AD-A065 831 VIRGINIA POLYTECHNIC INST AND STATE UNIV BLACKSBURG F/G 11/2
THERMAL-MECHANICAL AND THERMAL BEHAVIOR OF HIGH-TEMPERATURE STR--ETC(U)
DEC 78 D P HASSELMAN, M P KAMAT N00014-78-C-0431
UNCLASSIFIED NL

1 OF 2
AD A065831

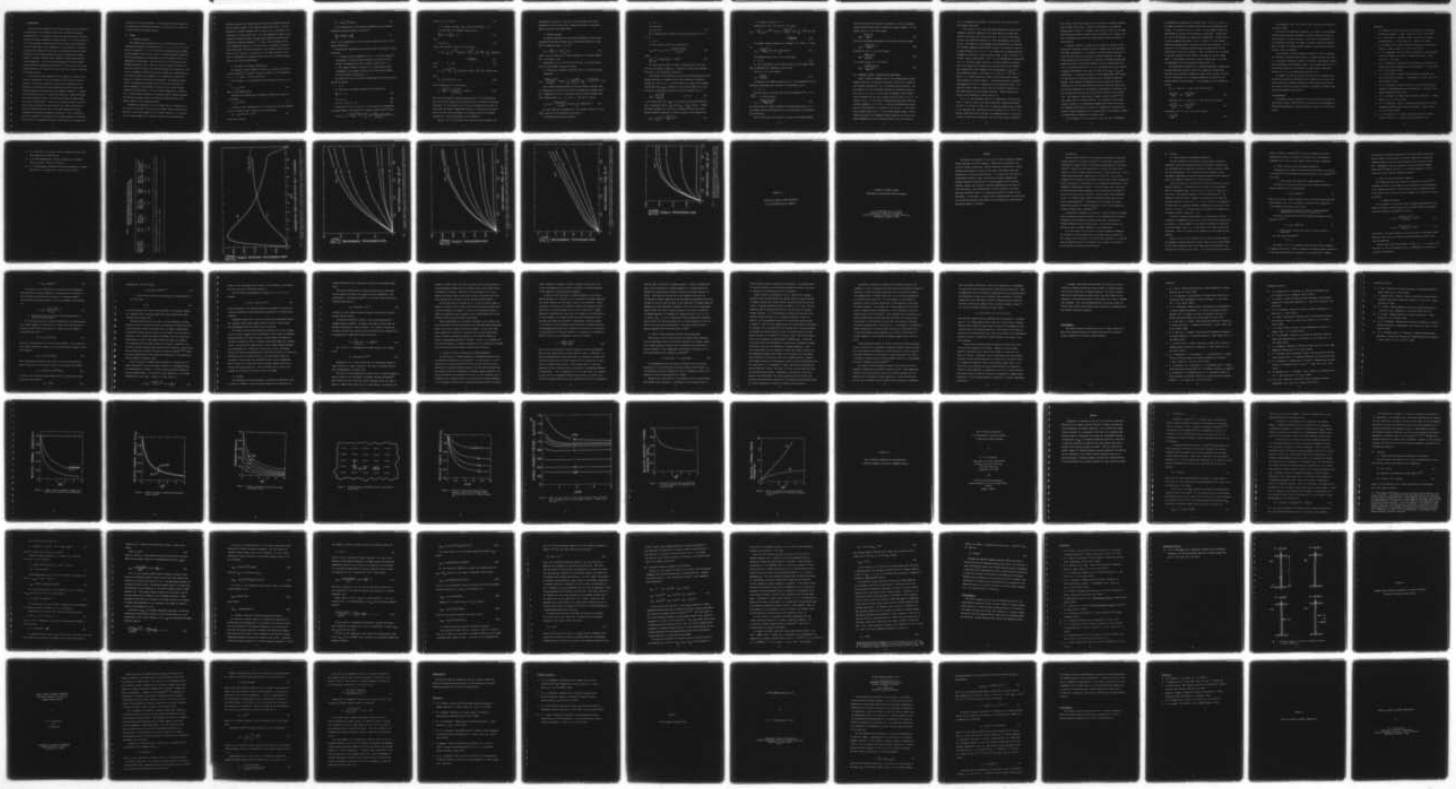

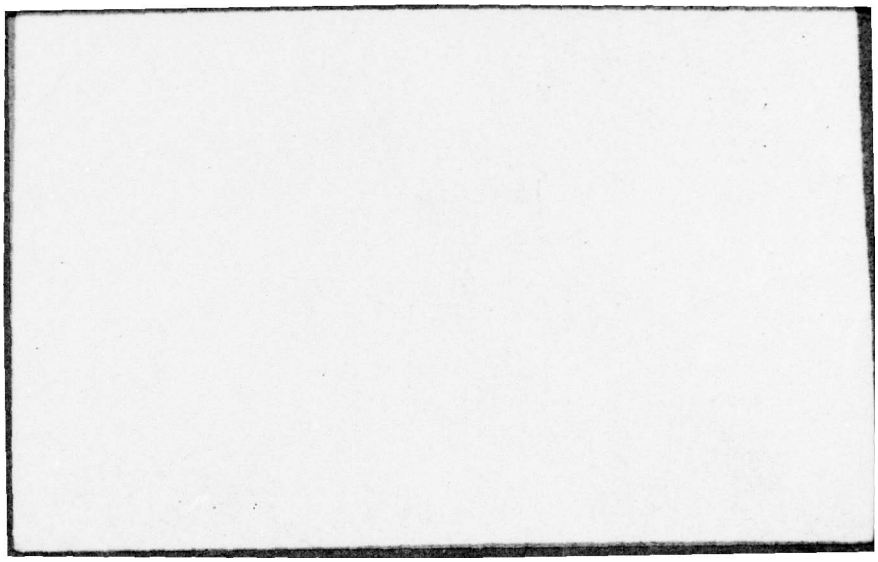

THERMAL-MECHANICAL AND THERMAL BEHAVIOR OF HIGH-TEMPERATURE STRUCTURAL MATERIALS,

(9) Interim Report, to ONR 1 Apr-31 Dec 78,

Agreement No.: N0014-78-C-0431

(15)

April 1, 1978 - December 31, 1978

by

(10) D.P.H. Hasselman and M.P. Kamat

(11) 31 Dec 78

in cooperation with

E.K. Beauchamp, L. Bentsen, K. Chyung, J. Heinrich, J.W. McCauley, H. Knoch, K. Satyamurthy, J.P. Singh, J.C. Swearengen, J.R. Thomas, G.E. Youngblood, Y. Tree and W.A. Zdaniewski

(12) 174p.

Departments of Materials Engineering and
Engineering Science and Mechanics
Virginia Polytechnic Institute and State University
Blacksburg, Virginia 24061

...classified

SECURITY CLASSIFICATION OF THIS PAGE (When Data Entered)

REPORT DOCUMENTATION PAGE		READ INSTRUCTIONS BEFORE COMPLETING FORM
1. REPORT NUMBER	2. GOVT ACCESSION NO.	3. RECIPIENT'S CATALOG NUMBER
4. TITLE (and Subtitle) Thermo-Mechanical and Thermal Behavior of High-Temperature Structural Materials		5. TYPE OF REPORT & PERIOD COVERED Interim Report 4/1/78-12-31-78 6. PERFORMING ORG. REPORT NUMBER
7. AUTHOR(s) D. P. H. Hasselman and M. P. Kamat		8. CONTRACT OR GRANT NUMBER(s)
9. PERFORMING ORGANIZATION NAME AND ADDRESS Virginia Polytechnic Institute and State University Blacksburg, VA 24061		10. PROGRAM ELEMENT, PROJECT, TASK AREA & WORK UNIT NUMBERS
11. CONTROLLING OFFICE NAME AND ADDRESS		12. REPORT DATE December 31, 1978 13. NUMBER OF PAGES 160
14. MONITORING AGENCY NAME & ADDRESS(if different from Controlling Office)		15. SECURITY CLASS. (of this report) Unclassified 15a. DECLASSIFICATION/DOWNGRADING SCHEDULE

16. DISTRIBUTION STATEMENT (of this Report)

See distribution list. ~~Do not release to NTIS~~

17. DISTRIBUTION STATEMENT (of the abstract entered in Block 20, if different from Report)

18. SUPPLEMENTARY NOTES

19. KEY WORDS (Continue on reverse side if necessary and identify by block number)

Absorption coefficient, micro-cracking, thermal stress resistance, thermal fatigue, figure-of-merit, ice, thermal conductivity, thermal diffucivity, glass-ceramic, mica-alumina, borosilicate glass, thermal buckling, reaction-sintered silicon nitride

20. ABSTRACT (Continue on reverse side if necessary and identify by block number)

-OVER-

DD FORM 1 JAN 73 1473 EDITION OF 1 NOV 65 IS OBSOLETE

Unclassified

SECURITY CLASSIFICATION OF THIS PAGE (When Data Entered)

This report presents the results obtained over the period of 4/1/78 to 12/31/78 on a research program on the thermo-mechanical and thermal behavior of high-temperature structural materials. A total of eleven studies were completed and reported in the form of individual chapters as follows:

I. "Thermal Stress Analysis of Partially Absorbing Brittle Ceramics Subjected to Radiation Heating".

II. "Analysis of Thermal Stress Resistance of Micro-Cracked Brittle Ceramics".

III. "Role of Physical Properties in the Resistance of Brittle Ceramics to Fracture in Thermal Buckling"

IV. "Thermal Stress Resistance Parameters for Brittle Materials Subjected to Thermal Stress Fatigue"

V. "On the Thermal Fracture of Ice".

VI. "Effect of Cracks on Thermal Conductivity",

VII. "Effect of Oxidation on Thermal Diffusivity of Reaction-Sintered Silicon Nitride".

VIII. "Effect of Crystallization on the Thermal Diffusivity of a Cordierite Glass-Ceramic",

IX. "Thermal Diffusivity of Ba-Mica/Alumina Composites".

X. "Effect of Alumina Dispersions on the Thermal Conductivity/Diffusivity and Thermal Stress Resistance of a Borosilicate Glass",

XI. "Figures-of-Merit for the Thermal Stress Resistance of High-Temperature Brittle Ceramics: A Review".

THERMO-MECHANICAL AND THERMAL BEHAVIOR OF HIGH-TEMPERATURE STRUCTURAL MATERIALS

PREFACE

Technical ceramics because of their chemical inertness, high melting point, good wear resistance, excellent mechanical stability at high temperature and other unique properties, represent a class of materials eminently suited for many critical engineering applications. Unfortunately, because of their brittleness and unfavorable combination of pertinent material properties, technical ceramics generally are highly susceptible to catastrophic failure in non-uniform thermal environments, which give rise to thermal stresses of high magnitude.

Thermal stress failure analysis of structural materials represents a multi-disciplinary problem which involves the principles of heat transfer, mechanics and materials engineering. Over the last few decades much general understanding of the nature of thermal stress failure of brittle materials has been generated. However, due to the multi-disciplinary nature of the problem, the ability to predict thermal stress failure quantitatively for design or other purposes has lagged behind the progress made in other engineering fields. The objective of the present program is to improve the qualitative and quantitative understanding of the nature of thermal stress failure of brittle structural materials. In order to achieve this objective, the participating investigators and scope of the program are organized in a

manner which takes full advantage of the combined inputs from a number of engineering disciplines including mechanical engineering, applied mechanics and materials science and engineering. This report presents, in the form of individual chapters, completed studies prepared for publication over the contracting period of 4/1/78 to 12/31/78.

The effort devoted to this program can be divided into three separate individual areas, namely: (A) Analysis of thermal stress failure; (B) measurement and analysis of material properties relevant to thermal stress failure and (C) reports with the objective of the dissemination of technical information on thermal stress failure. The completed studies are grouped together in these three major technical areas with brief descriptions of current work in progress as follows:

A. Analysis of Thermal Stress Failure.

Chptr. I. D. P. H. Hasselman, J. R. Thomas, Jr., M. P. Kamat and K. Satyamurthy, "Thermal Stress Analysis of Partially Absorbing Brittle Ceramics Subjected to Radiation Heating," J. Am. Ceram. Soc., (in review).

Chptr. II. D.P.H. Hasselman and J.P. Singh, "Analysis of Thermal Stress Resistance of Micro-cracked Brittle Ceramics," J. Am. Ceram. Soc., (in review).

Chptr. III. D.P.H. Hasselman, "Role of Physical Properties in the Resistance of Brittle Ceramics to Fracture in Thermal Buckling," J. Am. Ceram. Soc., (in press).

Note: This study was initiated under previous support provided by ARO and revised substantially as part of the present program.

Chptr. IV. D.P.H. Hasselman and W.A. Zdaniewski, "Thermal Stress Resistance Parameters for Brittle Materials Subjected to Thermal Stress Fatigue," J. Am. Ceram. Soc., 61 (7-8) 375 (1978).

Chptr. V. D.P.H. Hasselman and Y. Tree, "On the Thermal Fracture of Ice," J. Mat. Sc., (in press).

Research currently underway in this phase of the program includes a number of studies involving finite element modelling of transient thermal stresses and an analysis of non-linear convective heat transfer in thermal stress failure of brittle materials.

B. Measurement and Analysis of Material Properties Relevant to Thermal Stress Failure.

Chptr. VI. D.P.H. Hasselman, "Effect of Cracks on Thermal Conductivity," J. Comp. Mat., 12, 403-07 (1978).

Chptr. VII. W. Zdaniewski, H. Knoch, J. Heinrich and D.P.H. Hasselman, "Effect of Oxidation on Thermal Diffusivity of Reaction-Sintered Silicon Nitride," Ceram. Bull. (in press).

Chptr. VIII. K. Chung, G.E. Youngblood and D.P.H. Hasselman, "Effect of Crystallization on the Thermal Diffusivity of a Cordierite Glass-Ceramic," J. Amer. Ceram. Soc., (in press).

Chptr. IX. G.E. Youngblood, L. Bentsen, J.W. McCauley and D.P.H. Hasselman, "Thermal Diffusivity of Ba-Mica/Alumina Composites," J. Amer. Ceram. Soc., (in press).

Chptr. X. D.P.H. Hasselman, J.C. Swearengen, E.K. Beauchamp and W.A. Zdaniewski, "Effect of Alumina Dispersions on the

Thermal Conductivity/Diffusivity and Thermal Stress Resistance of a Borosilicate Glass," J. Am. Ceram. Soc., (in review).

It should be noted that the above studies were carried out in cooperation with other organizations and also received considerable internal VPI support. Chptrs. VIII and IX represent completion of brief studies carried out under previous ONR-support.

As part of the on-going research, the observations reported in Chptr. VIII are being pursued further in the form of quenching studies of reaction-sintered silicon nitride subjected to various oxidation treatments. Experimental data obtained at MERDI (under previous ONR-support) on a temperature dependent boundary resistance of glass-metal composites with a rather strong positive temperature dependence of the thermal diffusivity are being analyzed.* Also, thermal properties of a polycrystalline alumina used in experimental thermal stress studies are being determined. Other measurements in progress serve to verify the analytical findings reported in Chptrs. II and VI.

C. Dissemination of Technical Information on Thermal Stress Fracture of Brittle Materials.

Chptr. XI. D.P.H. Hasselman, "Figures-of-Merit for the Thermal Stress Resistance of High-Temperature Brittle Materials," Ceramurgia International (in press)

---

* Of interest to note is that similar observations are being made in parallel studies on potential MHD-materials: J.J. Rasmussen, Task N, "Materials Evaluation," Report to DOE-MHD, Jan.-March, 1978.

Effort currently underway as part of this phase of the program is devoted to the assembling of literature references and other information on thermal stress fracture of brittle materials for the purpose of compiling an extensive bibliography and the preparation of an in-depth review acticle. Furthermore, a conference is being organized with the tentative title: "Thermal Stresses in Structures and Materials in High Heat Flux Environments." This conference will take place in the early part of 1980. Exact dates and details of the program will be announced shortly.

CHAPTER I.

THERMAL STRESS ANALYSIS OF PARTIALLY ABSORBING BRITTLE CERAMICS SUBJECTED TO RADIATION HEATING

THERMAL STRESS ANALYSIS OF PARTIALLY ABSORBING BRITTLE CERAMICS SUBJECTED TO RADIATION HEATING

by

D.P.H. Hasselman, J. R. Thomas, Jr., M. P. Kamat and K. Satyamurthy

Departments of Materials Engineering, Mechanical Engineering
and Engineering Science and Mechanics
Virginia Polytechnic Institute and State University
Blacksburg, Virginia 24061

ABSTRACT

Thermal stresses in partially transparent brittle ceramics subjected to radiation heat transfer were analyzed for two convective cooling conditions. The absorption coefficient is introduced as a material property which affects thermal stress resistance. Appropriate thermal stress resistance parameters were derived.

I. INTRODUCTION

Brittle ceramic materials for structural purposes are well-known to be susceptible to catastrophic failure under conditions involving thermal stress[1]. For purposes of proper design and selection of materials for structures subjected to thermal stress, it is critical that the role of the physical properties which affect thermal stress resistance of brittle materials is well understood. For this purpose, literature solutions were presented for the role of the pertinent physical properties which control thermal stress fracture for conditions of steady-state[2] or transient convective heat transfer[3], thermal buckling[4] and crack propagation[5]. For the solutions presented, so-called "thermal stress resistance" parameters were derived[6,7] on the basis of which the optimum material can be selected for prescribed heat transfer conditions and failure criteria.

At sufficiently high temperatures heat transfer by radiation also can play a significant role in the thermal stress fracture of brittle materials. Previously, analytical solutions were presented for the thermal stress resistance of opaque materials for which the incident black-body radiation was absorbed in the immediate surface[8]. A further solution addressed itself to a material subjected to radiation heating which was transparent below a prescribed wave-length and opaque above this value of wave-length[9]. As far as the authors are aware to date no thermal stress analysis has been presented for ceramic materials subjected to radiant energy in which the incident radiation is being transmitted and absorbed throughout the material. Such an analytical solution is presented in this paper, with primary emphasis on establishing the role of the appropriate physical properties which determine the

thermal stress fracture behavior. The boundary conditions chosen for the analysis are those which will meet the objectives of the study in the most simple and expedient manner.

II. THEORY

A. Boundary Conditions

The analysis will be carried out for an infinite flat plate of thickness 2a located in the yz-plane and $-a < x < a$. At $x = a, -a$ the plate is subjected at $t = 0$ to a steady-state perpendicularly incident uniform radiation such as from a laser or focused black-body radiation. The optical properties of the material will be considered "grey", i.e., independent of wave-length. The reflectivity of the material will be assumed sufficiently low, so that the effect of multiple internal reflections within the plate on the absorbed energy can be neglected. The choice of symmetric heating of the plate simplifies the expressions for the thermal stresses as the moments of the temperature distributions around $x = 0$ vanish and need not be considered. The properties which control the magnitude of thermal stress, such as the coefficient of thermal expansion, Young's modulus, Poisson's ratio and the thermal conductivity and diffusivity, also are assumed independent of temperature. Other boundary conditions or wavelength and/or temperature-dependent materials properties can be considered by modifications of the present analysis or by numerical methods.

Throughout the analysis it will be assumed that the temperature of the plate is sufficiently low so that the radiant energy emitted by the material is very small compared to the incident radiation. For justification of this assumption, it should be noted that in transient heat

transfer, generally the thermal stresses reach their maximum values during the initial stages of the transient temperature history. For the derivation of thermal stresses then, the plate can be considered to be subjected to a constant heat flux. This same approach was taken in the analysis of thermal stresses in opaque bodies heated by radiation and validated by numerical examples[8]. Of course, for an estimate of the total temperature history or if the intensity of incident radiation is sufficiently high that surface melting or visco-elastic effects occur before brittle fracture can take place in the cooler interior of the plate, the assumption of constant radiant heat flux for thermal stress analysis will require modification.

B. Derivation of Transient Temperatures.

For normally incident radiation intensity q_o outside of the plate, the heat absorbed by the surface equals εq_o, where ε is the emissivity or $\varepsilon = (1 - r)$ where r is the reflectivity.

The intensity, q, of the radiation after entering the plate at x = a is:

$$q = \varepsilon q_o e^{-\mu(a-x)} \tag{1}$$

where μ is the absorptivity.

Similarly the intensity due to radiation entering the plate at x = -a becomes:

$$q = \varepsilon q_o e^{-\mu(a+x)} \tag{2}$$

The rate of heat absorption g''' at x is the sum of the heat absorbed due to the fluxes of Eqs. (1) and (2) and is expressed:

$$g''' = \mu\varepsilon q_o e^{-\mu a}(e^{\mu x} + e^{-\mu x}) \tag{3}$$

which can be written:

$$g''' = 2\mu\varepsilon q_o e^{-\mu a}\cosh(\mu x) \tag{4}$$

For the derivation of the transient temperatures, the following differential equation needs to be solved[10]:

$$\frac{\partial^2 T}{\partial x^2} + \frac{g''' (x)}{K} = \frac{1}{\beta}\frac{\partial T}{\partial t} \tag{5}$$

where T is the temperature, K is the thermal conductivity and β is the thermal diffusivity.

Solutions were obtained for two limiting cases for external cooling conditions:

1. A constant surface temperature at x = a, -a, which physically corresponds to the plate being contained in a convective heat transfer environment with a heat transfer coefficient $h = \infty$.
2. The complete absence of cooling at the plate surface which corresponds to an external convective heat transfer environment with heat transfer coefficient h = 0.

For these two cases, the transient temperature distributions can be derived as follows:

1. $h = \infty$

For this case the boundary conditions can be expressed:

$$\frac{\partial T}{\partial x}(0,\ t) = 0 \tag{6a}$$

$$T(x,\ 0) = T_o \tag{6b}$$

$$T(a,\ 0) = T(-a,\ 0) = T_o \tag{6c}$$

Substitution of Eq. (4) into Eq. (5) and solution by mathematical techniques common to the solution of transient temperatures[10] yields:

$$T(x,t) = T_o + \frac{4\mu\varepsilon q_o e^{-\mu a}\cosh(\mu a)}{aK} \sum_{n=o}^{n=\infty} \left[\frac{(1-e^{-\beta\lambda_n^2 t})(-1)^n \cos(\lambda_n x)}{(\mu^2+\lambda_n^2)\ \lambda_n}\right] \tag{7}$$

where $\lambda_n = (n + 1/2)\pi/a$ (8)

2. No surface cooling. Heat transfer coefficient, h = 0.

For this case, the boundary conditions are:

$$\frac{\partial T}{\partial t}(0, t) = \frac{\partial T}{\partial x}(a, t) = 0 \tag{9}$$

and

$$T(x, 0) = T_o \tag{10}$$

which, with the aid of Eqs. (4) and (5) yield:

$$T = T_o + \sum_{n=1}^{\infty} C_n e^{-\beta\lambda_n^2 t}\cos(\lambda_n x) + \frac{\varepsilon q_o e^{-\mu a}}{K}\left[\left(\frac{x^2}{a} + \frac{2\beta t}{a} + \frac{2}{a\mu^2} - \frac{a}{3}\right)\sinh(\mu a) - \frac{2\cosh(\mu x)}{\mu}\right] \tag{11}$$

where $\lambda_n = n\pi/a$ (12)

and

$$C_n = N_n^{-1}\frac{\varepsilon q_o e^{-\mu a}}{K}\int_0^a \cos(\lambda_n x)\left[\frac{2}{\mu}\cosh(\mu x) - \frac{x^2}{a}\sinh(\mu a)\right]dx \tag{13a}$$

with:

$$N_n = \int_0^a \cos^2(\lambda_n x)dx = a/2 \tag{13b}$$

After integration, Eq. (13a) yields:

$$C_n = \frac{4\varepsilon q_o e^{-\mu a}}{aK}\left\{\frac{\mu^2(-1)^{n+1}}{\lambda_n^2(\mu^2+\lambda_n^2)}\right\}\sinh(\mu a) \tag{13c}$$

Note that the boundary conditions underlying Eq. (11) as expressed by Eqs. (9) and (10) assume that the material does not re-emit the absorbed radiation. For this reason, Eq. (11) must be considered valid only for plates with low initial temperatures and over a time period sufficiently short such that the plate remains cool enough so that the re-emitted radiation to a first approximation can be neglected.

From Eq. (11) it may be noted that after an initial transient the

temperature in the plate at any point rises uniformly with time as expressed by the last term, with a temperature profile in the plate given by the third and fourth terms.

C. Thermal Stresses.

The general expression for the thermal stresses in a plate with a temperature distribution which varies through-the-thickness only and which is symmetric about x = 0, is[11]:

$$\sigma_{y,z} = \frac{\alpha E}{(1-\nu)} \left[-T + \frac{1}{2a} \int_{-a}^{a} T dx\right] \tag{14}$$

where α is the coefficient of thermal expansion, E is Young's modulus, and ν is Poisson's ratio.

Substitution of Eq. (7) or Eq. (11) into Eq. (14) yields expressions for the thermal stresses as follows:

1. Infinite heat transfer coefficient ($h=\infty$), or constant surface temperature.

$$\sigma_{y,z} = \frac{4\alpha E(\mu a)\varepsilon q_o e^{-\mu a}}{(1-\nu)Ka^2} \cosh(\mu a) \sum_{n=0}^{\infty} \frac{(1-e^{-\beta\lambda_n^2 t})}{(\mu^2+\lambda_n^2)} \left\{\frac{1}{a\lambda_n^2} - \frac{(-1)^n \cos(\lambda_n x)}{\lambda_n}\right\} \tag{15}$$

Since ceramic materials generally are much weaker in tension than in compression, the values of the tensile stresses are of primary interest. Examination of Eq. (15) indicates that the tensile stresses have their maximum values at x = -a, a and t = ∞ and can be written:

$$\sigma_{y,z}(a,\infty) = \frac{4\alpha E(\mu a)\varepsilon q_o e^{-\mu a}}{(1-\nu)Ka^2} \cosh(\mu a) \sum_{n=0}^{\infty} \{(\mu^2+\lambda_n^2)(a\lambda_n^2)\}^{-1} \tag{16}$$

Eq. (16) shows that the magnitude of the thermal stresses is a nonlinear function of the absorption coefficient μ.

Two limiting cases can be discussed:

a. $\mu a \to \infty$

For this case:

$$\sigma_{y,z}(x,\infty) = 0 \tag{17}$$

Eq. 17 implies that no thermal stresses are generated for $h = \infty$, $\mu a = \infty$.

b. $\mu a \to 0$

For this case Eq. (16) can be simplified to:

$$\sigma_{y,z}(a,\infty) = \sigma_{y,z}(-a,\infty) = \frac{64\alpha E\mu(1-\mu a)\varepsilon q_o a^2}{\pi^4(1-\nu)K} \tag{18}$$

using:

$$\lim_{\mu a \to 0} \sum_{n=0}^{\infty} \{(\mu^2+\lambda_n^2)(a\lambda_n^2)\}^{-1} = 16a^3/\pi^4 \tag{19}$$

Eq. (18) indicates that for lightly absorbing plates with $\mu a \to 0$ and $h=\infty$, the thermal stresses are a parabolic function (with downward curvature) of the absorption coefficient.

For purposes of the selection of partially absorbing materials with optimum resistance to thermal fracture when subjected to radiation heating, Eq. (18) for $\mu a << 1$ can be rewritten in terms of the maximum radiant heat flux, q_{max}, to which the plate can be subjected, so that the tensile stresses do not exceed the tensile strength, S_t, by:

$$q_{max} = \frac{S_t(1-\nu)K\pi^4}{64\alpha E\mu\varepsilon a^2} \qquad (\mu a << 1) \tag{20}$$

If the radiant heat flux, q_{max}, is the result of black-body radiation from a temperature source, T_{max}, with $q_{max} = \rho T_{max}^4$, (where ρ = Stefan-Boltzmann constant), Eq. (20) can be expressed also in terms of the maximum radiation temperature to which the plate can be subjected by:

$$T_{max} = \left(\frac{1}{64a\rho^2}\right)^{1/4} \left\{\frac{S_t(1-\nu)K}{\alpha E\mu\varepsilon}\right\}^{1/4} \tag{21}$$

2. No surface cooling (h = 0)

Substitution of Eq. (11) into Eq. (14) yields:

$$\sigma_{y,z} = -\frac{\alpha E}{1-\nu}\sum_{n=1}^{\infty} C_n e^{-\beta\lambda_n^2 t}\cos(\lambda_n x) + \frac{\varepsilon q_o \alpha E e^{-\mu a}}{K(1-\nu)}\left[\left(\frac{a}{3} - \frac{2}{a\mu^2} - \frac{x^2}{a}\right)\sinh(\mu a) + \frac{2\cosh(\mu x)}{\mu}\right] \quad (22)$$

The tensile thermal stresses are a maximum at x = 0 and t = ∞ given by:

$$\sigma_{y,z} = \frac{\alpha E \varepsilon q_o e^{-\mu a}}{(1-\nu)K}\left\{\frac{2}{\mu} + \left(\frac{a}{3} - \frac{2}{a\mu^2}\right)\sinh(\mu a)\right\} \quad (23)$$

Two limiting cases of Eq. 23 can be discussed:

a. $\mu a \to \infty$. (24)

Eq. (24) corresponds to the condition that all the incident radiant heat is absorbed in the immediate surface layer.

With $\mu a = \infty$, Eq. (23) becomes:

$$\sigma_{y,z} = \frac{\alpha E \varepsilon q_o a}{6(1-\nu)K} \quad (25)$$

As expected, the thermal stresses for $\mu a = \infty$ are independent of the absorption coefficient and a function of the emissivity only.

b. $\mu a \ll 1$.

For this case Eq. (23) with the aid of the expansion $e^{\mu a} \simeq 1 + \mu a + \frac{\mu^2 a^2}{2} + \ldots$, can be written:

$$\sigma_{y,z} = \frac{7\alpha E \varepsilon q_o \mu^3 (1-\mu a) a^4}{180(1-\nu)K} \quad (26)$$

which shows that for lightly absorbing (uncooled) plates with $\mu a \ll 1$, the thermal stresses are proportional to the third power of the absorption coefficient.

Eqs. (25) and (26) can be written in terms of the maximum radiant

heat flux to which the plate can be submitted, so that the maximum tensile thermal stress does not exceed the tensile strength. In this manner, for $\mu a = \infty$, Eq. (25) becomes:

$$q_{max} = \frac{6S_t(1-\nu)K}{\alpha E \varepsilon a} \tag{27}$$

which for the maximum temperature of black-body radiation becomes:

$$T_{max} = \{\frac{6S_t(1-\nu)K}{\alpha E \varepsilon a \rho}\}^{1/4} \tag{28}$$

Similarly for $\mu a << 1$, Eq. (26) becomes:

$$q_{max} = \frac{180S_t(1-\nu)K}{7\alpha E \varepsilon \mu^3 a^4} \tag{29}$$

or in terms of T_{max}, Eq. (29) becomes:

$$T_{max} = \{\frac{180S_t(1-\nu)K}{7\alpha E \varepsilon \rho \mu^3 a^4}\}^{1/4} \tag{30}$$

III. NUMERICAL RESULTS, DISCUSSION AND CONCLUSIONS

Figure 1 shows the maximum value of the non-dimensional tensile thermal stress as a function of the product μa for the two values of heat transfer coefficient $h = 0, \infty$, considered in the analysis. For both cases ($h = 0, \infty$) the thermal stresses are identically equal to zero, for $\mu a = 0$. For $h = 0$, the value of maximum tensile thermal stress increases with μa, with a maximum value of 0.167, as $\mu a \to \infty$. In contrast, for $h = \infty$, the values of maximum non-dimensional stress go through a maximum at $\mu a = 1.344$ at a value of non-dimensional stress equal to 0.279 followed by a decrease to zero as $\mu a \to \infty$. The latter effect arises because as $\mu a \to \infty$ the absorbed radiant energy is transformed into heat in the immediate surface regions of the plate to be removed immediately by the surrounding medium. For this reason as

$\mu a \to \infty$ no temperature increase in the plate will occur and the plate will remain stress-free.

It is critical to note that the present analysis was based on the assumption that the temperature of the plate when the stresses have reached a value near their final value (Fig. 1) is still sufficiently low that the re-emitted radiation to a first approximation can be neglected. The validity of this assumption was established by calculating the transient temperature and thermal stresses as a function of time for a range of values of μa. For $h = \infty$, the values for the temperatures and stresses as a function of time are shown in Figs. 2 and 3, and for $h = 0$ in Figs. 4 and 5, respectively. For $h = 0$, the temperatures are unbounded as $t \to \infty$. For this reason, as done in a previous study[8], the temperatures in the plate were calculated for the time at which the stresses have reached 95% of their maximum value corresponding to q_{max} for a given numerical example. For values of $h = \infty$ and $\mu a = 1.344$ and $h = 0$ and $\mu a = 2.5$, these temperatures together with the physical property values chosen are listed in Table I. These property values correspond approximately to those of a high-density polycrystalline alumina. The numerical results indicate clearly that the re-emitted radiation is a very small fraction of the incident radiation. Similar quantitative results can be obtained for other values of μa.

For $h = \infty$, the calculated value of the temperature in the plate at $\beta t/a^2 = 1$ also is close to the final steady-state temperature attained as $\beta t/a^2 \to \infty$, so that, at least for the numerical example given in Table I, the radiative heat losses need not be considered at all. For $h = 0$, however, after the initial transient the temperatures will rise linearly in time, so that after a sufficient time period has elapsed, radiation

heat losses, thermo-visco-elastic stress relaxation or melting phenomena need be taken into account. However, as indicated by the numerical example given in Table I, if thermal stress fracture occurs it will take place during the initial transient before the plate is hot enough to re-emit the absorbed heat flux and at temperatures at which the plate is still brittle.

In general, however, it should be noted that the validity of neglecting the re-emitted radiation should be examined for each individual case under consideration. For instance, for ultra-strong structures or those with low values of coefficient of thermal expansion, the heat fluxes required for failure may be so high with corresponding high plate temperatures that the re-emitted radiation may be an appreciable fraction of the incident heat flux. If so, the expressions for the stresses represent overestimates, such that the equations for q_{max} or T_{max} are conservative. In principle, solutions for the temperatures and stresses for high levels of re-emitted radiation can be obtained by numerical methods. Such numerical calculations also may include the effect of temperature on the pertinent material properties, multiple reflections, the spectral dependence of the emissivity and absorption coefficient, as well as non-linear effects such as thermo-visco-elastic stress relaxation. Such numerical evaluations as judged by other studies[12,13] are more complex than the present analysis. The advantage of the present analysis in spite of its simplifying assumptions is that the stresses are expressed analytically in terms of the appropriate variables, which permits a direct assessment of the relative role of each material property in establishing the magnitude of thermal stress.

In this respect, it is of interest to note the role of absorption

in determining the magnitude of thermal stress. For $\mu a << 1$ and $h = \infty$ the thermal stresses are linearly proportional to the absorption coefficient. In contrast, for $\mu a << 1$ and $h = 0$, the thermal stresses are proportional to the cube of the absorption coefficient. Coupled with the role of the absorption in governing the magnitude of thermal stress is also an unusual size effect. For $h = \infty$ and $\mu a << 1$, the thermal stresses are proportional to the square of the plate thickness. For $h = 0$ and $\mu a << 1$, the maximum thermal stresses are proportional to the fourth power of the plate thickness. These size effects are in contrast to those for convective heat transfer[3], for which at low Biot number ($ah/K < 1$) the thermal stresses are directly proportional to the size and independent of size for high Biot number ($ah/K \to \infty$).

The expressions developed for the maximum permissible incident heat flux and black-body radiation permit the formulation of additional "thermal stress resistance" parameters, which can be used for the selection of the material with the optimum combination of properties for maximum thermal stress resistance. These parameters can be defined as follows:

For $h = \infty$ and $\mu a << 1$, Eqs. (20) and (21) yield:

$$\left\{\frac{S_t(1-\nu)K}{\alpha E\varepsilon\mu}\right\} \quad \text{and} \quad \left\{\frac{S_t(1-\nu)K}{\alpha E\varepsilon\mu}\right\}^{1/4} \tag{31}$$

Similarly, for $h = 0$ and $\mu a << 1$, Eqs. (29) and (30) yield:

$$\left\{\frac{S_t(1-\nu)K}{\alpha E\varepsilon\mu^3}\right\} \quad \text{and} \quad \left\{\frac{S_t(1-\nu)K}{\alpha E\varepsilon\mu^3}\right\}^{1/4} \tag{32}$$

Furthermore, for $h = 0$, $\mu a \to \infty$, Eq. (27) yields:

$$\left\{\frac{S_t(1-\nu)K}{\alpha E\varepsilon}\right\} \tag{33}$$

The parameter of Eq. (33) raised to the 1/4 power was presented in an earlier study[8].

With these five additional parameters, the number of non-redundant thermal stress resistance parameters available for material selection now has grown to a total near thirty. Also, with the introduction of the absorption coefficient the number of material properties presently known to affect the thermal stress resistance of brittle materials has reached a total of eighteen.

From the point of view of material selection in order to minimize the incidence of thermal stress fracture, it should be noted that for $h = 0$, a partially transparent ceramic is expected to have greater thermal stress resistance than an opaque ceramic. On the other hand, for $h = \infty$, low thermal stresses can be achieved for either highly transparent ceramics ($\mu a \to 0$) or for opaque materials with $\mu a \to \infty$.

In summary, an analysis has been presented for the thermal stress resistance of partially absorbing brittle ceramics in the form of flat plates subjected to symmetric normally incident radiation heating for two specific convective cooling conditions. Appropriate thermal stress resistance parameters were derived.

Acknowledgements

The present study was supported in part by the Office of Naval Research under contract N00014-78-C-0431 and in part by the Department of Mechanical Engineering of Virginia Polytechnic Institute and State University.

References

1. W. D. Kingery, "Factors Affecting the Thermal Stress Resistance of Brittle Ceramics", J. Amer. Ceram. Soc., 38(1) 3-15 (1955).
2. R. L. Coble and W. D. Kingery, "Effect of Porosity of Thermal Stress Fracture", J. Amer. Ceram. Soc., 38(1) 33-37 (1955).
3. W. B. Crandall and J. Ging, "Thermal Shock Analysis of Spherical Shapes", J. Amer. Ceram. Soc., 38(1) 44-56 (1955).
4. D. P. H. Hasselman, "Role of Physical Properties in the Resistance of Brittle Ceramics to Failure in Thermal Buckling", J. Amer. Ceram. Soc., (in press).
5. D. P. H. Hasselman, "Unified Theory of Thermal Shock Fracture Initiation and Crack Propagation of Brittle Ceramics", J. Amer. Ceram. Soc., 52(11) 600-04 (1969).
6. D. P. H. Hasselman, "Thermal Stress Resistance Parameters for Brittle Refractory Ceramics: A Compendium", Am. Ceram. Soc. Bull., 49(12) 1933-37 (1970).
7. D. P. H. Hasselman, "Figures-of-Merit for the Thermal Stress Resistance of High-Temperature Brittle Materials: A Review", Ceramurgia International (in press).
8. D. P. H. Hasselman, "Thermal Shock by Radiation Heating", J. Amer. Ceram. Soc., 46, 229-34 (1963).
9. D. P. H. Hasselman, "Theory of Thermal Stress Resistance of Semi-Transparent Ceramics Under Radiation Heating", J. Amer. Ceram. Soc., 49, 103-04 (1966).
10. H. S. Carslaw and J. C. Jaeger, Conduction of Heat in Solids, 2nd Ed., Oxford, at the Clarendon Press (1960), 510 pp.

11. B. A. Boley and J. H. Weiner, Theory of Thermal Stresses, John Wiley and Sons, NY (1960) 586 pp.

12. O. S. Narayanaswamy and R. Gardon, "Calculation of Residual Stress in Glass", 52(10) 554-58 (1969).

13. O. S. Narayanaswamy, "Stress and Structural Relaxation in Tempering Glass," J. Am. Ceram. Soc., 61(3-4) 146-152 (1978).

TABLE I. Calculated Maximum Heat Flux and Temperature in Partially Absorbing Flat Plate Subjected to Radiation Heating at 95% of Maximum Thermal Stress Level.

Heat Transfer Coefficient (Watts. cm^{-2})	Value of μa	Time at 95% stress ($\beta t/a^2$)	Max. Heat Flux, q_{max} Watts. cm^{-2}	Surface Temp. (K°)	Emitted heat flux Watts cm^{-2}	Ratio Incident to Emitted Heat Flux
0	2.5	0.25	244	480	0.27	0.1%
∞	1.344	1	64	580	0.57	0.9%

Property values for calculation: $S_t = 200$ MN.m^{-2}; $E = 4 \times 10^5$ MN.m^{-2}; $\nu = 0.25$, $K = 0.3$ Watts. $cm^{-1}.°C^{-1}$; $\varepsilon = 0.9$; $\alpha = 7 \times 10^{-6} °C^{-1}$, $a = 1$ cm; $T_o = 273°K$.

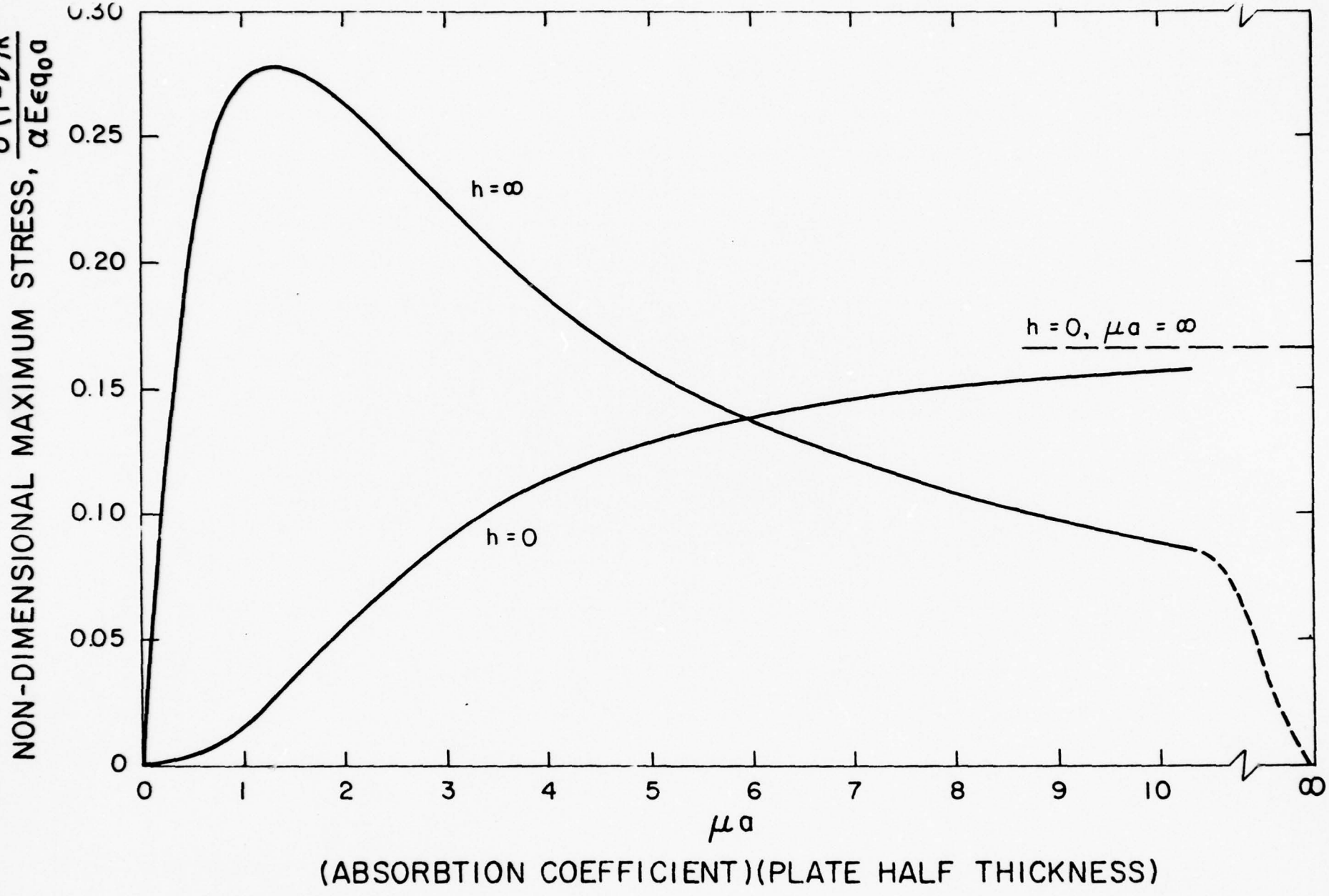

Fig. 1. Maximum tensile thermal stresses in partially absorbing flat plate symmetrically heated by normally incident radiation and cooled by convection with heat transfer coefficients, h = o and h = ∞.

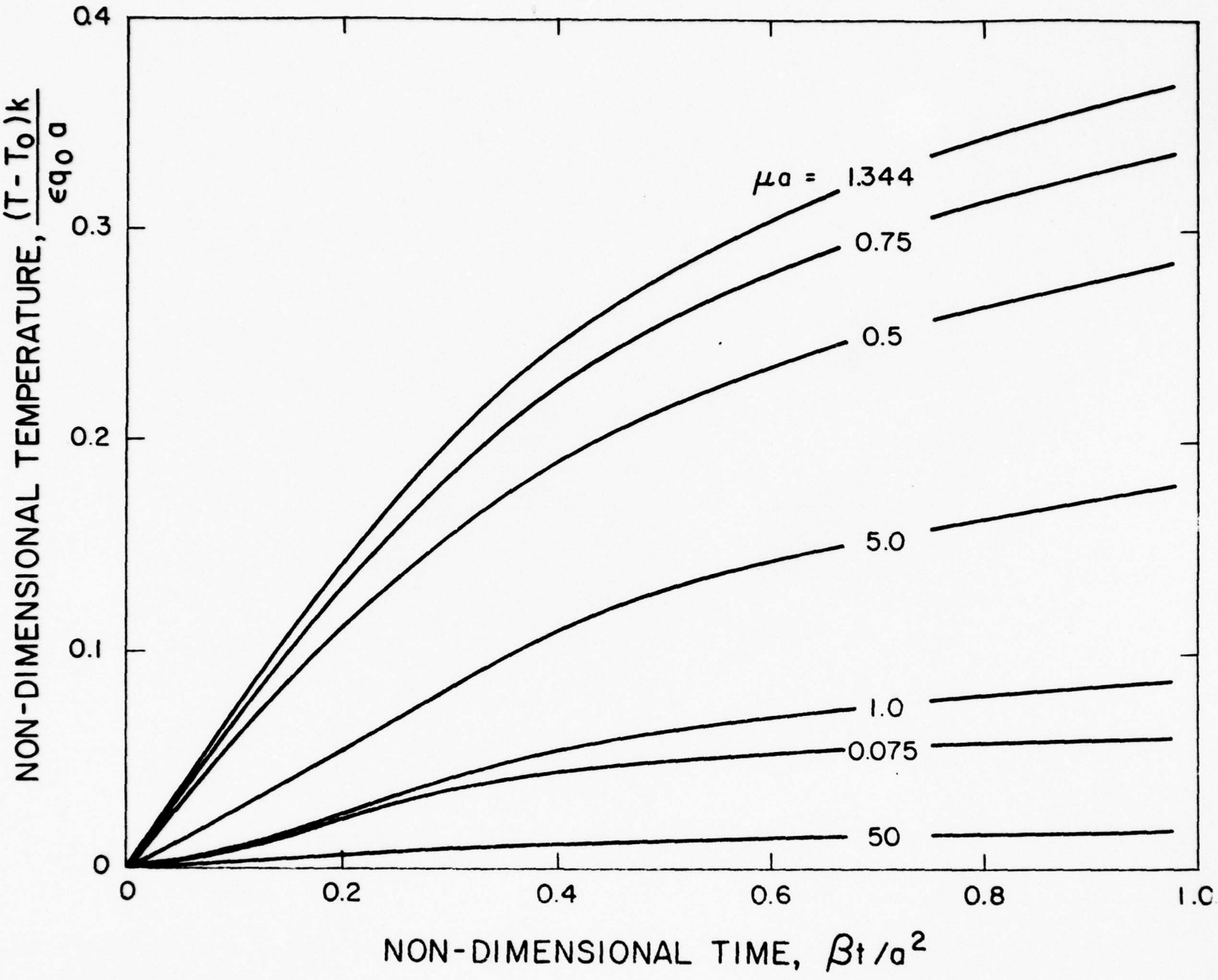

Fig. 2. Transient temperatures at center of partially absorbing flat plate symmetrically heated by normally incident radiation and cooled by convection with heat transfer coefficient, $h = \infty$.

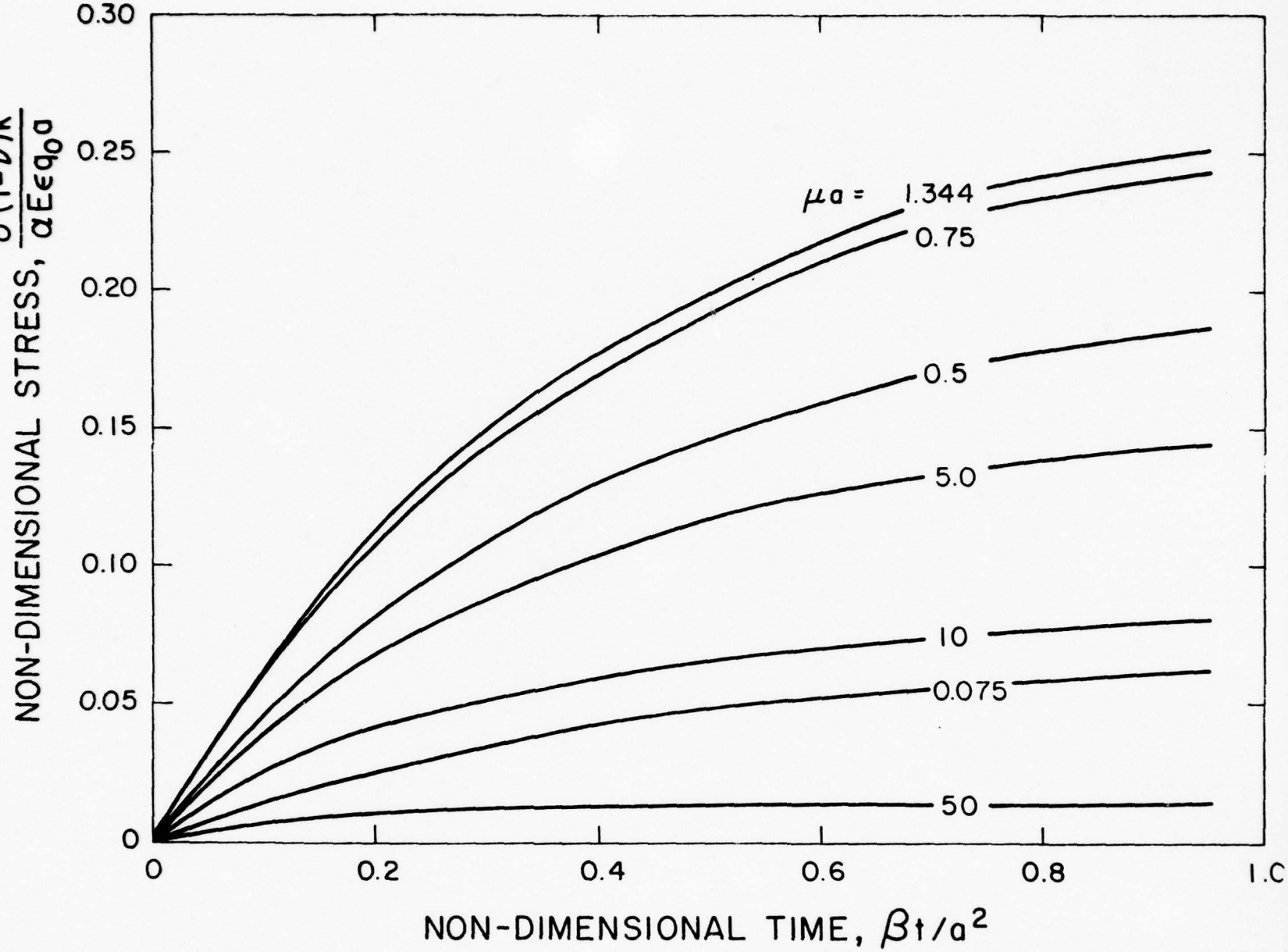

Fig. 3. Transient tensile thermal stresses at surface of partially absorbing flat plate symmetrically heated by normally incident radiation and cooled by convection with heat transfer coefficient, $h = \infty$.

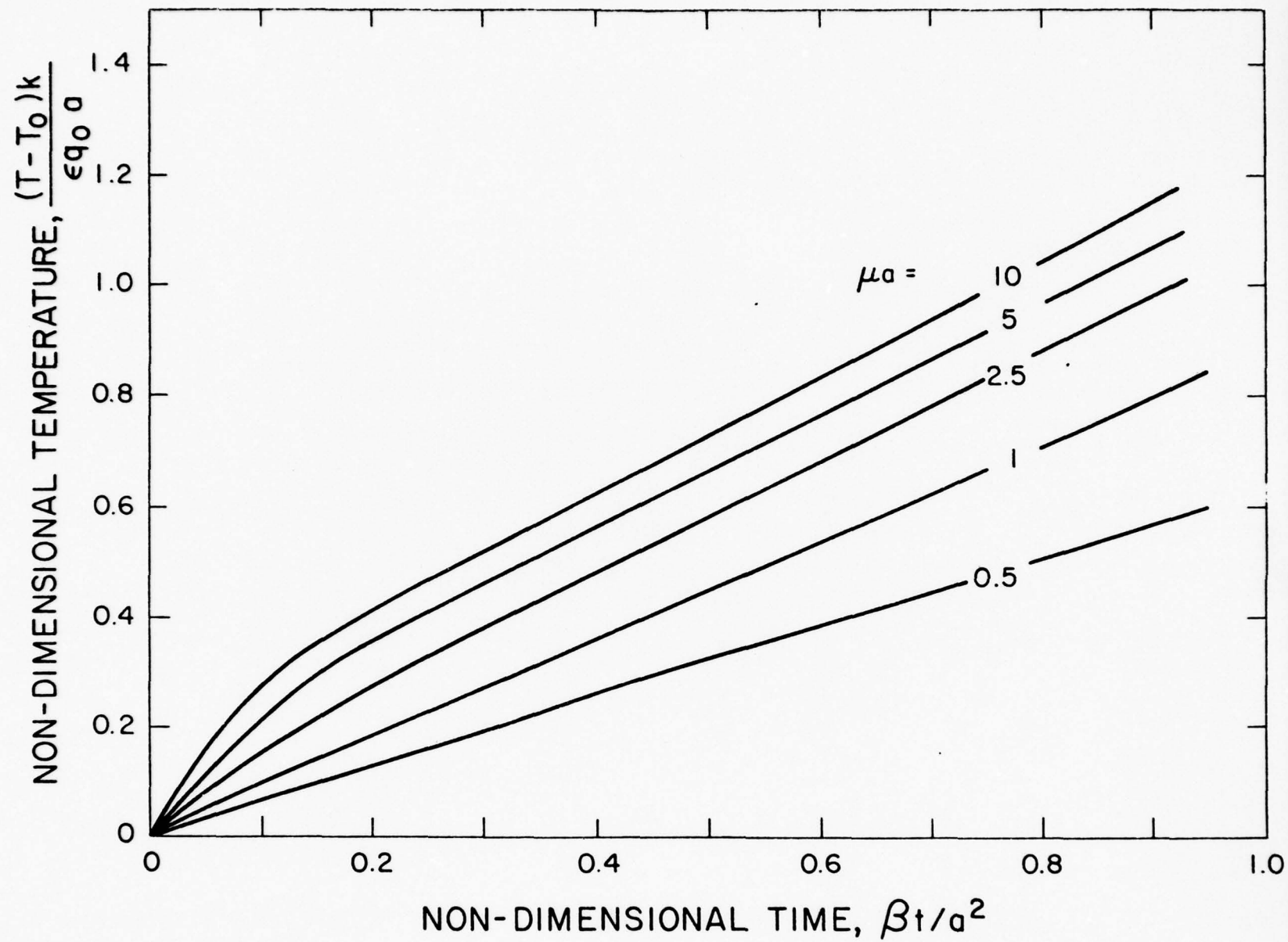

Fig. 4. Transient temperatures at surface of partially absorbing flat plate symmetrically heated by normally incident radiation and cooled by convection with heat transfer coefficient, h = o.

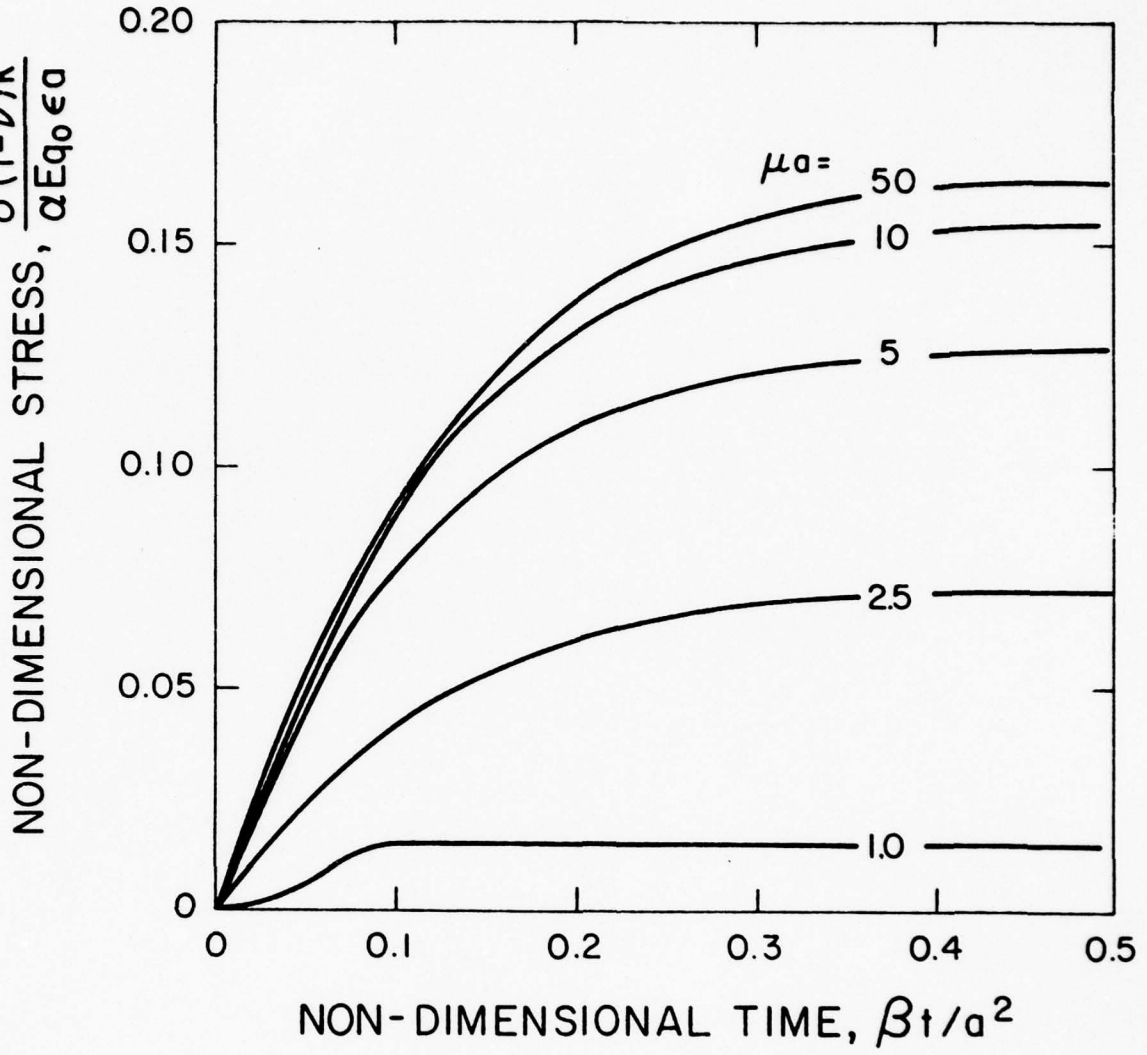

Fig. 5. Transient tensile thermal stresses at center of partially absorbing flat plate symmetrically heated by normally incident radiation and cooled by convection with heat transfer coefficient, h = o.

CHAPTER II.

ANALYSIS OF THERMAL STRESS RESISTANCE OF MICRO-CRACKED BRITTLE CERAMICS.

ANALYSIS OF THERMAL STRESS

RESISTANCE OF MICRO-CRACKED BRITTLE CERAMICS

D. P. H. Hasselman and J. P. Singh
Department of Materials Engineering
Virginia Polytechnic Institute and State University
Blacksburg, Virginia 24061

ABSTRACT

An analysis is presented for the effect of micro-cracking on thermal stress resistance of brittle ceramics. Expressions are obtained or derived for thermal conductivity, elastic properties, coefficient of thermal expansion and strength in terms of crack-size, crack density and crack interaction for a micro-cracked material. It is shown that the values of Young modulus, Poisson's ratio, coefficient of thermal expansion and thermal conductivity decrease with increasing degree of micro-cracking. Strength, however, may increase or decrease depending upon the nature of crack interaction. The combined effect of micro-cracking on the above mentioned properties results in a significant increase in thermal stress resistance. In particular, it makes a micro-cracked material very attractive for the application where high thermal stress resistance with good thermal insulating property is required.

I. Introduction

Brittle ceramic materials for structural applications at high temperature generally are highly susceptible to catastrophic failure under conditions of thermal stress. As demonstrated experimentally[1] and analytically[2,3], materials with high densities of micro-cracks may offer a solution to the low thermal stress resistance of brittle materials. Micro-cracked materials exhibit high strains-at-fracture[4,5], high fracture toughness[6] and on thermal failure should undergo stable crack propagation[2,3] rather than unstable (catastrophic) crack propagation encountered for many homogeneous high-strength ceramics. The high thermal stress resistance of micro-cracked materials primarily can be attribured to the effect of the micro-cracks on elastic behavior. Heavily micro-cracked materials, in fact, can exhibit elastic moduli substantially lower than the non-micro-cracked materials[4,5]. Unfortunately micro-cracking can cause a significant decrease in thermal conductivity, with a corresponding decrease in thermal stress resistance[7,8,9].

A quantitative assessment of the effect of micro-cracking on thermal stress resistance requires an analysis of the combined effects of micro-cracking on elastic behavior, thermal conductivity, coefficient of thermal expansion and the fracture stress. This latter property, in particular, may be strongly affected by crack interaction.

It is the purpose of this study to present literature information on the effect of micro-cracking on the principal properties which affect thermal stress resistance or to derive such information, if required. From the combined results, an assessment then is made of the effect of micro-cracking on thermal stress resistance.

II. Analysis

A. General Approach and Boundary Conditions.

For the information on the effect of micro-cracks on material properties, only those expressions will be presented or derived which are sufficient for an analysis of the effect of micro-cracking on thermal stress resistance. For a review and critical analysis of the mathematical approaches to and the assumptions underlying the equations given, the reader is referred to the cited literature.

As will be shown, the relative effect of micro-cracking on a given material property, q is derived in the literature or in the present paper in the general form: $q = q_o(1-\varepsilon)$ or $q = q_o(1+\varepsilon)^{-1}$, where q_o is the value of the material property of the crack-free material. The quantity ε, which includes a constant is a function of the crack density and crack size. Since for $\varepsilon << 1$, $(1-\varepsilon) \simeq (1+\varepsilon)^{-1}$, for simplicity of comparison, all equations, whenever appropriate will be given in the form of $q = q_o(1+\varepsilon)^{-1}$. This also avoids the problem of obtaining zero or negative property values for $\varepsilon \geq 1$.

In order to reduce the total number of solutions which could be presented to a manageable total, for so far as possible the analysis will be limited to a crack geometry in the form of ellipsoids of revolution of very low aspect ratio (i.e., cracks which in the limit approach zero thickness). Also, all cracks will be assumed to be of uniform size and geometry.

Finally, also it will be assumed that the crack sizes and temperature gradients involved during the thermal stress are sufficiently small, so that crack instability due to the temperature non-uniformity in the vicinity of the cracks does not occur. As is easily ascertained from the

theory of Goodier and Florence[10], this latter assumption is easily satisfied for cracks of the order of Griffith flaws and temperature gradients of the order of those usually found in ceramic technology.

B. Effect of Micro-cracks on Thermal Conductivity

Solutions for the effect of micro-cracks in the shape of ellipsoids of revolution of zero thickness on thermal conductivity are available[11,12] as follows:

1. Micro-cracks with statistical random orientation.

The effect of micro-cracks with statistical random orientation on thermal conductivity can be expressed[12]:

$$K = K_o(1 + 8Nb^3/9)^{-1} \tag{1}$$

where K, K_o are the thermal conductivities of the micro-cracked and crack-free material, resp., N is the number of cracks per unit volume and b is the radius of revolution of the cracks.

2. Micro-cracks oriented with plane of crack propagation perpendicular to the direction of heat flow.

The effect of micro-cracks with this preferred orientation can be derived to be[11,12]:

$$K = K_o(1 + 8Nb^3/3)^{-1} \tag{2}$$

3. Micro-cracks oriented with plane of cracks parallel to heat flow.

For this crack orientation[12]:

$$K \simeq K_o \tag{3}$$

The result of eq. 3 is reasonable since the cracks are not expected to impede the heat flow. Figure 1 compares the relative thermal conductivity for the three orientations as a function of the quantity Nb^3. Cracks

with preferred orientation perpendicular to the direction of heat flow have the highest relative effect on thermal conductivity, followed by randomly oriented cracks and cracks parallel to the direction of heat flow. Experimental data for the effect of micro-cracking on thermal conductivity[7,8] suggest that $Nb^3 \simeq 2$, so that the range of $0 < Nb^3 < 5$ chosen for figure 1 must be considered realistic.

C. Effect of Cracks on Elastic Properties

This subject has received considerable theoretical attention[13-19], including the effect of the absence and the presence of crack interaction. As for thermal conductivity, crack orientation plays a significant role in the effect of micro-cracks on elastic behavior, as presented or derived as follows:

1. Random orientation

For the purpose of the present study, convenient expressions for the effect of randomly oriented micro-cracks on Young's modulus and Poisson's ratio were obtained by Salganik[16] as follows:

$$E = E_o\left[1 + \frac{16(10-3\nu_o)(1-\nu_o^2)}{45(2-\nu_o)} Nb^3\right]^{-1} \tag{4}$$

$$\nu = \nu_o\left[1 + \frac{16(3-\nu_o)(1-\nu_o^2)}{15(2-\nu_o)} Nb^3\right]^{-1} \tag{5}$$

where E and ν are Young's modulus and Poisson's ratio of the micro-cracked material, and E_o and ν_o are Young's modulus and Poisson's ratio of the crack-free material.

Figures 2 and 3 show the dependence of E/E_o and ν on the quantity Nb^3. Note that to a first approximation, E/E_o is independent of the value of ν_o and can be expressed:

$$E \simeq E_o[1 + 16Nb^3/9]^{-1} \tag{6}$$

For purpose of the discussion of the effect of micro-cracking on the coefficient of thermal expansion, an expression for the effect of micro-cracking on bulk modulus is required. As derived by Walsh[14] (also directly obtainable from eqs. 4 and 5) this effect can be expressed:

$$B = B_o\left[1 + \frac{16(1-\nu_o^2)Nb^3}{9(1-2\nu_o)}\right]^{-1} \tag{7}$$

2. Micro-cracks with crack plane oriented perpendicular to uni-axial stress direction.

For circular micro-cracks oriented perpendicular to the stress direction, Young's modulus in the direction of stress can be derived from the solution of Sack[20] which shows that for a single crack the change in potential energy (ΔW) is:

$$\Delta W = 8(1-\nu_o^2)\sigma^2 b^3/3E_o \tag{8}$$

where E_o is Young's modulus of the crack-free material. For N cracks per unit volume, assuming the absence of crack interaction, the change in potential energy is:

$$\Delta W_N = 8(1-\nu_o^2)\sigma^2 Nb^3/3E_o \tag{9}$$

Since the potential energy per unit volume in the crack-free material equals $\sigma^2/2E_o$, the total potential energy in the material with cracks:

$$W_t = \sigma^2/2E_o + 8(1-\nu_o^2)\sigma^2 Nb^3/3E_o \tag{10}$$

In terms of the effective Young's modulus (E) of the material the potential energy (W_t) becomes:

$$W_t = \sigma^2/2E \tag{11}$$

Equating eqs. 10 and 11 yields:

$$E = E_o[1+16(1-\nu_o^2)Nb^3/3]^{-1} \tag{12}$$

3. Micro-cracks with crack plane parallel to stress direction.

For this case:

$$E \simeq E_o \tag{13}$$

as can be derived easily from the upper bound[21] for the Young's modulus of a composite with a dispersed phase with Young's modulus and volume fraction which approach zero.

The above expressions for the effect of micro-cracking on elastic behavior strictly are valid for dilute concentrations of cracks for which crack interaction effects can be neglected. At higher concentrations at which the distance between cracks is on the order of or less than the crack size, crack interaction effects undoubtedly can play a major part. Unfortunately, as far as the present writers are aware, no solutions for interaction effects between cracks in the form of ellipsoids of revolution on elastic behavior have appeared in the literature. Nevertheless, such solutions are available for arrays of cracks in plates[3,15,18], which can give a qualitative or semi-quantitative indication of the interaction effects between ellipsoidal cracks.

From the solution of Yokobori and Ichikawa[22] for co-planar rows of cracks, Hasselman[15] derived the elastic behavior of a rectangular array of cracks depicted in figure 4, in which interaction effect between the rows was assumed absent. The effective Young's modulus (E) of the plate perpendicular to the plane of cracks (for plane strain) is:

$$E = E_o\left[1 - \frac{16Nd^2(1-\nu_o^2)}{\pi} \ln \cos \frac{\pi a}{2d}\right]^{-1} \tag{14}$$

where a is the half-length of the cracks, N is the density of the cracks per unit area and d is defined in figure 4.

For very dilute concentrations of cracks ($N \to o$, $d \to \infty$) eq. 14 becomes:

$$E = E_o[1 + 2\pi N(1-\nu_o^2)a^2]^{-1} \tag{15}$$

which corresponds to the solution obtained by Hasselman[3] for dilute concentration (absence of crack interactions) adjusted for the plane stress condition.

Comparison between eqs. 14 and 15 indicates that interaction between the co-planar cracks causes Young's modulus to drop to a value below the corresponding value for lack of crack interaction.

The effect of interaction between the parallel rows of the co-planar cracks on Young's modulus can be ascertained from the results of Delameter, Herrman and Barnett[18], shown in figure 5, which combine the effects of interaction between the rows of co-planar cracks and between the co-planar cracks. As expected, for a given value of 2a/c, Young's modulus decreases with increasing 2a/d. However, for a given value of 2a/d, the upward curvature of E/E_o with increasing 2a/c, shows that the nature of interaction between the rows of co-planar cracks is such that Young's modulus is increased; in other words, the interaction effect between neighboring rows of cracks is to reduce the effect on Young's modulus due to an individual non-interacting crack. This observation will be shown to be critical to the effect of the micro-cracks on strength.

D. Strength

The introduction of micro-cracking in a material is expected to have an effect on strength. The micro-cracks themselves can constitute the

failure-initiating flaws or may have an effect on pre-existing larger flaws.

For dilute concentrations of micro-cracks for which crack interactions effects are absent, the strength will be independent of the crack density. As derived by Sack[20] for a circular crack the critical fracture stress (S_t) is:

$$S_t = [\pi E \gamma_f / 2a(1-\nu_o^2)]^{1/2} \tag{16}$$

in which γ_f is the surface fracture energy per unit area of the newly created fracture surface.

At high crack densities, however, crack interaction effects on strength cannot be ignored. To examine this effect, reliance must be placed on solutions for cracks in plates. For a single co-planar row of cracks, the fracture stress as derived by Yokobori and Ichikawa[22] can be expressed (for conditions of plane strain) as:

$$S_t = \left[\frac{E\gamma_f}{2(1-\nu_o^2)d} \cot\left(\frac{\pi a}{2d}\right)\right]^{1/2} \tag{17}$$

Eq. 17, as $d \to \infty$, approaches the Griffith solution for a single crack:

$$S_t = [E\gamma_f / \pi a(1-\nu_o^2)]^{1/2} \tag{18}$$

Comparison of eq. 17 and 18 shows that the interaction between co-planar cracks is to cause a decrease in the value of strength from the value corresponding to a single crack.

The effect of crack interactions between rows of co-planar cracks (as shown in figure 4) was calculated by Delameter, Herrman and Barnett[18]. Their results in terms of relative stress intensity factor are shown in figure 6. These results show that for a given value of the distance (d)

between co-planar cracks, the stress intensity factor decreases with decreasing distance between rows of co-planar cracks, which should lead to an increase in strength. This leads to the surprising result that a material with many cracks of the proper relative orientation and inter-crack spacing can be stronger than the non-microcracked material.

On the other hand, as indicated by eq. 17 and the results shown in figure 6 for small values of d/2a, the interaction between cracks can be such that strength is decreased. In part, this explanation serves to explain the generally lower strength of micro-cracked materials in comparison to their non-microcracked counterparts.

Another explanation for a decrease in strength can be based on the fact that failure of brittle materials can be initiated from pre-existing flaws of sizes much larger than the micro-cracks. In this case, some micro-cracks which form may lie co-planar with the pre-existing flaw, which in effect experiences an increase in its effective length and causes a corresponding decrease in strength. In fact, it is thought that this latter mechanism is primarily responsible for the decrease in strength of brittle materials which exhibit extensive micro-cracking.

E. Effect of Cracks on Coefficient of Thermal Expansion

The coefficient of thermal expansion of a homogeneous material does not depend on the geometry of the material. For this reason, it is not expected that a brittle material with cracks of zero width will have a coefficient of thermal expansion different from the non-cracked material. For materials which are heterogeneous in thermal expansion behavior, the above conclusion is not expected to be valid. In such materials, such as composites with a mismatch between the coefficients of thermal expansion of the individual components or in polycrystalline materials which exhibit

thermal expansion anisotropy, internal stresses can arise which can control the magnitude of the overall coefficient of thermal expansion of the composite or polycrystalline aggregate.

In general, the coefficient of thermal expansion of such heterogeneous materials is a function of the coefficients of thermal expansion, the volume fraction and the elastic moduli of each component. Micro-cracking as the result of the internal stresses will change the elastic moduli with a resulting change in the overall coefficient of thermal expansion. Quantitatively, this effect will depend on the distribution of each component, the internal stress with the heterogeneous system and other microstructural variables. Some general features, however, of the effect of micro-cracking on the coefficient of thermal expansion of heterogeneous materials can be examined on the basis of an expression for the coefficient of thermal expansion of a composite (α_c) derived by Turner[23], which for a two-component system can be written:

$$\alpha_c = \frac{\alpha_1 V_1 B_1 + \alpha_2 V_2 B_2}{V_1 B_1 + V_2 B_2} \tag{19}$$

where α is the coefficient of thermal expansion, B is the bulk modulus and V is the volume fraction of each component 1 and 2. Generally, for materials manufactured at high temperature, on cooling the component with the higher coefficient of thermal expansion will be subjected to a high level of residual tensile stress. These stresses when of sufficient magnitude can cause extensive micro-cracking and a corresponding decrease in bulk modulus. If so, examination of eq. 19 reveals that in a composite in which one of the components develops micro-cracks, the overall coefficient of thermal expansion (α_c) will approach the value for the component

with the lower coefficient of thermal expansion. Similar considerations apply to the coefficient of thermal expansion of a polycrystalline aggregate of a material which exhibits anisotropy in thermal expansion behavior. This explains the very low or even negative values for the coefficient of thermal expansion of micro-cracked polycrystalline materials, in spite of the fact that the value of the coefficient of thermal expansion averaged over crystallographic orientation still can be quite appreciable. Figure 7 shows the effect of micro-cracking on the relative coefficient of thermal expansion of a hypothetical composite with $B_1 = B_2$, $V_1 = V_2 = 0.5$ and $\alpha_2 = 4\alpha_1$. It can be noted that the micro-cracking for reasonable values for Nb[3] can reduce the coefficient of thermal expansion to half the value of the non-microcracked material. The above conclusions are in general agreement with the observations of Rossi[24].

F. Effect of Micro-Cracking on Thermal Stress Resistance

The relative effect of micro-cracking on thermal stress resistance by the simultaneous effects of the micro-cracking on the thermal conductivity, Young's modulus, Poisson's ratio, strength and the coefficient of thermal expansion, can be judged most conveniently on the basis of the well-known thermal stress resistance parameters[25]:

$$R = S_t(1-\nu)/\alpha E, \quad R' = S_t(1-\nu)K/\alpha E \tag{20}$$

For heterogeneous materials such as composites or micro-cracked materials with a micro-structural scale much smaller than the body size, the individual properties involved in R and R' correspond to those of the composite or micro-cracked material as a whole.

Materials with high values of the parameters R and R' should exhibit good thermal stress resistance. Accordingly, for the present case, if

micro-cracking increases thermal stress resistance, the combined effect of the micro-cracking on the individual properties should be such that an increase in the parameters R and R' is achieved.

Figure 8 shows the variation of R and R' with Nb^3 for randomly oriented cracks calculated from the combined effects of micro-cracking on thermal conductivity, Young's modulus, Poisson's ratio and the coefficient of thermal expansion as shown in figures 1, 2, 3 and 7 with the assumption that crack-interaction effects are such that the strength remains invariant. For crack-interaction effects such that the stress intensity factor decreases (i.e., strength increases) as shown in figure 6, the corresponding values for R will lie above the ones shown in figure 8. Even for crack interactions such that strength is decreased, an increase in R is expected since the combined effect of micro-cracking on strength and Young's modulus at least for moderate values of crack density is such as to increase[15] the ratio of S_t/E. This latter observation is well documented by experimental[4,5] observations. An increase in S_t/E will lead to an increase in R irrespective of additional changes in Poisson's ratio and the coefficient of thermal expansion. Since crack interactions also are expected to affect the thermal conductivity, no unambiguous statement with respect to the changes in R' can be made, until theoretical solutions for this effect become available. However, since Young's modulus is affected more strongly by micro-cracking than thermal conductivity, it is reasonable to expect that with crack-interaction effects taken into account, the value of R' will not drop below the value for the non-cracked material. Regardless of the details of the crack geometry and interactions, the present analytical results clearly substantiate the experimental observation[1] that randomly oriented micro-cracks can lead to significant increases in thermal stress resistance.

Significant increases in thermal stress resistance should be obtainable, at least in principle for micro-cracks with preferred orientation. Generally, in cases involving severe heat flux, at least near surfaces the maximum values of thermal stress arise in a direction perpendicular to the direction of heat flow. For this reason, it is desirable to maintain a value of thermal conductivity in the direction of heat flow as high as possible. At the same time, Young's modulus and the coefficient of thermal expansion perpendicular to the direction of heat flow should be kept as low as possible. This condition can be achieved by promoting oriented micro-cracking such that the plane of the micro-cracks lies parallel to the direction of heat flow, with random or preferred orientation perpendicular to the heat flow. In this manner, the effective thermal conductivity in the direction of heat flow as indicated by eq. 3 is unaffected whereas Young's modulus (eq. 12) and the coefficient of thermal expansion in the direction of maximum thermal stress can be reduced.

A non-uniform distribution of cracks of random or preferred orientation can also be used to advantage in improving thermal stress resistance. Such a non-uniform distribution of cracks results in a spatial variation in thermal conductivity, which under the proper conditions will lead to a decrease in maximum value of tensile thermal stress and a corresponding increase in thermal stress resistance[26].

The effect of micro-cracking on thermal stress resistance can be regarded as beneficial from another viewpoint as well. High-temperature materials often are expected to perform as thermal insulators for the purpose of the containment of high temperatures. Such materials then may have the requirement of high thermal stress resistance in combination

with low thermal conductivity. This latter requirement is incompatible with the first which generally requires high thermal conductivity. This incompatibility may be satisfied by using heavily micro-cracked materials. The requirement of high ratio of thermal stress resistance to thermal conductivity can be expressed in terms of "figures-of-merit" which are derived by dividing the thermal stress resistance parameters R and R' (eq. 20) by the thermal conductivity which yields:

$$R_r = S_t(1-\nu)/\alpha EK \quad \text{and} \quad R'_r = S_t(1-\nu)/\alpha E$$

Note that the figure-of-merit R'_r dimensionally is equivalant to the parameter R. It is demonstrated earlier that due to their effect on Young's modulus, micro-cracks can cause a major increase in the parameter R, and therefore also in the figure-of-merit R'_r. This effect is even more pronounced for the figure-of-merit R_r, which as the result of the simultaneous decrease in E and K, should show a major increase as the result of the micro-cracking.

For the above derivations and discussions the crack density and crack size were assumed to be constant. However, in micro-cracked materials the number and the size of the cracks is a function of the degree of cooling. Furthermore, due to crack-closure and crack healing, reheating of micro-cracked materials can result in the recovery of many of the physical properties close to the non-microcracked values. For this reason, the properties of micro-cracked materials are expected to exhibit a strong dependence on temperature as well as on thermal history. This aspect should be taken into account in assessing the thermal stress resistance of a micro-cracked material intended for a specific engineering application.

In summary, expressions were presented for the effect of micro-cracking on thermal conductivity, Young's modulus, strength, Poisson's ratio and the coefficient of thermal expansion. The results indicate that micro-cracked materials should exhibit excellent thermal stress resistance. Oriented micro-cracks, in principle, can be used to considerable advantage. Also, micro-cracked materials can be very useful for purposes which require high thermal stress resistance in combination with high thermal insulating properties.

Acknowledgment

The present study was conducted as part of a larger research program on the thermal-mechanical and thermal properties of structural ceramics supported by the Office of Naval Research.

References

1. R. C. Rossi, "Thermal-Shock Resistant Ceramic Composites," Ceramic Bulletin, 48 (7) 736-37 (1969).
2. D. P. H. Hasselman, "Unified Theory of Thermal Shock Fracture Initiation and Crack Propagation in Brittle Ceramics," J. Am. Ceram. Soc., 52 (11) 600-04 (1969).
3. D. P. H. Hasselman, "Thermal Stress Crack Stability and Propagation in Severe Thermal Environments," pp. 89-103 in Materials Science Research, Vol. V, Ceramics in Severe Environments, Ed. by W. W. Kriegel and Hayne Palmour III, Plenum Press, New York (1971).
4. E. A. Bush and F. A. Hummel, "High-Temperature Mechanical Properties of Ceramic Materials: I, Magnesium Dititanate," J. Amer. Ceram. Soc., 41 (6) 189-95 (1958).
5. E. A. Bush and F. A. Hummel, "High-Temperature Mechanical Properties of Ceramic Materials: II, Beta-Eucryptite," J. Amer. Ceram. Soc., 42 (8) 388-91 (1959).
6. J. A. Kuszyk and R. C. Bradt, "Influence of Grain Size on Effects of Thermal Expansion Anisotropy in $MgTi_2O_5$," J. Amer. Ceram. Soc., 56 (8) 420-23 (1973).
7. H. J. Siebeneck, D. P. H. Hasselman, J. J. Cleveland and R. C. Bradt, "Effect of Microcracking on the Thermal Diffusivity of Fe_2TiO_5", J. Amer. Ceram. Soc., 59 (5-6) 241-44 (1976).
8. H. J. Siebeneck, J. J. Cleveland, D. P. H. Hasselman and R. C. Bradt, "Grain Size Microcracking Effects on the Thermal Diffusivity of $MgTiO_5$."
9. W. R. Manning, G. E. Youngblood and D. P. H. Hasselman, "Effect of Microcracking on the Thermal Diffusivity of Polycrystalline Aluminum Niobate", J. Am. Ceram. Soc., 60, 469-70 (1977).

References (Cont'd)

10. J. N. Goodier and A. L. Florence, pp. 562-68 in Proceedings XIth Int. Congress of Appl. Mechanics, Munich (1964).

11. J. R. Willis, "Bounds and Self-Consistent Estimates for the Overall Properties of Anisotropic Composites," J. Mech. Phys. Solids 25, 185-202 (1977).

12. D. P. H. Hasselman, "Effects of Cracks on Thermal Conductivity," J. Comp. Mat. 12 403-07 (1978).

13. J. P. Berry, "Some Kinetic Considerations of the Griffith Criterion For Fracture," I and II, J. Mech. Phys. Solids, 8 (3), 194-206; 206-17 (1960).

14. J. B. Walsh, "Effect of Cracks on the Compressibility of Rocks," J. Geophys. Res., 70 (2) 381-99 (1965).

15. D. P. H. Hasselman, "Analysis of the Strain at Fracture of Brittle Solids with High Densities of Microcracks," J. Am. Ceram. Soc., 52 (8), 458-59 (1969).

16. R. L. Salganik, "Mechanics of Bodies with Many Cracks," Izv. An. SSSR Mekhanika Tverdogo Tela, 8 (4) 149-158 (1973).

17. R. J. O'Connell and B. Budiansky, "Seismic Velocities in Dry and Saturated Cracked Solids," J. Geophysical Research, 79 (35) 5412-26 (1974).

18. W. R. Delameter, G. Hermann and D. M. Barnett, "Weakening of an Elastic Solid by a Rectangular Array of Cracks," J. Appl. Mech. (43), 74-80 (1975).

19. B. Budiansky and R. J. O'Connell, "Elastic Module of a Cracked Solid," Int. J. Solid Structures," 12, 81-97 (1976).

20. R. A. Sack, "Extension of Griffith's Theory of Rupture to Three Dimensions," Proc. Phys. Soc., London 729-36 (1946).

References (Cont'd)

21. B. Paul, "Prediction of Elastic Constants of Multiphase Materials," Trans. AIME, 218 (2), 36-41 (1960).

22. T. Yokobori and M. Ichikawa, "Elastic Solid with an Infinite Row of Collinear Cracks and the Fracture Criterion," J. Phys. Soc., Japan, (19) 2341-42 (1964).

23. P. S. Turner, "Thermal-Expansion Stresses in Reinforced Plastics," J. Res. Natl. Bur. Standards, 37 (4) 239-50 (1946): RP 1745.

24. R. C. Rossi, "Thermal Expansion of BeO-SiC Composites," J. Amer. Ceram. Soc., 52 (5) 290-91 (1969).

25. D. P. H. Hasselman, "Thermal Stress Resistance Parameters for Brittle Refractory Ceramics: A Compendium," Amer. Ceram. Soc. Bull., 49 (12), 1933-37 (1970).

26. D. P. H. Hasselman and G. E. Youngblood, "Enhanced Thermal Stress Resistance of Structural Ceramics with Thermal Conductivity Gradient," J. Amer. Ceram. Soc., 61, (1) 49-52 (1978).

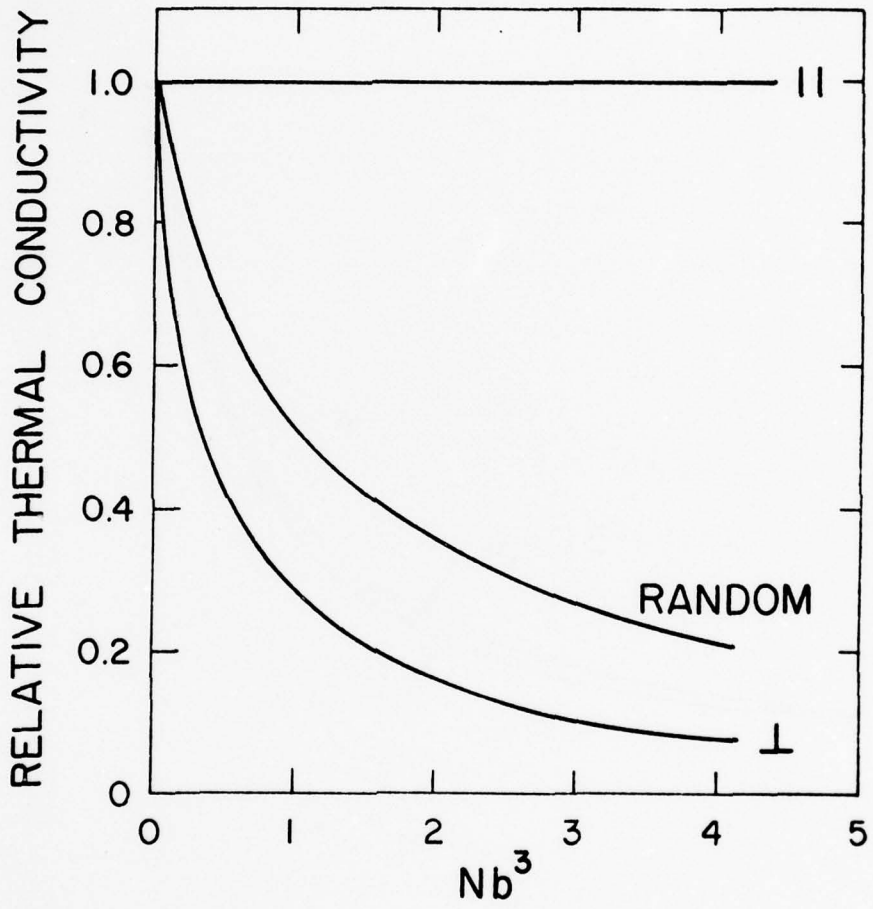

Figure 1. Effect of micro-cracking on thermal conductivity for various crack orientations.

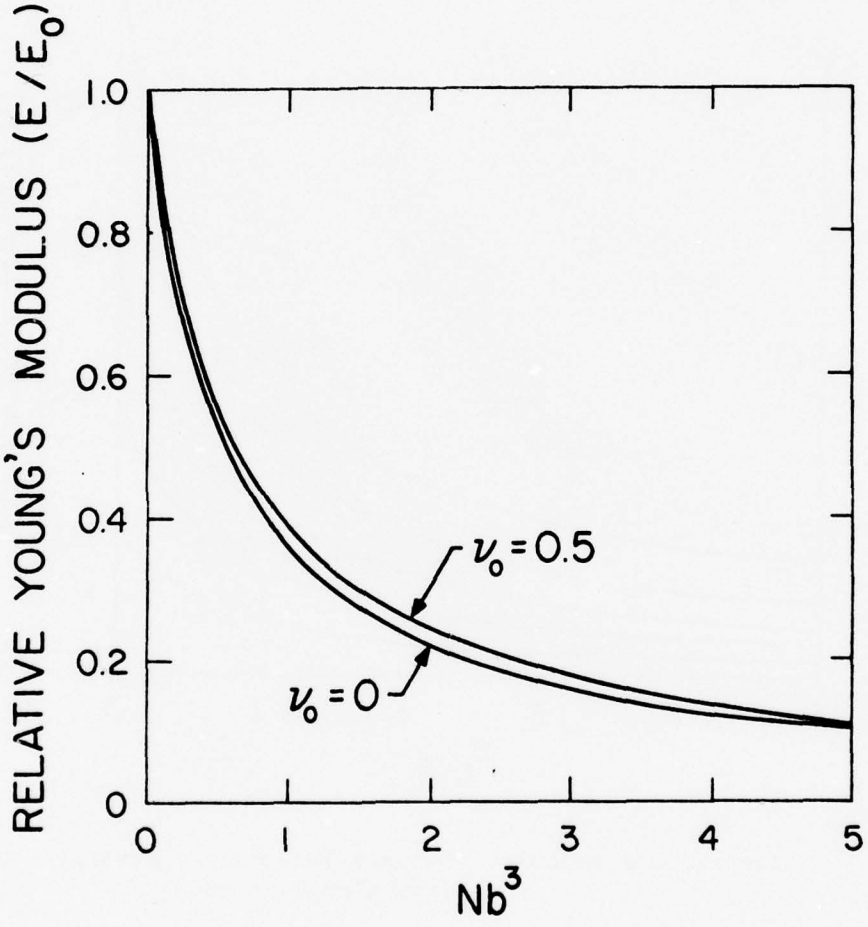

Figure 2. Effect of randomly oriented micro-cracks on Young's modulus.

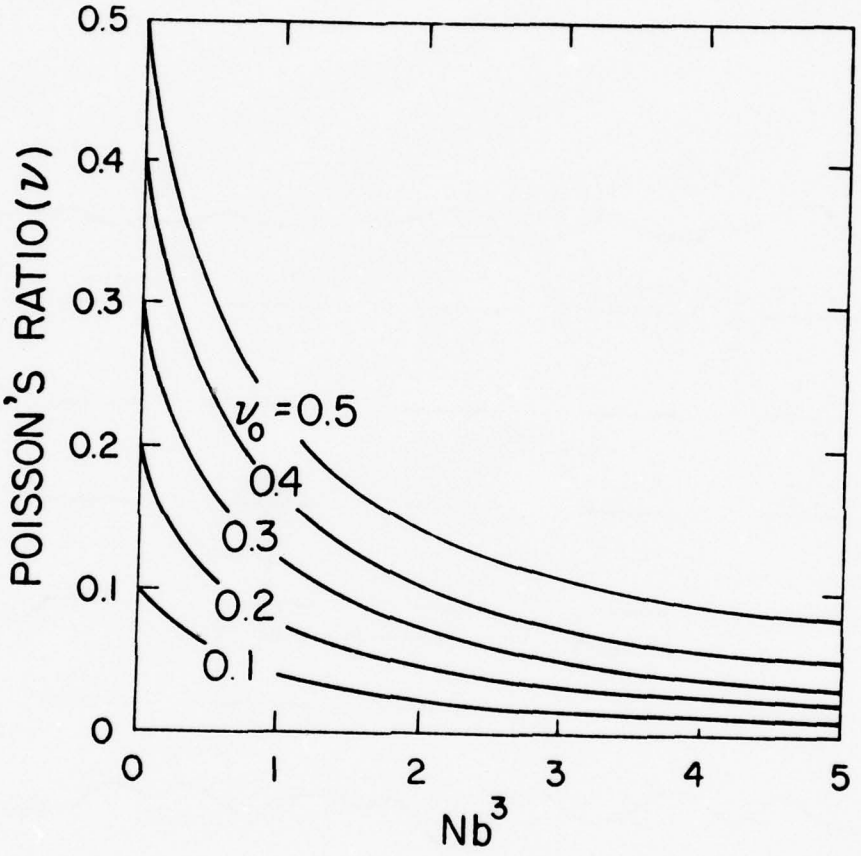

Figure 3. Effect of randomly oriented micro-cracks on Poisson's ratio.

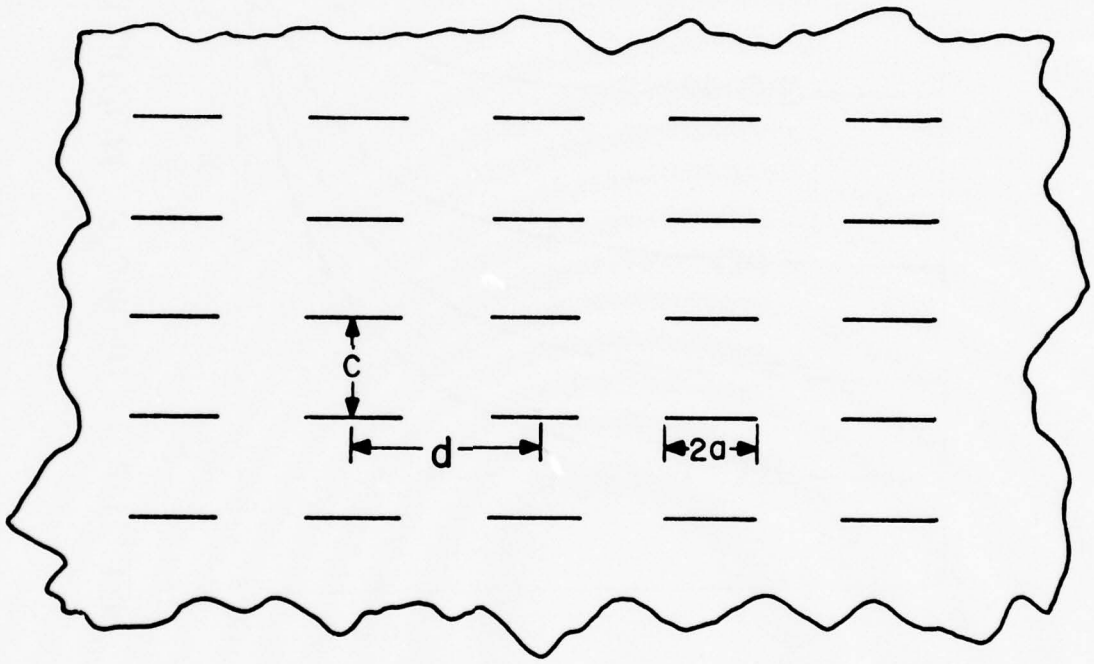

Figure 4. Flat plate with rectangular array of cracks (after footnote 18).

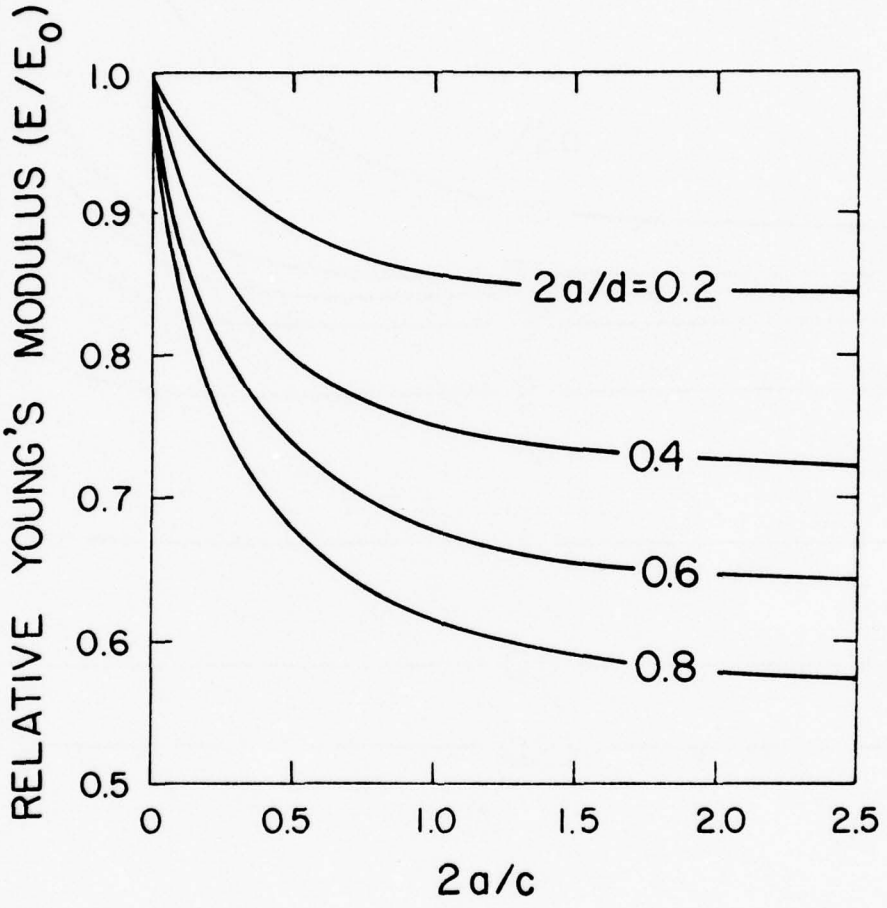

Figure 5. Effect of interacting cracks on Young's modulus of plate with rectangular array of cracks shown in Fig. 4. (After footnote 18).

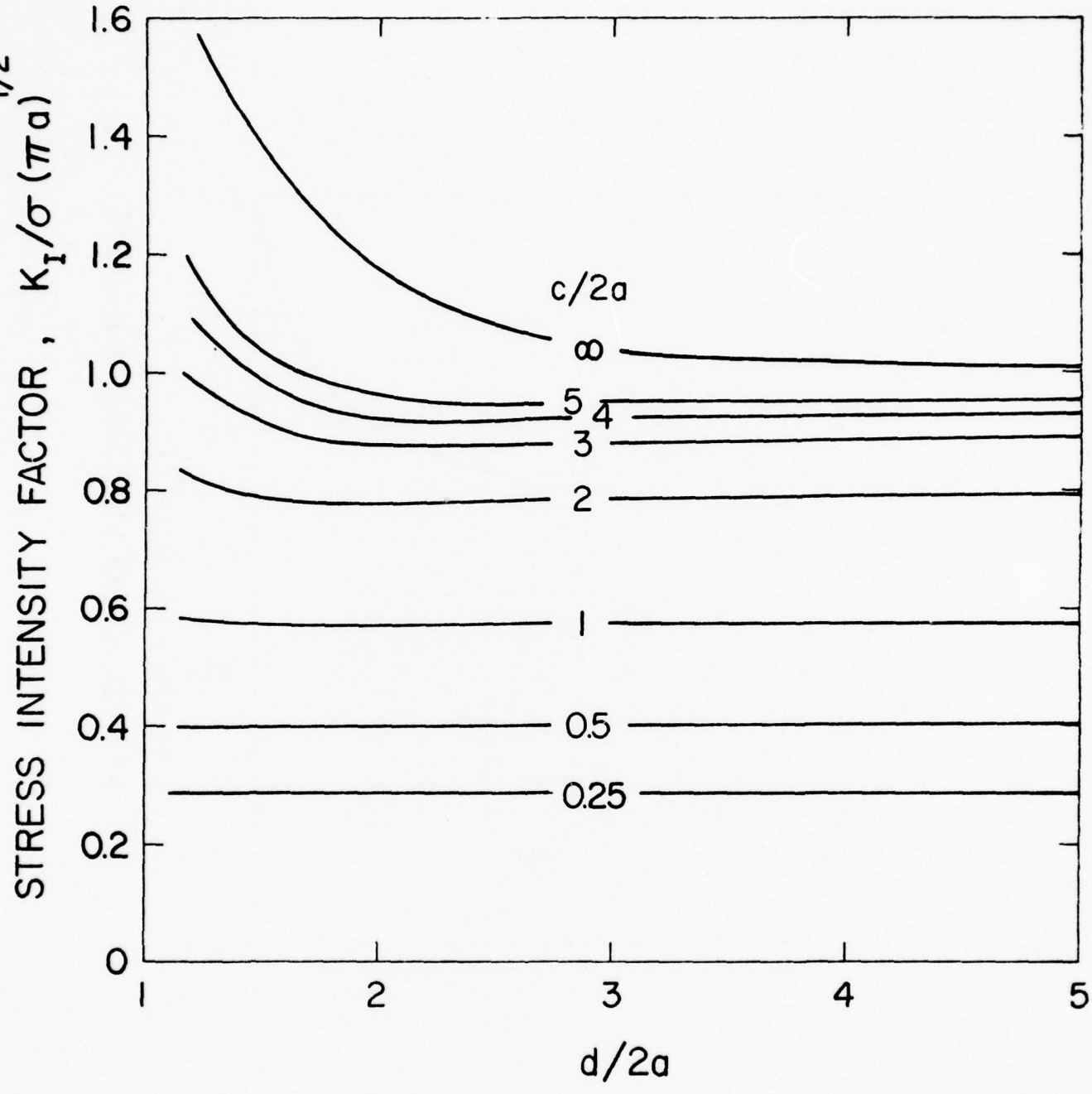

Figure 6. Effect of crack interaction on stress intensity factor for plate with rectangular array of cracks shown in Fig. 4. (After footnote 18).

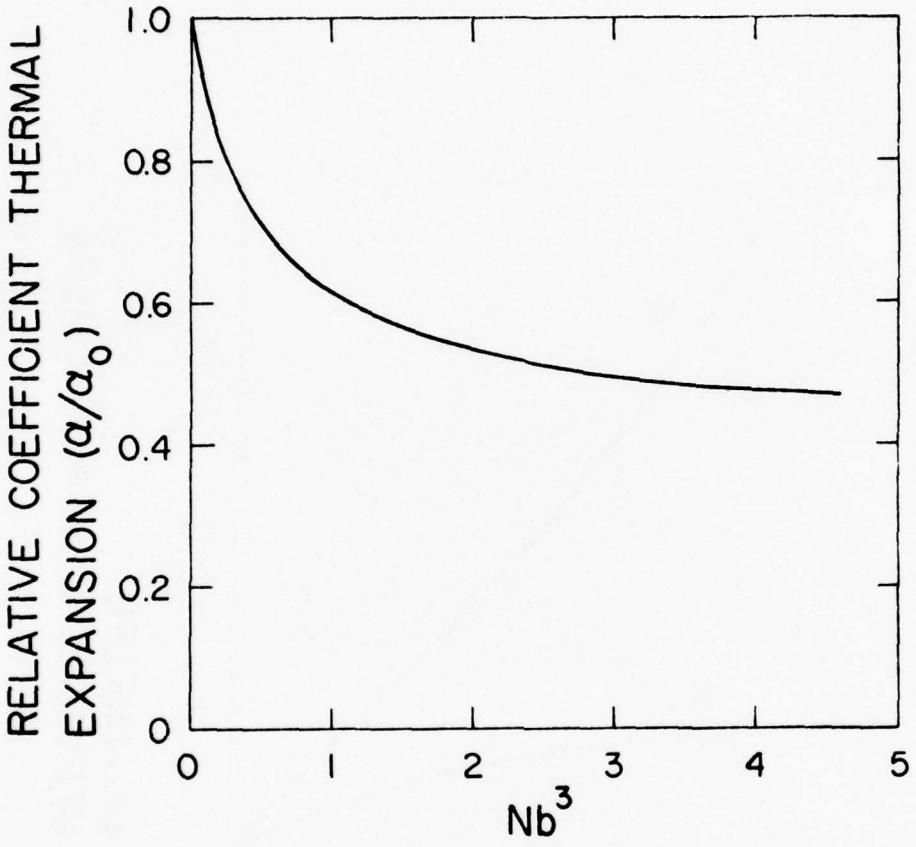

Figure 7. Effect of micro-cracking on coefficient of thermal expansion of composites (see text for data).

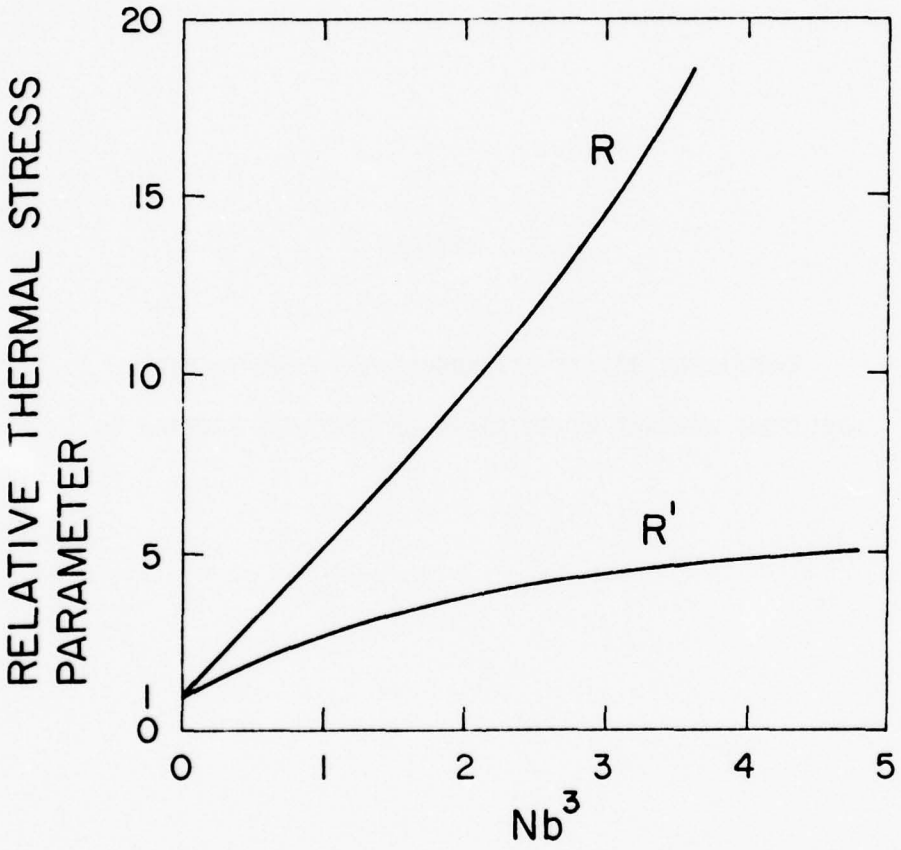

Figure 8. Effect of randomly oriented micro-cracks on the thermal stress resistance parameters R and R'.

CHAPTER III.

ROLE OF PHYSICAL PROPERTIES IN THE RESISTANCE OF BRITTLE CERAMICS TO FRACTURE IN THERMAL BUCKLING.

Role of Physical Properties in the Resistance of Brittle Ceramics to Failure by Thermal Buckling

by

D. P. H. Hasselman

Department of Materials Engineering
Virginia Polytechnic Institute
and State University
Blacksburg, Va. 24061

and

Institute for Materials Research
German Laboratory for Air and Space Flight
(DFVLR)
Cologne, Germany

ABSTRACT

An analysis is presented of the role of the physical properties which affect the thermal buckling behavior of ceramic materials for various geometric and thermal conditions. For a column with slight initial curvature, or a curvature as the result of a transverse temperature gradient, expressions are derived for the maximum increase in temperature, ΔT_{max} or transverse temperature gradient or heat flux to which the column can be subjected such that failure under the influence of the bending stresses is avoided. From the solutions obtained a number of "thermal buckling resistance parameters" are defined for the comparison of the relative thermal buckling resistance of brittle materials. Numerical examples indicate that thermal buckling of brittle materials of the proper geometry can occur relatively easily.

I. Introduction

Theoretical analyses[1-5] of the thermal stress resistance of brittle ceramics generally are based on the assumption that failure occurs in tension or shear. Although an extensive literature[6-10] on the analysis of the thermal buckling in engineering structures is available, little consideration appears to have been given to the possibility of thermal buckling of ceramic materials used for structural purposes.

In previous theoretical studies, Fridman[6] and Burgermeister and Steup[7] presented solutions for the thermal buckling of an initially straight column with uniform cross-section prevented from expanding against rigid constraints. Under these conditions the column remains straight up to a critical temperature difference, ΔT_c at which the column exhibits instability which (for column with ends free to rotate) is given by:

$$\Delta T_c = \pi^2 I/L^2 \alpha A \tag{1}$$

where I is the cross-sectional moment of inertia, L is the length of the column, α is the coefficient of thermal expansion and A is the cross-sectional area of the column.

For $\Delta T \geq \Delta T_c$, the column exhibits post-thermal buckling bending analyzed by Boley and Wiener[8]. For the failure criterion that the maximum bending stresses in the column should not exceed the tensile strength, it was shown recently[11] that the maximum temperature difference, ΔT_{max} over which a column with square cross-section can be heated, is:

$$\Delta T_{max} = \Delta T_c + S_t^2 L^2/\pi^2 \alpha E^2 d^2 \tag{2}$$

where S_t is the tensile strength. E is Young's modulus and d is the smaller dimension of the cross-section.

For purpose of the analyses to be presented in the present paper, it should be emphasized that the solution for ΔT_c represents an instability problem. In contrast, the solution for ΔT_{max} considers failure in tension as the result of the bending moment induced as the result of the curvature of the column after instability has occurred.

The purpose of this study is to present additional solutions for the thermal buckling of ceramic materials for geometric and thermal conditions of interest to ceramic technology. As for the aforementioned studies, the specific specimen geometry chosen for the present analyses consists of a long slender column (rod or narrow plate) constrained from expanding at the ends so that, on a temperature increase, the column (etc.) is subjected to a compressive load. For this geometry and thermal loading the buckling behavior is analyzed for, a) a column which exhibits a slight initial curvature, b) an initially straight column with a curvature caused by a temperature gradient in the column perpendicular to the column length and c) an initially curved column with a temperature gradient as for b, which causes either an additional positive or negative curvature. Under all conditions, the column will be considered to have a uniform cross-section along its total length. Furthermore for simplicity, the analysis will be limited to deflections which are sufficiently small that the curvature (R^{-1}) of the column to a good approximation can be expressed by:

$$R^{-1} = d^2y/dx^2[1 + (dy/dx)^2]^{-3/2} \simeq d^2y/dx^2 \qquad (3)$$

i.e., such that the square of the slope is small compared to unity and that the total deflections are much less than the column thickness.

The incidence of buckling of a column is a function of the mechanical constraints at the column's ends. The present analyses will be carried out for columns which are free to rotate at their ends, with an end geometry such that on rotation the effective length of the column between the constraints and therefore the mechanical load, $P = \alpha E \Delta T A$ remain invariant.* For different boundary conditions, solutions can be obtained by the general mathematical techniques given in the literature.[6,7,8,9,10] Differences in boundary conditions will affect only the geometric constants in the solutions obtained, not the relative role of the physical properties, easily verified by dimensional analysis.

II. Analysis

A. Uniformly Heated Column with Slight Initial Curvature.

For this column, the deflection (w) in the y-direction due to a uniform initial curvature with radius R can be expressed:

$$w = (x^2 - Lx)/2R \tag{4}$$

The condition of equilibrium for the column is:[12]

$$I\ddot{y} = -\alpha\Delta TA\{y + (x^2 - Lx)/2R\} \tag{5}$$

where y is the deflection of the column in addition to the deflection due to the initial curvature.

---

* For a rod of finite width and square ends held between perfectly rigid planar constraints, the load will increase for deflections of the column up to about twice the column thickness. The assumption of constant load implies that the geometric conditions of the column ends and constraints are such that for small deflections, on rotation the net length of the column between the constraints remains invariant. A detailed analysis of such geometric conditions is beyond the scope and purpose of this paper. In general, for other boundary conditions such as large deflections or fixed ends, the non-extensible bending of the column needs to be considered. This turns the problem into a non-linear one, which is less convenient for the derivation of the thermal buckling resistance parameters.

Eq. 5 has the general solution:

$$y = B \sin(kx) + C \cos(kx) - (x^2 - Lx)/2R + (k^2R)^{-1} \quad (6)$$

where $k^2 = \alpha\Delta TA/I$ and B and C are constants.

From the boundary conditions $y = 0$ when $x = 0$, L and when $x = L/2$, $\dot{y} = 0$ eq. 6 becomes:

$$y = -(Rk^2)^{-1}\tan(kL/2) \sin(kx) - (Rk^2)^{-1} \cos(kx)$$
$$-(x^2 - Lx)/2R + (Rk^2)^{-1} \quad (7)$$

The bending moment due to the load $P = \alpha E\Delta TA$ is a maximum at the value $y = y_{max}(x = L/2)$. From eq. 7:

$$y_{max} = -(Rk^2)^{-1}\{\sec(kL/2)-1\} + L^2/8R \quad (8)$$

The total deflection (y_t) of the column at $x = L/2$ is the sum of y_{max} and $w(x = L/2)$ of eq. 4, which yields:

$$y_t = -(Rk^2)^{-1}\{\sec(kL/2)-1\} \quad (9)$$

For the purpose of deriving thermal buckling resistance parameters it is more convenient to express eq. 9 by an expansion.

Substitution of the first three terms of the general series

$$\sec z = 1 + z^2/2! + 5z^4/4! + \ldots \quad (10)$$

where $z = kL/2$. Dividing eq. 10 by Rk^2 and retaining terms linear in ΔT only yields:

$$y_t = -5k^2L^4/384R - L^2/8R \quad (11)$$

The maximum tensile stress (σ_{max}) in the column is the sum of the bending stresses (σ_b) provided by the moment of the total deflection and

thermal load $P = \alpha E \Delta T A$ and the compressive stress $\sigma_c = \alpha E \Delta T$ in the column.

Using $\sigma_b = Mc/I$ (12)

where $M = Y_t P$ and c is the distance from the neutral axis to the outer fiber of the column, yields for the maximum tensile stress, (σ_{max}):

$$\sigma_{max} = \frac{5\alpha^2 (\Delta T)^2 E A^2 L^4 c}{384 R I^2} + \alpha E \Delta T \left\{\frac{A L^2 c}{8RI} - 1\right\} \tag{13}$$

In eq. 13, for slender columns (high L/d values) the major contribution to the bending stresses is made by the second term linear in ΔT, followed by the first term quadratic in ΔT. The compressive stresses are expected to be minor only. The bending stresses linear in ΔT arise from the deflection of the column due to the initial curvature which is independent of ΔT. The bending stresses quadratic in ΔT are due to the deflections which occur in addition to the original deflection. These additional deflections are a function of ΔT, which results in a quadratic or higher order dependence on ΔT, depending on the number of terms retained in the expansion of eq. 10.

A solution of ΔT_{max}, the maximum temperature difference to which the column can be heated without fracture, can be obtained from eq. 13, by substitution of the tensile strength, S_t for σ_{max} and solving the following quadratic equation:

$$\frac{5\alpha^2 (\Delta T)^2_{max} E A^2 L^4 c}{384 R I^2 S_t} + \frac{\alpha E \Delta T_{max}}{S_t}\left\{\frac{A L^2 c}{8RI} - 1\right\} - 1 = 0 \tag{14a}$$

In view of its quadratic form, eq. 14a is less convenient for the derivation of thermal resistance parameters. For this purpose two specific, albeit unusual cases, will be examined. If in eq. 13 the compressive stresses are equal to the bending stresses linear in ΔT, eq. 13 becomes:

$$\sigma_{max} = 5\alpha^2 E(\Delta T)^2 A^2 L^4 c/384RI^2 \tag{14b}$$

which for $\sigma_{max} = S_t$ yields for ΔT_{max}:

$$\Delta T_{max} = (S_t/\alpha^2 E)^{1/2}(384RI^2/5A^2L^4c)^{1/2} \tag{14c}$$

If, in eq. 13, the compressive stress term is equal to the bending stress quadratic in ΔT:

$$\sigma_{max} = \alpha E \Delta T A L^2 c/8RI \tag{15a}$$

which yields:

$$\Delta T_{max} = (S_t/\alpha E)(8RI/AL^2 c) \tag{15b}$$

B. Straight column with transverse temperature gradient.

The initially straight column to be considered is subjected to a uniform heat flow perpendicular to the length of the column and parallel to the direction of the shortest dimension of the cross-section. Such heat flow under steady-state conditions and temperature independent properties will cause a linear temperature distribution (constant temperature gradient) through the thickness of the column. In general, a body of any shape subjected to a uniform temperature gradient $\nabla = dT/dy$

will deform to exhibit a uniform curvature with radius R equal to[8]:

$$R = (\alpha\nabla)^{-1} \tag{16}$$

where α is the coefficient of thermal expansion. As a result, the analysis of the thermal buckling of a straight column with transverse temperature gradient in the y direction is identical to the analysis of a column with slight initial curvature considered under A, simply by replacing R in eqs. 4 through 16 by $(\alpha\nabla)^{-1}$, which yields:

$$\sigma_{max} = \frac{5\alpha^3 E(\Delta T)^2 \nabla A^2 L^4 c}{384 I^2} + \alpha E \Delta T \left\{\frac{\alpha \nabla A L^2 c}{8I} - 1\right\} \tag{17}$$

Note that in contrast to eq. 13, the first and second terms in eq. 17 are proportional to the cube and square of the coefficient of thermal expansion, resp.

Again, similar to eq. 13, ΔT_{max} for a given gradient ∇, can be obtained from eq. 17 by substituting S_t for σ_{max} and solving the quadratic equation:

$$\frac{5\alpha^3 (\Delta T)^2_{max} E \nabla A^2 L^4 c}{384 I^2 S_t} + \frac{\alpha E \Delta T_{max}}{S_t} \left\{\frac{\alpha \nabla A L^2 c}{8I} - 1\right\} - 1 = 0 \tag{18a}$$

For the purpose of obtaining the appropriate thermal stress resistance parameters, in analogy to eq. 14a, it is convenient to derive ΔT_{max} and ∇_{max} for specific cases.

If in eq. 18a the compressive stress equals the bending stress linear in ΔT, ΔT_{max} for the straight column subjected to a transverse temperature gradient ∇ becomes:

$$\Delta T_{max} = (S_t/\alpha^3 E)^{1/2}(384I^2/5A^2L^4\nabla c)^{1/2} \quad (18b)$$

For a given value of ΔT, the maximum temperature gradient ∇_{max} becomes:

$$\nabla_{max} = (S_t/\alpha^3 E)\{384I^2/5(\Delta T)^2A^2L^4c\} \quad (18c)$$

Eq. 18c also can be expressed in terms of the maximum heat flux, $Q_{max} = K\nabla_{max}$, where K is the thermal conductivity, which yields:

$$Q_{max} = (S_tK/\alpha^3 E)\{384I^2/5(\Delta T)^2A^2L^4c\} \quad (18d)$$

If in eq. 17 the compressive stresses are equal to the tensile bending stresses quadratic in ΔT, ΔT_{max} can be derived to be:

$$\Delta T_{max} = (S_t/\alpha^2 E)(8I/AL^2\nabla c) \quad (19a)$$

Similarly, for a given value of ΔT, ∇_{max} becomes:

$$\nabla_{max} = (S_t/\alpha^2 E)\{8I/AL^2(\Delta T)c\} \quad (19b)$$

which for the maximum transverse heat flux, yields:

$$Q_{max} = (S_tK/\alpha^2 E)\{8I/AL^2(\Delta T)c\} \quad (19c)$$

C. Curved column with transverse temperature gradient.

This column with slight initial curvature of radius R is shown in Fig. 1D, is subjected to the identical thermal conditions as the column considered under example B above. The effect of the transverse heat

flow is to add an additional component $\nabla\alpha$ to the original curvature of radius R such that the final radius R_f can be written:

$$R_f = R(1 + \alpha\nabla)^{-1} \tag{20}$$

In eq. 20, it should be noted the quantity ∇ can have a positive or negative value depending on the direction of heat flow. Heat flow directed towards the concave side (∇ negative) will decrease the curvature (increase R_f), whereas heat flow directed towards the convex side (∇ positive) will increase the curvature. For this column, the analysis is identical to the initially curved column or the straight column with a curvature caused by a transverse heat flow, simply by replacing R in eqs. 4 through 15 by R_f as expressed by eq. 20, with an appropriate change in sign depending on the direction of heat flow. Heat flow, directed at the concave side, will cause a decrease in the maximum stresses due to the reduction in the net deflection of the column. Conversely, heat directed at the convex side of the column, which increases the net deflection, will lead to an increase in the value of bending-stresses and a corresponding reduction in the ΔT_{max}.

An interesting condition occurs when the decrease in curvature due to heat flow at the concave side is identical to the original curvature of the column. This occurs when:

$$|\nabla| = (\alpha R)^{-1} \tag{21}$$

Under this condition, the column is straight and the compressive load caused by the constraints causes no bending moment and corresponding bending stresses but places the column in pure compression with a stress

of $\alpha E \Delta T$. Rather than a bending problem, the column is governed by the criterion of stability for a straight column as expressed by eq. 1. For values of ∇ in excess of the value given to eq. 22, the column will take on a net curvature opposite in direction to the initial curvature in the absence of heat flow.

III. Discussion, Numerical Examples and Conclusions

From eq. 14, 15, 18 and 19 a number of new thermal stress resistance parameters can be obtained appropriate to thermal buckling. Together with those from eqs. 1 and 2 presented previously[11], these parameters can be defined by:

$$R_{1b} = \alpha^{-1} \quad R_{2b} = (S_t^2/\alpha E^2) \quad R_{3b} = (S_t/\alpha E)$$

$$R_{4b} = (S_t/\alpha^2 E)^{1/2} \quad R_{5b} = (S_t/\alpha^2 E) \quad R_{6b} = (S_t K/\alpha^2 E) \tag{22}$$

$$R_{7b} = (S_t/\alpha^3 E)^{1/2} \quad R_{8b} = (S_t/\alpha^3 E) \quad R_{9b} = (S_t K/\alpha^3 E)$$

It may be noted that the role of the physical properties in these parameters differs from that in parameters for other thermal environments and criteria for thermal stress resistance[5,11,14]. With those given by eq. 22 this brings the number of non-redundant thermal stress resistance parameters to a total of some twenty-five. This large number again serves to emphasize the well-known conclusion that the relative thermal stress resistance of different ceramic materials can be established only if the thermal conditions are well known quantitatively and the performance criteria and mode of failure are pre-determined.

It should be noted that in the general case of buckling failure as described by eqs. 13 and 17, ΔT_{max}, ∇_{max} or Q_{max} are described by at

least two of the parameters given in eq. 22, their relative influence decided by the geometry of the column.

Note that the parameter R_{1b} depends only on the coefficient of thermal expansion and in contrast to the other parameters does not depend on strength and Young's modulus as variables. This difference is pointed out to re-emphasize that eq. 1 defines a condition of instability only for a straight column and not one of failure which is determined by the post-thermal buckling behavior defined by eq. 2 and the parameter R_{2b}. The seven remaining parameters were derived on the basis of a definition of fracture, rather than instability and therefore include strength and Young's modulus as variables. It may also be noted that with the exception of R_{1b} that the parameters of eq. 22 can be expressed in fracture-mechanical terms, by means of the appropriate relations between strength, critical stress intensity factor and the crack-depth. Furthermore, it may be noted that eqs. 1, 2, 15, 18 and 19 do not depend on the width of the column. For columns which are relatively wide, the stiffness in bending is greater than for a thin column[13]. This can be accounted for by replacing E by $E/(1-\nu^2)$, where ν is Poisson's ratio and the appropriate substitutions in the parameters of eq. 22.

It is of interest to illustrate the various expressions for the thermal buckling resistance by a number of numerical examples. For an initially straight column this was done earlier[11], but will be included again for comparative purposes.

An initially straight column with square cross-section (with $A = bd$ and $I = bd^3/12$, where b = width and d = thickness) can be considered to be composed of an alumina substrate material with $\alpha \simeq 7\times10^{-6}{}^{\circ}C^{-1}$, $E = 4.1\times10^{5} MN.m^{-2}$, $S_t = 4.1\times10^{2} MN.m^{-2}$, d = 0.2 cm and L = 20 cms. Eqs. 1 and 2 yields:

$$\Delta T_c \simeq 12°C \text{ and } \Delta T_{max} \simeq 92°C \tag{23}$$

For the same alumina substrate with slight initial curvature with a radius of R = 100 cms, eq. 13 for ΔT_{max} yields*:

$$\Delta T_{max} \simeq 6.5°C \tag{24}$$

If the curvature of R = 100 cm of the above example were the result of transverse heat flow through an initially flat or straight substrate, a value of $\Delta T_{max} \simeq 6.5°C$ (eq. 24) would have been achieved at a temperature gradient of approximately 92°C/cm.

The analytical results obtained for the curved column subjected to a transverse heat flow, in general are of technical interest for such structures as refractory arch-roofs or walls of circular vertical furnaces such as the blast or basic oxygen furnace. In general, it is the curvature which lends some degree of stability to such structures since it tends to place the refractory under some degree of compression as the result of either gravitational forces or thermal expansion with external constraints. If, however, such a structure is heated to too high internal temperatures or is heated too rapidly such that excessive temperature gradients are encountered, the net curvature of the roof or wall may well be of opposite direction. Under these conditions, such a structure, unless well constrained, will have a tendency to buckle inward. For a linear temperature gradient, this condition for eq. 21 occurs at a value of critical temperature gradient, ∇_{cr} given by:

$$\nabla_{cr} \simeq (\alpha R)^{-1} \tag{25}$$

*This value should not be compared directly with ΔT_{max} of eq. 23 in view of the different boundary conditions used for the derivations of eq. 2 and 15. A solution for ΔT_{max} by means of eq. 13 yields a value of $\Delta T_{max} \simeq 8°C$.

Taking, for example, a magnesia brick wall with $\alpha \simeq 12 \times 10^{-6} {}^{\circ}C^{-1}$ and $R = 1000$ cms,

$$\nabla_{cr} \simeq 80 {}^{\circ}C m^{-1} \tag{26}$$

Although the numerical examples presented above were based on arbitararily selected dimensions and property values, the numerical results nevertheless indicate that thermal buckling should be considered a potential failure mechanism for brittle ceramic materials and should be taken into account in the design of high-temperature structures. Buckling can be minimized if the structures are free to expand or are constrained in a manner that either deflections are minimized or very large deflections can occur at low levels of tensile bending stresses (i.e. very high L/d ratio), if practical.

Acknowledgments

The theory presented in this paper was developed in part at the German Research Institute for Air and Space Flight in Cologne, Germany, under auspices of a Senior Scientist Award presented to the author by the German Government and in part under auspices of a research program sponsored by the Army Research Office under Grant No. DAAG29-76-G-0091, and the Office of Naval Research under contract No. N00014-78-C-0431.

References

1. W. D. Kingery, "Factors Affecting the Thermal Stress Resistance of Ceramic Materials," J. Amer. Ceram. Soc., 38 (1) 3-15 (1955).
2. W. R. Bussem, "Resistance of Ceramic Bodies to Temperature Fluctuations," Sprechsaal, 93 (6) 137-41 (1960).
3. W. B. Crandall and J. Ging, "Thermal Shock Analysis of Spherical Shape," J. Amer. Ceram. Soc., 38 (1) 44-45 (1955).
4. D. P. H. Hasselman, "Thermal Shock by Radiation Heating," J. Amer. Ceram. Soc., 46 (5) 229-34 (1963).
5. D. P. H. Hasselman, "Thermal Stress Resistance Parameters for Brittle Refractory Ceramics: A Compendium," Amer. Ceram. Soc. Bull. 49 (12) 1033-37 (1970).
6. Y. B. Fridman, Strength and Deformation in Nonuniform Temperature Fields, Consultants Bureau New York (1964).
7. G. Buergermeister and H. Steup, Stabilitaets Theorie, Akademie Verlag, Berlin (1957).
8. B. A. Boley and J. H. Weiner, Theory of Thermal Stresses, John Wiley and Sons, New York (1960).
9. A. D. Kovalenko, Thermoelasticity, Wolters-Noordhoff Publishing, Groningen (1969).
10. B. E. Gatewood, Thermal Stress, McGraw-Hill, New York (1957).
11. D. P. H. Hasselman, "Role of Physical Properties in Post-Thermal Buckling Resistance of Brittle Ceramics," J. Amer. Ceram. Soc. (in press).
12. S. P. Timoshenko and J. M. Geve, Theory of Elastic Stability, 2nd Ed. pp 31-32, McGraw-Hill, New York (1961), 541 p.
13. R. J. Roark, Formulas for Stress and Strain, McGraw-Hill, NY, 1965, 432 pp.

References (Cont'd)

14. D. P. H. Hasselman and W. Zdaniewski, "Thermal Stress Resistance Parameters for Brittle Materials Subjected to Thermal Stress Fatigue," J. Am. Ceram. Soc. (in press).

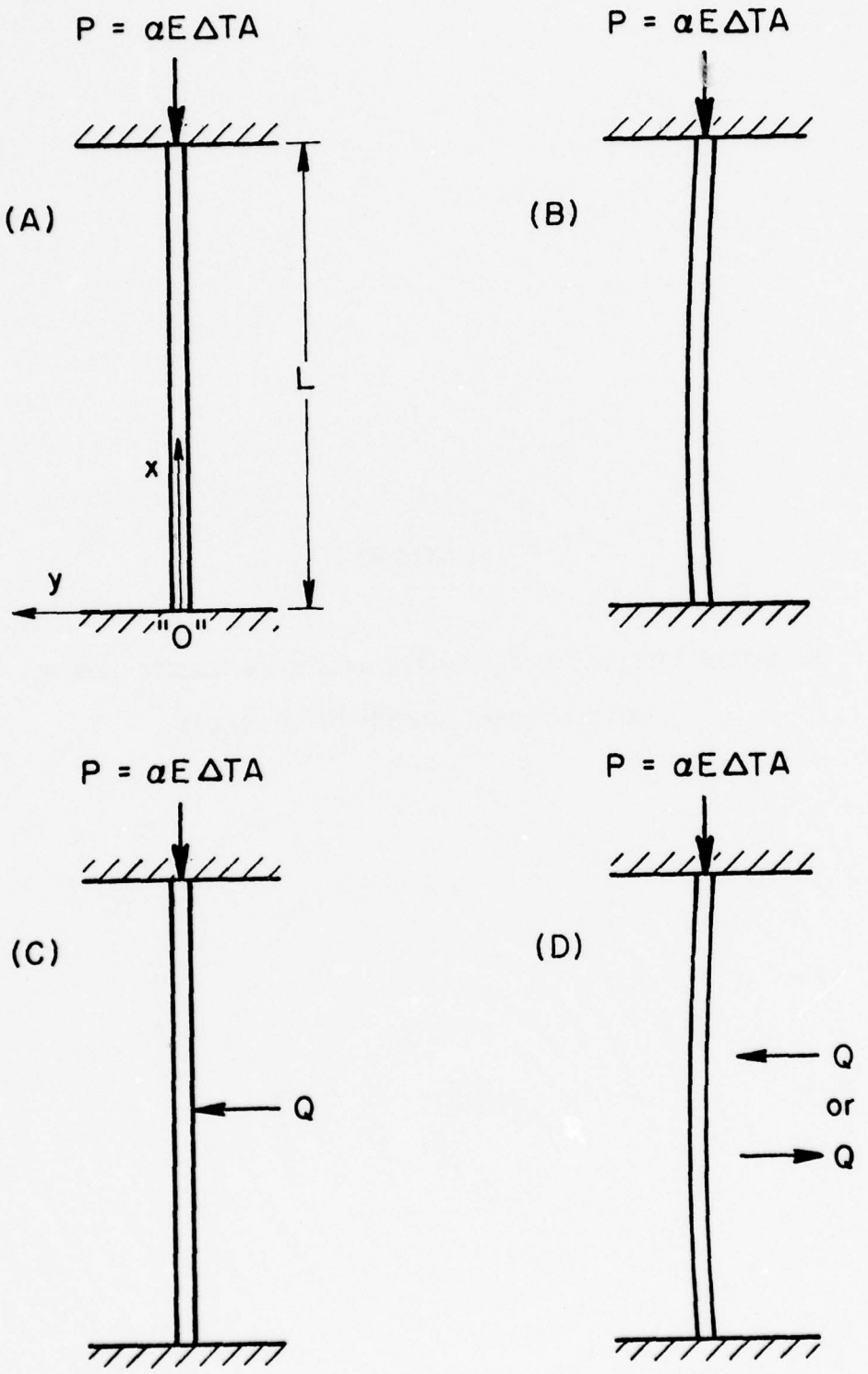

Fig. 1. Mechanical Models for Analysis of Thermal Buckling of Ceramic Materials.

CHAPTER IV.

THERMAL STRESS RESISTANCE PARAMETERS FOR BRITTLE MATERIALS SUBJECTED TO THERMAL STRESS FATIGUE.

THERMAL STRESS RESISTANCE PARAMETERS FOR BRITTLE MATERIALS SUBJECTED TO THERMAL STRESS FATIGUE

by

D. P. H. Hasselman

and

W. Zdaniewski

Department of Materials Engineering
Virginia Polytechnic Institute
Blacksburg, Va. 24061

Brittle materials for high-temperature applications usually are highly susceptible to premature failure under conditions in which they are subjected to thermal stress. The selection of the optimum material for a specific thermal environment and criterion of thermal stress resistance can be based on so-called "thermal stress resistance" figures-of-merit or parameters. A number of such parameters[1-8] are available for steady-state or transient heat transfer (including inertial effects), visco-elastic effects, thermal buckling as well as the effect of catastrophic crack propagation on physical properties of materials subjected to levels of thermal stress in excess of the failure stress.

It is conceivable that materials undergo fatigue under conditions of thermal stress as the result of sub-critical crack growth at stress levels below the failure stress. This condition can arise, for instance, in hollow tubes conducting heat such as furnace tubes or those used in heat exchangers or other applications. It is the purpose of this note to derive on the basis of fracture-mechanical principles, expressions for the time-to-failure of materials subjected to steady-state thermal stress, from which appropriate "thermal fatigue" resistance parameters can be obtained.

A material is considered which is subjected to a maximum value of steady-state tensile thermal stress, σ_t:

$$\sigma_t = C\alpha E\Delta T/(1-\nu) \qquad (1)$$

where α is the coefficient of thermal expansion, E is Young's modulus, ν is Poisson's ratio and C is a geometric constant, which for a circular hollow-cylinder with a temperature difference ΔT across the wall in radial heat flow can be obtained from the study by Kent.[9]

Fatigue of the material occurs as the result of sub-critical growth of a crack in the mode I crack displacement at a crack velocity, V:

$$V = AK_I^n \exp(-Q/RT) \tag{2}$$

where A and n are numerical constants, K_I is the mode I stress intensity factor, Q is the activation energy for crack growth, R is the gas constant and T is the absolute temperature. It will be assumed that over the total extent of crack-growth till the time-of-failure the size of the crack relative to the structure size is such that the compliance of the structure is not affected. Under this assumption the stress-intensity factor K_I is related to the stress and crack size by

$$K_I = \sigma_t Y a^{1/2} \tag{3}$$

where Y is a constant related to the crack geometry and a is the crack size.

As shown by Evans[10] the time-to-failure (t_f) can be expressed:

$$t_f = \frac{2}{\sigma_t^2 Y^2} \int_{K_{Ii}}^{K_{Ic}} \frac{K_I dK_I}{V} \tag{4}$$

where K_{Ic} is the critical stress intensity factor and K_{Ii} is the initial stress intensity factor at the imposition of the thermal stress at time, t = o.

Substitution of eq. 1 and 3 into eq. 4 followed by integration yields the time-to-failure for the condition $K_{Ii} << K_{Ic}$ and n > 2 as:

$$t_f = \frac{2(1-\nu)^2 \exp(Q/RT)}{(C\alpha E\Delta T)^2 Y^2 A(n-2) K_{Ii}^{(n-2)}} \tag{5}$$

Eq. 5 also can be expressed in terms of the time-to-failure for the situation that the value of ΔT is the result of a heat flux, q related to ΔT by $q = C'K\Delta T$, where C' is another geometric constant and K is the thermal conductivity. This yields for t_f:

$$t_f = \frac{2\{(1-\nu)KC'\}^2 \exp(Q/RT)}{\{C\alpha Eq\}^2 Y^2 A(n-2) K_{Ii}^{(n-2)}} \tag{6}$$

Separation of the geometric and material properties in eqs. 5 and 6 yield the "thermal fatigue" resistance parameters:

$$R_f = \frac{(1-\nu)^2 \exp(Q/RT)}{\alpha^2 E^2 (n-2)A} \quad \text{and} \quad R_f' = R_f K^2 \tag{7}$$

In principle under transient temperature conditions such as those encountered in thermal cycling, the number of cycles to failure can be derived at least for those conditions that the crack-growth at any instant occurs in a quasi-static manner. With this assumption the "thermal cycle fatigue" parameters should be identical to those given by eq. 7.

As a last remark it is of interest to point out that with the two parameters derived in this note, the number of independent non-redundant thermal stress resistance parameters available to the materials engineer amounts to a total of twenty-two. It appears almost superfluous to say that the selection of the optimum material for a given environment involving high levels of thermal stress requires detailed specification of the performance criterion and the thermal environment to which the materials are to be subjected.

Acknowledgment

The present study was conducted as part of a larger research program on the thermo-mechanical behavior of high-temperature structural materials sponsored by the Office of Naval Research.

References

1. W. D. Kingery, "Factors Affecting Thermal Stress Resistance of Ceramic Materials," J. Amer. Ceram. Soc., 38 (1) 3-15 (1955).

2. W. R. Buessum, "Resistance of Ceramic Bodies to Temperature Fluctuations," Sprechsaal, 93 (6) 137-41 (1960).

3. D. P. H. Hasselman, "Thermal Shock by Radiation Heating," J. Amer. Ceram. Soc., 46 (5) 229-34 (1963).

4. D. P. H. Hasselman, "Approximate Theory of Thermal Stress Resistance of Brittle Ceramics Involving Creep," J. Amer. Ceram. Soc., 50 (9) 454-57 (1967).

5. H. Bargmann, "Dynamic Thermal Shock Resistance," pp. 174-81 in Topics in Applied Continuum Mechanics, ed. by J. L. Zeman and F. Ziegler, Springer Verlag (1974).

6. D. P. H. Hasselman, "Role of Physical Properties in the Resistance of Brittle Ceramics to Fracture in Thermal Buckling," J. Amer. Ceram. Soc., (in press).

References (Cont'd)

7. D. P. H. Hasselman, "Unified Theory of Thermal Shock Fracture Initiation and Crack Propagation in Brittle Ceramics," J. Amer. Ceram. Soc., 52 (11) 600-04 (1969).

8. D. P. H. Hasselman, "Thermal Stress Resistance Parameters for Brittle Refractory Ceramics: A Compendium," American Ceramic Society Bulletin, 49 (12) 1033-37 (1970).

9. C. H. Kent, "Thermal Stresses in Spheres and Cylinders Produced by Temperature Varying with Time," J. Appl. Mech., 54 (18) 185-96 (1932).

10. A. G. Evans, "A Method of Evaluating the Time-Dependent Failure Characteristics of Brittle Materials - And its Application to Polycrystalline Alumina," J. Mat. Sc., 7 1137-46 (1972).

CHAPTER V.

ON THE THERMAL FRACTURE OF ICE

ON THE THERMAL FRACTURE OF ICE

by

D. P. H. Hasselman and Y. Tree

Department of Materials Engineering
Virginia Polytechnic Institute and State University
Blacksburg, Virginia 24061
USA

ON THE THERMAL FRACTURE OF ICE

D. P. H. Hasselman and Y. Tree
Department of Materials Engineering
Virginia Polytechnic Institute
and
State University
Blacksburg, Virginia 24061 USA

Brittle materials are known to be susceptible to catastrophic failure induced by thermal stresses. This is well known for brittle materials for engineering applications involving high temperature[1]. Thermal fracture, however, also can occur in materials at moderate or low temperature, such as ice, which can fail in a brittle manner even at temperatures close to its melting point. Thermal fracture of ice can be demonstrated experimentally by the immersion of ice-cubes in fluids for industrial or house-hold use. The resulting thermal fracture frequently is accompanied by acoustic emission easily perceived by the human ear.

The low thermal stress resistance of ice can be demonstrated by a numerical example. Considered will be a piece of ice of spherical geometry initially at -20°C suddenly immersed in H_2O at a temperature of 25°C. For an estimate of the heat transfer coefficient, it will be assumed that heat transfer to the ice occurs by laminar convection. The heat transfer coefficient, h, can be expressed[2].

$$h \approx \frac{K}{D} (0.56)(N_{pr} \cdot N_{gr})^{\frac{1}{4}} \qquad (1)$$

where K is the thermal conductivity of the water, D is the diameter of the sphere, N_{pr} is the Prandtl number and N_{gr} is the Grasshoff number.

From tabulations[3] of the properties of water the quantity $N_{pr} \cdot N_{gr}$ is approximately:

$$N_{pr} \cdot N_{gr} \simeq 2 \times 10^{4} D^{3} \Delta T \ cm^{-3} . {}^{\circ}C^{-1} \qquad (2)$$

where ΔT is the temperature difference between the ice surface and the mean temperature of the water. With D = 2.5 cms, ΔT = 45°C, $K_{H_2O} = 1.5 \times 10^{-3}$ cal. $cm.^{-1} {}^{\circ}C. {}^{-1} s^{-1}$[4], the heat coefficient becomes,

$$h \simeq 1.98 \times 10^{-2} cal.cm.^{-2} {}^{\circ}C^{-1} .s^{-1} . \qquad (3)$$

As shown by Crandall and Ging[5] the maximum value of tensile thermal stress (σ_m) in a spherical body heated in a convection heat transfer environment can be expressed:

$$\sigma_m \simeq [\alpha E \Delta T/(1-\nu)][2\beta/5(\beta+2)] \qquad (4)$$

where ΔT is the initial temperature difference between the ice and the water, α is the coefficient of thermal expansion, E is Young's modulus, ν is Poisson's ratio and β is the Biot number defined by $\beta = Rh/K$ where R is the sphere radius, h is the heat transfer coefficient and K is the thermal conductivity of the ice. Substitution of the following literature data for ice, $\alpha \simeq 1.13 \times 10^{-4} {}^{\circ}C^{-1}$[4], $E \simeq 10^{10} N.m^{-2}$, $\nu = 0.33$ and $K \simeq 5.4 \times 10^{-3}$ $cal.cm^{-1} .{}^{\circ}C^{-1} .s^{-1}$.[6], with the above value of h (eq. 3) yields:

$$\sigma_m \simeq 1.82 \times 10^{7} N.m^{-2} \qquad (5)$$

This value can be compared with a reported[6] value of the tensile strength, σ_f of ice with $\sigma_f \simeq 1.5 \times 10^{6} N.m^{-2}$, which clearly indicates that

for thermal conditions and dimensions chosen for the present calculation, the thermal fracture of ice is unavoidable. A reduction in size of the ice to a diameter of approximately 0.1 cms reduces the stress to a value comparable to the fracture stress. By raising the initial temperature of the ice to its melting point, thermal fracture on heating can be avoided also, regardless of the nature of magnitude of the heat transfer involved.

Acknowledgment

The present study was conducted as part of a larger research program on the thermo-mechanical and thermal properties of structural brittle materials supported by the Office of Naval Research.

References

1. W. D. Kingery, J. Am. Ceram. Soc., 38 (1955) 3.

2. J. Schenk and F. A. M. Schenkels, Appl. Sci. Res., 19 (1968) 465.

3. R. Hosmer Norris, "Heat Transfer and Fluid Flow Data Book," (General Electric, Heat Transfer Division, June 1976).

4. Charles D. Hodgman, "Handbook of Chemistry and Physics," 36 Edn. (Chemical Rubber Publishing Co., Cleveland, 1954).

5. W. B. Crandall and J. Ging, J. Am. Ceram. Soc., 38 (1955) 44.

6. E. R. Pounder, "The Physics of Ice," (Robert Maxwell, 1965).

CHAPTER VI.

EFFECT OF CRACKS ON THERMAL CONDUCTIVITY

EFFECT OF CRACKS ON THERMAL CONDUCTIVITY

by

D. P. H. Hasselman
Department of Materials Engineering
Virginia Polytechnic Institute and State University
Blacksburg, Virginia 24061

AD-A065 831 VIRGINIA POLYTECHNIC INST AND STATE UNIV BLACKSBURG F/G 11/2
THERMAL-MECHANICAL AND THERMAL BEHAVIOR OF HIGH-TEMPERATURE STR--ETC(U)
DEC 78 D P HASSELMAN, M P KAMAT N00014-78-C-0431
UNCLASSIFIED NL

2 OF 2
AD A065831

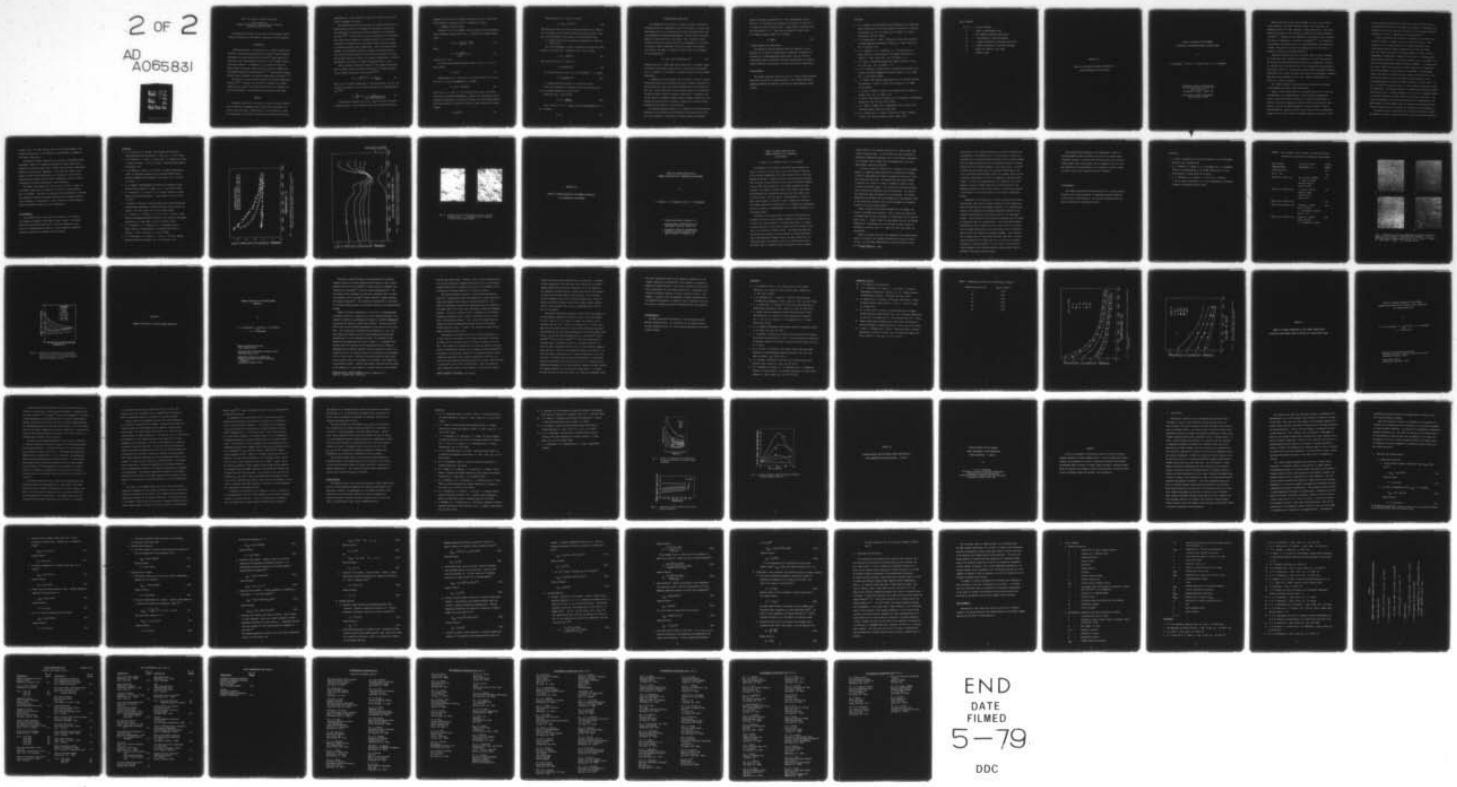

END
DATE FILMED
5-79
DDC

Effect of Cracks on Thermal Conductivity

D.P.H. Hasselman
Virginia Polytechnic Institute and State University
Blacksburg, Virginia 24061

Expressions are derived for the effect of penny-shaped cracks of various orientations on the thermal conductivity of solid materials.

INTRODUCTION

Tessellated stresses in composites due to thermal expansion mismatches in polycrystalline materials which exhibit thermal expansion anisotropy can cause excessive micro-cracking.[1] High densities of cracks can result from mechanical failure such as in thermal shock or from craze formation. The presence of such cracks can cause profound changes in strength, elastic behavior, fracture toughness and the thermal conductivity and diffusivity.[2,3] Heavily micro-cracked materials have a potential for extreme thermal stress resistance.[4,5]

The effect of cracks on elastic behavior has received theoretical attention.[6,7] Solutions for the effect of cracks on the thermal conductivity in terms of crack density and size do not, however, appear to be available. Such solutions are presented in this paper.

ANALYSIS

The present analysis for the effect of cracks on thermal conductivity is based on the assumption that cracks can be considered to be pores of very flat shape. Specifically, the crack geometry is taken to be equivalent to ellipsoids of revolution for which the minor axis

approaches zero. Heat transfer by radiation or convection across the cracks is assumed to be absent.

By treating the cracks as flat pores, the thermal conductivity of materials with cracks can be obtained from literature solutions for the conductivity of matrices with dilute dispersions of ellipsoidal particles.[8,9] In order that the thermal conductivity of the material with cracks can be treated as a continuum property, the size of the cracks will be considered to be much smaller than the size or volume of the matrix material under consideration. Also, the cracks will be assumed to be distributed uniformly throughout the matrix material. The cited literature equations on which the present analysis is based will be given directly in terms of the thermal conductivity of a matrix containing a second phase of thermal conductivity equal to zero.

From the general solution of Fricke,[12] the thermal conductivity (K) of a matrix material containing dispersions of ellipsoidal shape of zero thermal conductivity can be written:[8,9]

$$K = K_o - \frac{V/3}{1-V} \Sigma_i^{i=a,b,c} \frac{2K}{(2 - abcL_i)} \qquad (1)$$

where K_o is the thermal conductivity of the matrix phase, a,b, and c are the axis of ellipsoid, V is the volume fraction of the dispersed phase and:[9,10]

$$L_i = \frac{2A_i}{abc} = \int_o^\infty \frac{ds}{(s+i^2)\sqrt{s+a^2(s+b^2)(s+c^2)}} \qquad (2)$$

Closed form solutions for L_i of eq. 2 can be obtained for oblate ellipsoids (a<b=c). For the present study the crack geometry will be

assumed to be of the form of oblate ellipsoids, with a→o. Cracks with three different orientations will be considered as follows:

A. Randomly oriented cracks.

Solution of eq. 2 for randomly oriented pores of oblate ellipsoidal shape followed by substitution in eq. 1, yields for the thermal conductivity:

$$K = K_o - \frac{V}{3(1-V)}\left[\frac{K}{M} + \frac{4K}{2-M}\right] \tag{3}$$

where:

$$M = \left(\frac{\theta - \frac{1}{2}\sin 2\theta}{\sin^3\theta}\right)\cos\theta \tag{4}$$

in which $\cos\theta = a/b$.

For cracks with extreme ellipsoidal shape, as $a/b \to o$, $\theta \to \pi/2$, which yields:

$$M = \pi a/2b \tag{5}$$

Substitution of eq. 5 for M in eq. 3 and noting that $M << 2$, $K/M >> 2K$ and $V << 1$, upon rearrangement eq. 3 becomes:

$$K \simeq K_o(1 + 2bV/3\pi a)^{-1} \tag{6}$$

Note that as $a \to o$, and $V \to o$ for infinitely thin cracks, the second terms in eq. 6 becomes indeterminate. However, this indetermacy can be removed by noting that for an oblate ellipsoid, the volume equals $4\pi ab^2/3$. The volume fraction V occupied by N cracks of equal size per unit volume becomes:

$$V = 4\pi Nab^2/3 \tag{7}$$

Substitution of eq. 7 into eq. 6 yields:

$$K = K_o(1 + 8Nb^3/9)^{-1} \tag{8}$$

which gives the effect of cracks on thermal conductivity in terms of the crack density and crack size, rather than volume fraction. Note that b now corresponds to the radius of the penny-shaped crack.

B. Oriented cracks with crack-plane perpendicular to direction of heat flow.

This case corresponds to oblate ellipsoidal pores with the a-axis parallel to the heat flow. Solution of eqs. 1 and 2 yields:

$$K = K_o - VK/M(1-V) \tag{9}$$

which with the aid of eq. 5 results in:

$$K = K_o(1+2bV/\pi a)^{-1} \tag{10}$$

Eq. 10 with the aid of eqs. 5 and 7 and assuming $V << 1$, yields:

$$K = K_o(1+8Nb^3/3)^{-1} \tag{11}$$

C. Cracks with heat flow parallel to plane of cracks.

This case corresponds to ellipsoidal pores with the major axis (b or c) oriented parallel to the heat flow.

Solution of eqs. 1 and 2 gives:

$$K = K_o - \frac{2V}{1-V}\left[\frac{K}{2-M}\right] \tag{12}$$

Since, as $a/b \to o$, $M << 2$. Again, using the approximation $V << 1$, eq. 12 yields:

$$K \simeq K_o \tag{13}$$

DISCUSSION AND CONCLUSIONS

The expressions for the effect of cracks on thermal conductivity, presented herein are expressed in terms of crack density and crack size. This should prove to be of practical value since the density and crack size probably are determined experimentally far more easily than crack width (i.e. minor axis) and crack volume. Also, a measure of crack density and crack size may be obtainable by measurements of the effect of cracks on elastic properties, for which solutions are available. For instance, the effect of randomly oriented cracks on bulk modulus, B can be expressed:[7]

$$B = B_o[1 + 16(1-\nu^2)Nb^3/9(1-2\nu)]^{-1} \qquad (14)$$

Comparison with eq. 8 shows that the relative effect of randomly oriented cracks on bulk modulus, apart from the factors involving Poisson's ratio, is "similar" to the effect of randomly oriented cracks on thermal conductivity.

A comparison of the expressions for the effect of cracks of various orientations shows that the maximum reduction in thermal conductivity is achieved when all cracks are oriented perpendicular to the direction of heat flow. On the other hand, cracks oriented parallel to the direction of heat flow have no effect on thermal conductivity. As expected, the relative effect of randomly oriented cracks on thermal conductivity lies between the relative effect on thermal conductivity of cracks oriented perpendicular and parallel to the heat flow.

The present analytical results can be compared with the experimental observation that excessive micro-cracking in polycrystalline iron-titanate, which exhibits a large degree of thermal expansion anisotropy,

reduces the thermal conductivity by a factor approximately equal to three [3]. If the grains are considered to be cubical in shape, and to contain at least one crack each of a radius equal to the grain size, the crack density $N = \ell^{-3}$, such that the product $N\ell^3$ equals unity. For randomly oriented cracks, eq. 8 predicts:

$$K \simeq 9K_o/17 \tag{15}$$

in good agreement with observation.

The analytical results presented herein are expected to be appropriate to the areas of rock-mechanics, composites and materials of construction for high-temperature applications, such as refractory liners which often are expected to perform satisfactorily in a heavily cracked condition, as the result of failure under severe thermal shock.

Acknowledgments:

The present study was conducted as part of a larger research program supported by the Office of Naval Research, on the thermal and thermomechanical behavior of structural materials for high-temperature applications.

References

1. W. R. Buessum, "Internal Ruptures and Recombinations in Anisotropic Ceramic Materials," pp 127-48 in Mechanical Properties of Engineering Ceramics, Ed. by W. W. Kriegel and H. Palmour III. Wiley-Interscience, New York (1961).
2. J. A. Kuszyk and R. C. Bradt, "Influence of Grain Size on Effects of Thermal Expansion Anisotropy in $MgTi_2O_5$," J. Amer. Ceram. Soc., Vol. 56 (1973) p. 420.
3. H. J. Siebeneck, D. P. H. Hasselman, J. J. Cleveland and R. C. Bradt, "Effect of Microcracking on the Thermal Diffusivity of Fe_2TiO_5," J. Amer. Ceram. Soc., Vol. 59 (1976), p. 241.
4. R. C. Rossi, "Thermal-Shock-Resistant Ceramic Composites," Bull. Am. Ceram. Soc., Vol. 48 (1969) p. 736.
5. D. P. H. Hasselman, "Unified Theory of Thermal Shock Fracture Initiation and Crack Propagation in Brittle Ceramics," J. Am. Ceram. Soc., 52 (11) 600-04 (1969).
6. J. P. Berry, "Some Kinetic Considerations of the Griffith Criterion for Fracture," I and II, J. Mech. Phys. Solids, Vol. 8, (1960) pp 194 and 206.
7. J. B. Walsh, "Effect of Cracks on the Compressibility of Rock," J. Geophys. Res., Vol. 70, (1965) p 381.
8. H. Fricke, "The Electrical Conductivity of a Suspension of Homogeneous Spheroids," Phys. Rev. 24, 575-87 (1924).
9. A. E. Powers, "Conductivity in Aggregates," Knolls Atomic Power Laboratory Report, KAPL-2145, March 1961.
10. H. S. Carslaw and J. C. Jaeger, "Conduction of Heat in Solids," 2nd Ed. p 427, Oxford University Press, London, 1959.

List of Symbols

a, b, c,	-	axis of ellipsoid
b	-	radius of penny-shaped crack
B	-	bulk modulus of material with cracks
B_o	-	bulk modulus of crack-free material
K	-	thermal conductivity of material with cracks
K_o	-	thermal conductivity of crack-free material
N	-	number of cracks per unit volume
ν	-	Poisson's ratio

CHAPTER VII.

EFFECT OF OXIDATION ON THERMAL DIFFUSIVITY OF REACTION-SINTERED SILICON NITRIDE

EFFECT OF OXIDATION ON THE THERMAL DIFFUSIVITY OF REACTION-SINTERED SILICON NITRIDE

by

W. Zdaniewski,[†] H. Knoch,[§] J. Heinrich[§] and D. P. H. Hasselman[†]

[†]Department of Materials Engineering
Virginia Polytechnic Institute and
State University
Blacksburg, Virginia 24061, USA

[§]Institut fuer Werkstoff-Forschung,
DFVLR, Cologne, Germany

Reaction-sintered silicon nitride (RSSN), in view of its excellent creep resistance, low density and good thermal shock properties, is a candidate material for high temperature turbine applications. The thermodynamics and kinetics of the oxidation of RSSN have received considerable attention[1,2]. Depending on the temperature and specimen history, oxidation can lead to an enhancement or decrease of strength[3,4,5]. It is expected that oxidation also should affect the thermal diffusivity and conductivity of RSSN. The present note reports experimental data for the effect of oxidation of RSSN on its thermal diffusivity.

Specimens of RSSN in the form of circular discs 12.5 mm in diameter by 2.5 mm thick with a density of approximately 2.2 $g.cm^{-3}$ were prepared by nitriding of cold-pressed silicon compacts at a temperature of 1400°C, in a mixture of 90 vol.% N_2 and 10 vol.% H_2, following the firing schedule described by Heinrich[6]. The resulting silicon nitride consisted of approximately 80% of the α-phase, the rest consisting of the β-polymorph. Oxidation was carried out isothermally in air over a range of temperatures up to 1450°C for a period of 50 hours.

The thermal diffusivity was measured by the laser-flash technique[7] using equipment described in detail elsewhere[8].

Figure 1 shows typical data for the thermal diffusivity as a function of temperature for the RSSN oxidized at three different temperatures. Figure 2 shows the thermal diffusivity at a number of temperatures as a function of oxidation temperature, together with the percentage wt. gain. Figures 3a and 3b show SEM micrographs of fracture surfaces of the as-received RSSN and oxidized at 1200°C, which indicate that the oxidization appears to have in part closed the originally open pore structure. X-ray

analysis shows that oxidation at 1200°C for 50 hours resulted in an approximately 20% conversion of the RSSN into a mixture of crystobalite and amorphous silica, while oxidation at 1400°C for 50 hours produced smaller quantities of silica, in agreement with literature data[2,5].

Figure 2 indicates that the effect of oxidation on the thermal diffusivity of RSSN is a complex function of oxidation treatment. Most significant is the large decrease in the thermal diffusivity over a rather narrow range of oxidation temperature near 1100° and 1200°C. Also, the thermal diffusivity of the RSSN oxidized at 1200°C is nearly independent of temperature, a behavior characteristic of vitreous rather than crystalline materials. This general behavior can be explained on the basis of the known general oxidation behavior of RSSN[1,2]. At temperatures up to about 1000°C the oxidation rate slowly increases with temperature and occurs throughout the open porosity in the RSSN. At temperatures higher than 1200°C the oxidation product forms a protective layer on the surface which seals the pores and inhibits further oxidation, with a corresponding smaller decrease in thermal diffusivity than for 1200°C. In fact, at 1400° this protective layer, in fact, appears to enhance the thermal diffusivity. The apparent decrease in thermal diffusivity above 1400°C, possibly may be due to enhanced oxidation as the result of enhanced thermally activated diffusion of oxygen through the protective oxide layer. The relative independence of the thermal diffusivity from temperature for the RSSN oxidized at 1200°C suggests that the amorphous silica phase may have formed a continuous phase by preferential oxidation at grain boundaries.

The specific heat of silica and silicon nitride have similar values[9]. Furthermore, it should be noted that the wt. gain of the RSSN on oxidation

is small (<2%). For these reasons, most of the observed changes in the thermal diffusivity due to the oxidation are attributable to changes in the thermal conductivity.

A decrease in thermal conductivity is critical to the thermal stress resistance of RSSN. The significant decrease in thermal conductivity, especially for oxidation near 1100° to 1200°C, may well cause a measurable decrease in thermal stress resistance. This effect will depend on the nature of thermal shock encountered, but is expected to be most severe during transient heating from low ambient temperatures, where the effect of oxidation on thermal conductivity is most pronounced.

The present data suggest that from the point of view of changes in the thermal conductivity and diffusivity, oxidation of RSSN should be kept to a minimum. This may be accomplished by the development of high density products by improved nitriding, impregnation or closing of pores by vapor deposition. Alternatively, on prior oxidation at 1400°C should inhibit the extensive oxidation at lower temperatures.

Acknowledgments

The specimens used in this study were prepared at the Institut fuer Werkstoff-Forschung of the DFVLR, Cologne, Germany. The thermal diffusivity was measured by VPI and SU under the auspices of a program on the thermo-mechanical behavior of high-temperature structural materials, supported by the Office of Naval Research.

References

1. A. G. Evans and R. W. Davidge, "The Strength and Oxidation of Reaction-Sintered Silicon Nitride," J. Mat. Sc., 5, 314-25 (1970).
2. R. W. Davidge, A. G. Evans, D. Gilling and P. R. Wilyman; pp. 329-43 in Special Ceramics 5. Ed. by P. Popper. British Ceramic Research Association, 1972.
3. R. W. Davidge, G. Tappin, T. R. McLaren, "Strength Parameters Relevant to Engineering Applications for Reaction Bonded Silicon Nitride and REFEL Silicon Carbide," Powd. Metall. Int. 8 [3] 110-114 (1976).
4. S. C. Singhal, "Thermodynamics and Kinetics of Oxidation of Hot-Pressed Silicon Nitride," J. Mater. Sci., 11 [3] 500-509 (1976).
5. J. B. Warburton, J. E. Antill, R. W. M. Howes, "Oxidation of Thin Sheet Reaction-Sintered Si_3N_4," J. Amer. Ceram. Soc. 61 [1-2] 67-72 (1978).
6. J. Heinrich, "Influence of Silicon Grain Size on the Microstructure and Mechanical Properties of Reaction-Sintered Silicon Nitride (in German). Ber. Deut. Keram. Ges. 55 (4), 238-41 (1978).
7. W. J. Parker, R. J. Jenkins, C. P. Butler and G. L. Abbott, "Flash Method of Determining Thermal Diffusivity, Heat Capacity and Thermal Conductivity," J. Appl. Phys. 32 [9] pp. 1679-81, (1961).
8. H. J. Siebeneck, J. J. Cleveland, D. P. H. Hasselman and R. C. Bradt, "Effect of Microcracking on the Thermal Diffusivity of Fe_3TiO_5," J. Amer. Ceram. Soc., 59, 241-44 (1976).
9. Y. S. Touloukian, R. W. Powell, C. Y. Ho, M. C. Nicolaou, Thermophysical Properties of Matter, Vol. 10, IFI Plenun, 1973.

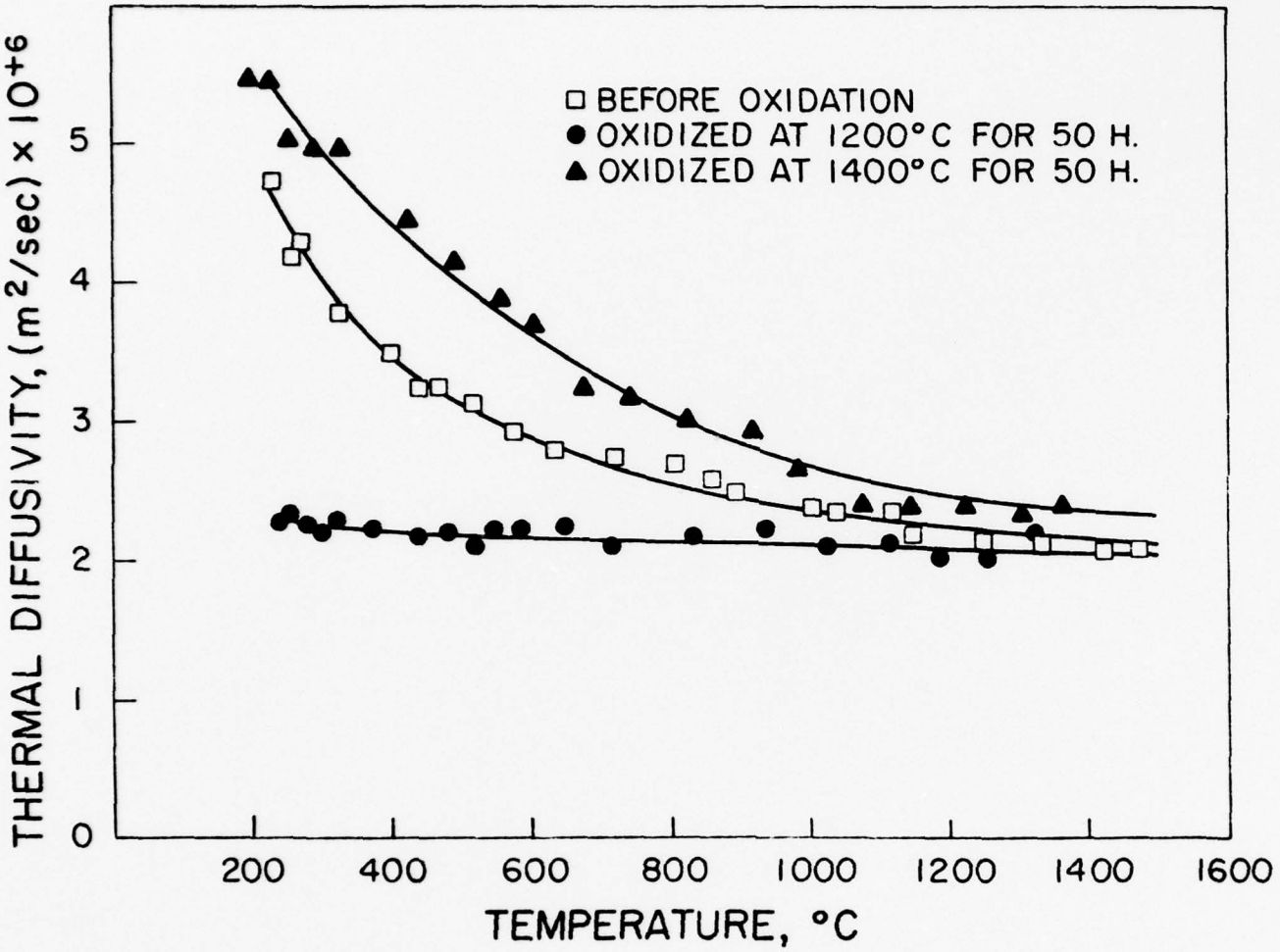

Fig. 1. Effect of temperature on the thermal diffusivity of reaction-sintered silicon nitride subjected to oxidation in air.

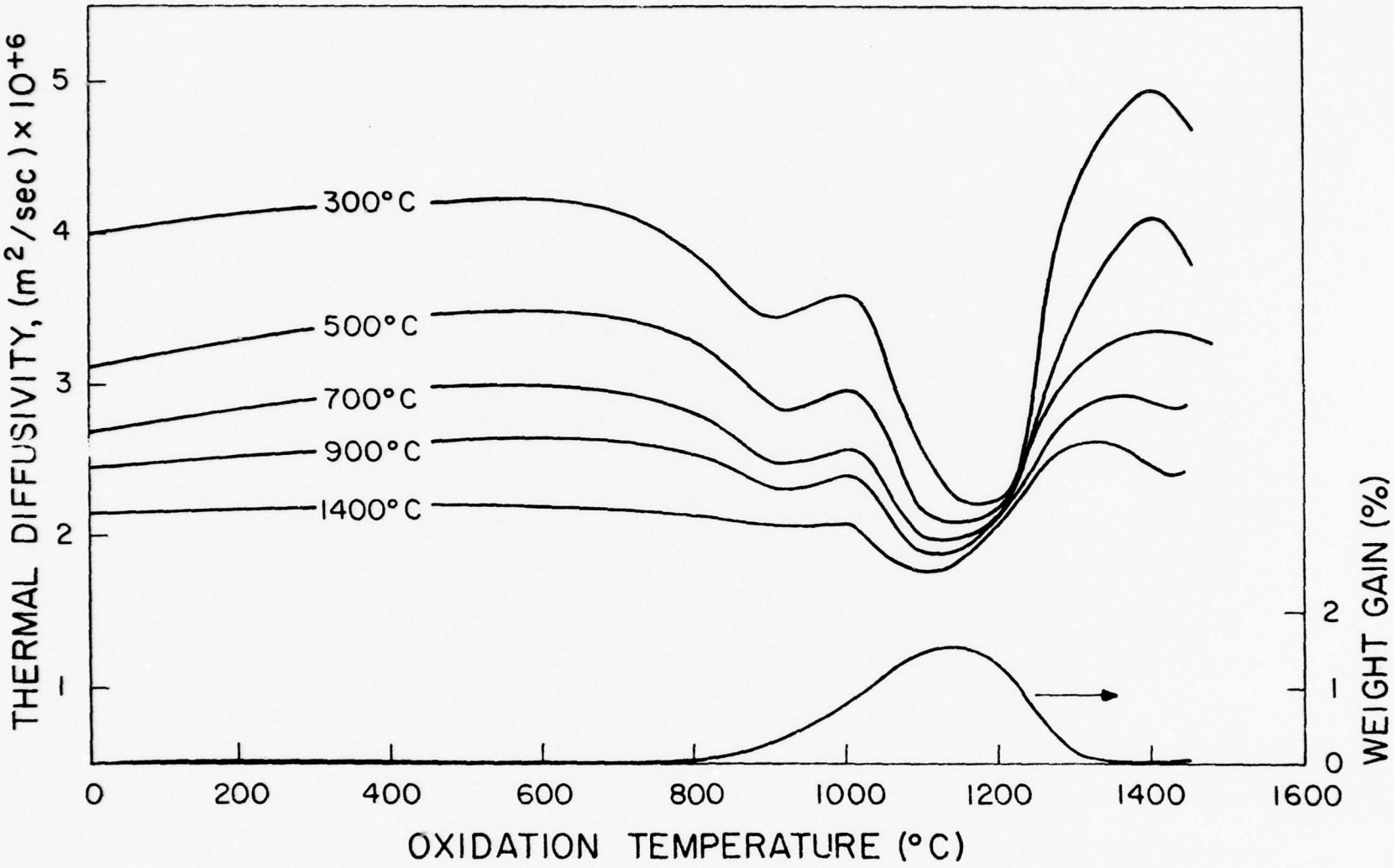

Fig. 2. Thermal diffusivity of reaction sintered silicon nitride oxidized for 50 hrs. in air as a function of oxidation temperature.

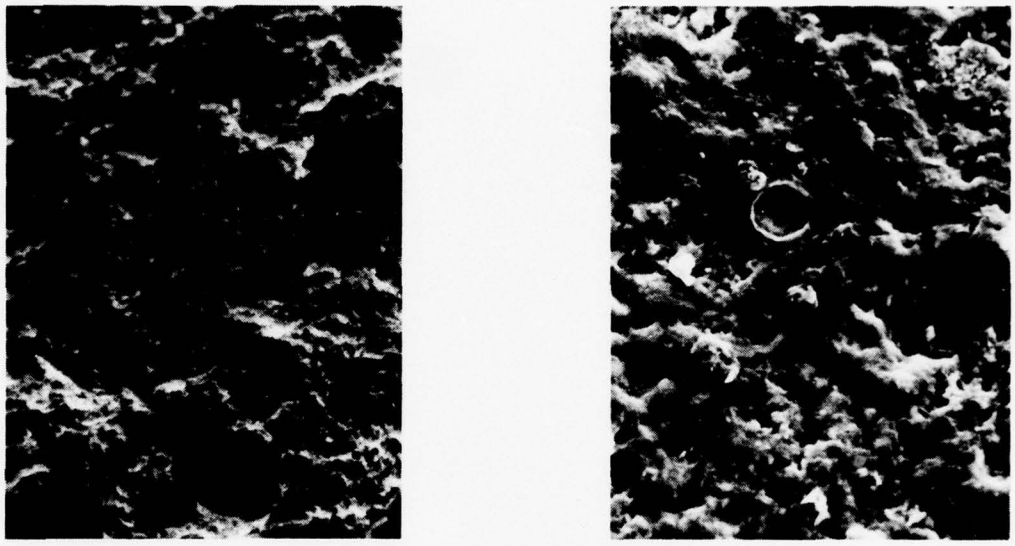

a b

Fig. 3. Scanning electron fractograph of reaction sintered silicon nitride. a, non-oxidized and b, oxidized at 1200°C for 50 hours (500x).

CHAPTER VIII.

EFFECT OF CRYSTALLIZATION ON THE THERMAL DIFFUSIVITY OF A CORDIERITE GLASS-CERAMIC

EFFECT OF CRYSTALLIZATION ON THE THERMAL DIFFUSIVITY OF A CORDIERITE GLASS-CERAMIC

by

K. Chyung*, G. E. Youngblood† and D. P. H. Hasselman§

* Corning Glass Works, Corning, N. Y.

† Montana Energy and MHD Research and Development Institute, Butte, MT.

§ Department of Materials Engineering, Virginia Polytechnic Institute and State University, Blacksburg, Va.

EFFECT OF CRYSTALLIZATION ON THE THERMAL DIFFUSIVITY OF A CORDIERITE GLASS-CERAMIC

K. Chyung, G. E. Youngblood and D. P. H. Hasselman

The magnitude of the thermal conductivity and diffusivity of solids is controlled by the specific heat, and transport properties of the carriers responsible for the heat transfer such as electrons, phonons and photons[1]. Dielectric glassy (non-crystalline) materials with low values of phonon mean free path at low and moderate temperatures at which phonon transport is the primary mechanism for heat transport, are expected to exhibit much lower thermal conductivity and diffusivity than crystalline materials with much higher values of mean free path. For this reason, crystallization of a glass to form a glass-ceramic is expected to cause a significant increase in the thermal conductivity and diffusivity, as confirmed by experimental data for the effect of crystallization on the thermal diffusivity of a mica-glass-ceramic[2].

In general, the relative effect of partial crystallization of a glass on the heat the heat transfer properties is expected to be a function of relative amount of the crystalline phase, its crystal structure and nature of the atomic bonding and other properties relevant to the transport of thermal energy. The phonon mean free path and velocity are expected to be much smaller in a mica-crystalline phase, with Vanderwaals bonding between the basal planes than in a crystalline phase with primarily ionic and co-valent atomic bonds. The latter type of crystalline phase is expected to cause a greater

relative effect on the thermal diffusivity of a glass-ceramic than a mica crystalline phase. In the present note this hypothesis is verified by comparing experimental data for the thermal diffusivity of a cordierite glass ceramic with corresponding data for a mica glass-ceramic reported previously[2].

A series of samples 1" high by 1/2" in diameter of the original glass of a commercial glass-ceramic* were crystallized by heating to 820°C in approximately 45 minutes followed by holding for 2 hours for crystallite nucleation. The samples were then heated rapidly to and held for 8 hours at a range of temperature levels in order to promote crystallite growth. The crystallite morphology was studied by replication transmission electron microscopy. The nature of the crystalline phase was measured by x-ray analysis. The thermal diffusivity was measured from room temperature to approximately 750°C by the laser-flash technique with the same equipment and procedures followed for the mica glass-ceramic[2].

Figure 1 shows the electron micrographs for four samples subjected to different heat treatments. Table I lists the density for all samples and the nature and amount of crystallinity for the samples shown in Fig. 1. Figure 2 shows the experimental data for the thermal diffusivity. No difference was noted between the data obtained on heating and cooling of two of the samples for which this effect was investigated.

Figure 2 indicates that near room temperature the crystallization caused an increase in the thermal diffusivity by a factor in excess of three. At the higher temperature the relative increase is less.

---

* Corning Glassworks, C9606

Qualitatively, these relative differences in thermal diffusivity are attributable to the combined effect of the decrease in thermal conductivity due to increased phonon-scattering in the crystalline phase, with increasing temperature and the simultaneous increase in thermal conductivity due to photon transport in the glassy phase. It should be noted that the present data for the thermal diffusivity of the fully crystallized glass-ceramic (1260°C) lie somewhat below the data collected by Touloukian et al[3] for the commercial cordierite glass-ceramic. In part, this difference may be attributable to the difference in the heat schedule used for the crystallization of the commercial material and the present samples, which may have resulted in differences in the relative amounts of the various crystalline phases.

Comparison of the present data with those reported for the mica glass-ceramic shows that the original glasses for both studies have about the same value of the thermal diffusivity. On crystallization, however, the increases in the thermal diffusivity obtained for the cordierite glass-ceramic are far greater than for the mica glass-ceramic. This observation is in qualitative agreement with the original hypothesis that for a glass-ceramic a crystalline phase without Vanderwaals bonding is expected to be far more effective in increasing the thermal diffusivity of the glass-ceramic than a crystalline phase in part held together by Vanderwaals bonding. This conclusion also is demonstrated by the present data which show that at crystallization temperatures of 1000°C and above, the increase in thermal diffusivity is governed primarily by the change in the nature and relative amounts of the various crystalline phases rather than the decrease in the amount in glassy phase.

Exact quantitative estimates of this phenomenon in terms of lattice-dynamical theory are beyond the scope of the present study. In general, however, the present data and those obtained for the mica glass-ceramics offer strong support for the suggestion that the thermal diffusivity of glass-ceramics can be tailored to specific values by careful control over composition and heat treatment.

Acknowledgment:

The thermal diffusivity was measured as part of a larger research program on the thermal properties of engineering ceramics supported by the Office of Naval Research. The electron micrographs and x-ray data were obtained at Corning Glass Works.

References:

1. C. Kittel, Introduction to Solid State Physics, 3rd Ed. John Wiley and Sons, Inc., New York 1966.

2. H. J. Siebeneck, K. Chyung, D. P. H. Hasselman and G. E. Youngblood, "Effect of Crystallization on the Thermal Diffusivity of a Mica Glass-Ceramic," Ceramic Bulletin (in press).

3. Y. S. Touloukian, R. W. Powell, C. Y. Ho and M. C. Nicolaou, p. 581 in Thermal Diffusivity, Vol. 10 of Thermophysical Properties of Matter, IFI/Plenum, New York (1973).

TABLE I. Heat Treatment, Type and Amount of Crystalline Phases and Densities of Heat-Treated Cordierite Glass-Ceramics.

Heat Treatment (Temp and Time)	Crystalline Phases and Volume %	Density gms/cc
As-Received Glass	-	2.65
820°C, 2 hrs.	-	2.66
820°C-2hrs; 905°C-8 hrs.	Mg - Petalite (60-80%) β - Quartz (10-20%) Enstatite (Trace) Glass (10-20%)	2.76
820°C-2 hrs; 1000°C-8 hrs.	β - Quartz (85-90%) Spinel (5-10%) Enstatite (5%) Glass (2-5%)	2.92
820°C-2 hrs; 1100°C-8 hrs.	-	2.67
820°C-2 hrs; 1150°C-8 hrs.	Cordierite (70-80%) Rutile (5-10%) α - Cristobalite (10-15%) Glass (~ 2%)	2.66
820°C-2 hrs; 1260°C-8 hrs.	Cordierite (70-80%) $MgTiO_5$ (10-15%) α - Cristobalite (10-15%)	2.60

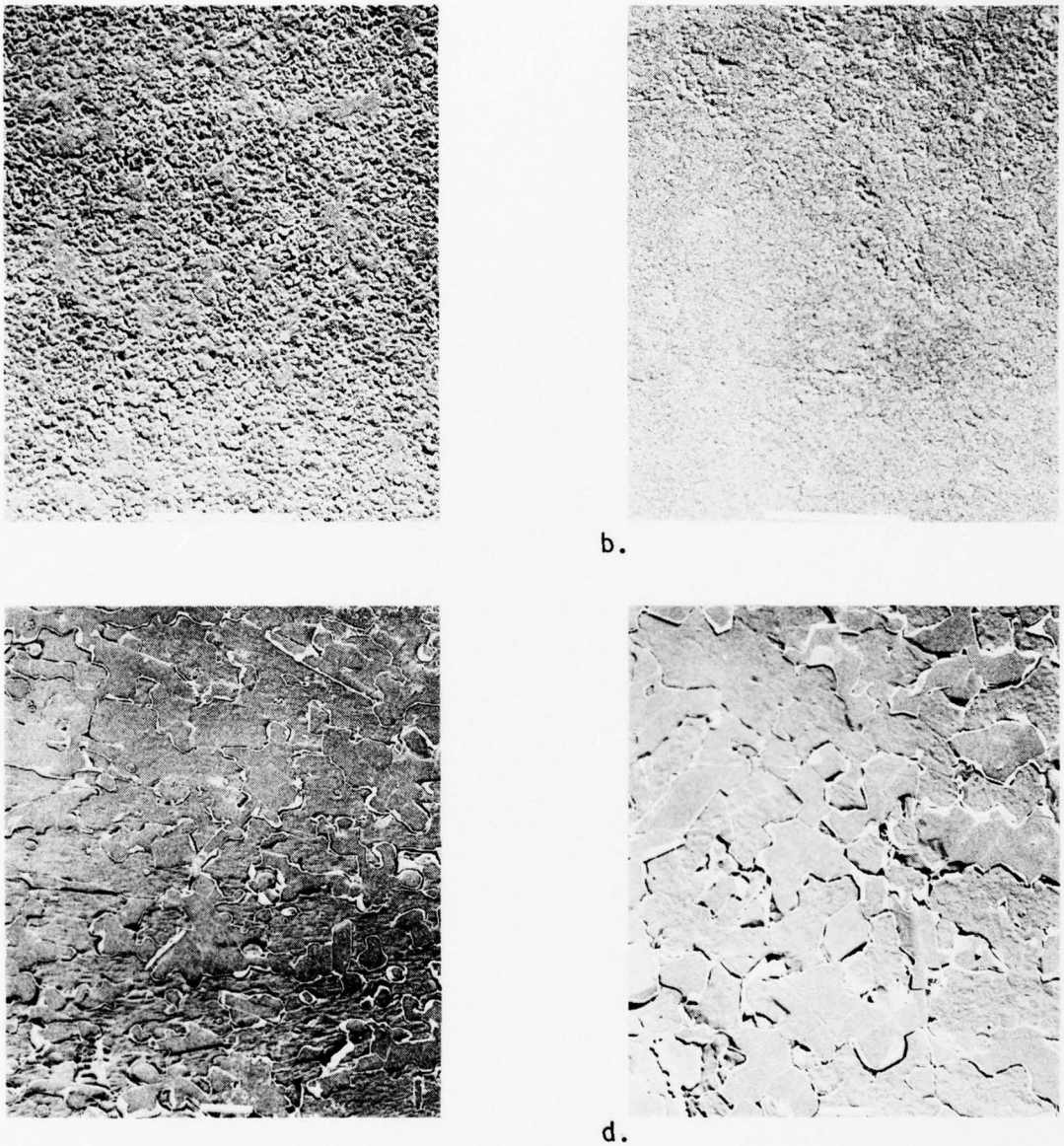

Fig. 1. Replication electron micrographs of partially crystallized cordierite glass-ceramics. Nucleation heat treatment: 2 hrs at 820°C followed by crystal growth for 8 hrs at a: 905°C; b: 1000°C; c: 1150°C and d: 1260°C. Bar indicates one μm.

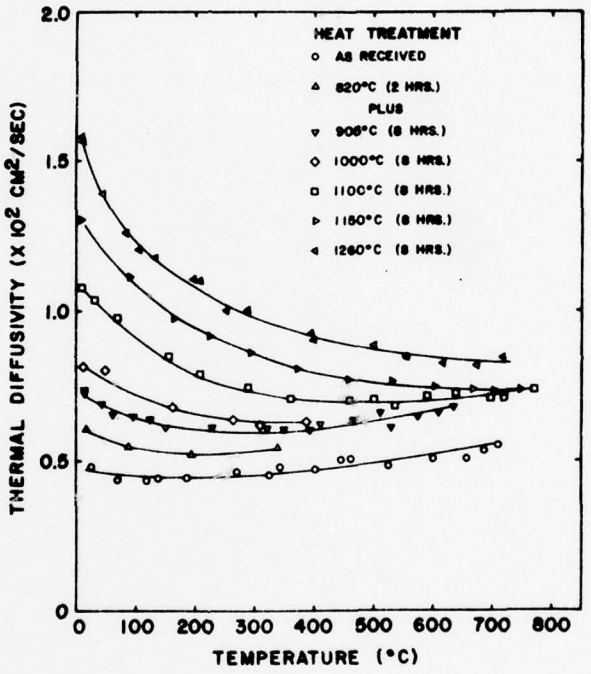

Figure 2. Effect of crystallization on the thermal diffusivity of a Cordierite Glass-Ceramic. Open (solid) symbols indicate measurements made during heating (cooling).

CHAPTER IX.

THERMAL DIFFUSIVITY OF BA-MICA/ALUMINA COMPOSITES

THERMAL DIFFUSIVITY OF BA-MICA/ALUMINA COMPOSITES

by

G. E. Youngblood*, L. Bentsen*, J. W. McCauley†
and
D. P. H. Hasselman§

*Montana Energy R&D Institute
Butte, Montana 59701

†Army Materials and Mechanics Research Center
Watertown, Mass. 02172

§Department of Materials Engineering
Virginia Polytechnic Institute and State University
Blacksburg, Virginia 24061

Particulate composites based on mica-dispersions are excellent candidate materials for many engineering applications in view of their improved friction and wear behavior[1], enhanced fracture toughness[2] and thermal shock resistance[3,4] as well as enhanced machinability[5]. The mica-phase of such composites can also have a profound effect on physical properties such as strength[6], elastic behavior[6], thermal expansion and thermal conductivity[7]. The present note reports data for the effect of a Ba-mica dispersed phase on the thermal diffusivity of polycrystalline alumina.

Samples of alumina containing up to 50 vol.% of a dispersed phase of Ba-mica, identical in composition to those studied previously[6], were prepared by uniaxial hot-pressing mixed powders of nominally $BaMg_3Al_2Si_2O_{10}F_2$ mica* and γ-Al_2O_3§ at 1250°C and 7,000 psi. The mica was in the form of thin circular flakes[6] approximately 10 μm thick by 30 μm in diameter. The γ-Al_2O_3 had an average particle diameter of 1.1 μm. The mica flakes were oriented with their long dimension and basal plane perpendicular to the hot-pressing direction. The densities of the samples at room temperature are listed in Table I. In agreement[8] with previous data, the densities with increasing mica-content showed an approximate linear negative deviation from the theoretical density calculated by the rule of mixtures, giving a total deviation of approximately 6% at 50 vol.% mica. The micro-structures showed that their deviations in density cannot be attributed to an increase in pore phase with increasing mica content. Instead these density variations are the result of the formation of a small amount of a glassy reaction product between

*Synthane Taylor, Mybroy Ceramics Division, Ledgewood, N.J.
§Cerac Co., Menomee Falls, Wisconsin.

the mica and alumina phase. Possibly, also, the lower densities may be due to micro-cracking by cleavage within the mica due to the internal stresses which result on cooling as the result of the mismatch in the coefficients of thermal expansion of the mica and alumina.

The thermal diffusivity parallel to the hot-pressing direction from 25°C to approximately 800°C was measured by the laser-flash technique with equipment and procedures described elsewhere[9]. Fig. 1 shows the experimental data for all compositions with the exception of the sample with 20 vol.% mica, which exhibited an apparently anomalous behavior. In order to provide a basis of comparison of the relative temperature dependence, Fig. 1 includes experimental data for a pure dense polycrystalline alumina*. Fig. 2 shows the compositional dependence for various temperatures obtained from the curves drawn through the data of Fig. 1. Figure 2 also includes the data for the sample containing 20 vol.% mica.

The anomaly in the present data for the thermal diffusivity at 20 vol.% mica was also found for the thermal conductivity[7], with the exception that in the latter study, the anomaly occurred at 15 vol.% mica. This anomaly is attributable to the type and amount of reaction products formed between the mica and the alumina during hot-pressing[10]. Preparation of full-density composites is accomplished within a narrow temperature range below which complete densification does not occur and above which undesirable reaction products are formed. This situation is particularly critical near 15-20% Ba-mica. Below this amount an excess temperature results in the formation of a glass and a spinel,

*SN60, Feldmühle, Plochingen, West Germany

whereas above this amount a glassy phase is formed only. In support of this explanation it was found that x-ray analysis of the present samples showed diffraction peak intensities, for the mica-phase of the composite containing 20% mica, smaller than for the other samples as expected from initial amount of mica present. For the present data the anomalous value for the thermal diffusivity most likely is because the reaction products either have a higher thermal conductivity or a lower specific heat than the corresponding value for the mica or the alumina.

The relative temperature dependence of the thermal diffusivity of the mica-alumina composites is similar to that for the pure alumina. In fact, a plot of α^{-1} vs T shows a straight line behavior with an intercept near zero at T = 0°K for all compositions. It may be noted again that the present data are for the thermal diffusivity with heat flow through the mica occurring perpendicular to the weakly bonded basal planes. As expected from experimental data for other micas[11], boron nitride[12,13] and pyrolytic graphite[14,15], heat flow perpendicular to the basal plane is expected to result in a thermal conductivity at least an order of magnitude less than that of polycrystalline aluminum oxide and also to result in a temperature dependence less than T^{-1}, expected for phonon conduction over the range of temperature of the present data. The reason that the temperature dependence of the thermal conductivity/diffusivity of the mica has little or no influence on the temperature dependence of the Ba-mica/alumina composites is that the heat is conducted primarily by the continuous alumina phase. If, however, the mica had been the continuous phase, its temperature dependence would

have had a significant effect on the temperature dependence of the thermal conductivity and diffusivity of the composite, especially at higher mica volume fractions. This latter conclusion is easily verified by expressions for the thermal conductivity of composites or by analogy by equivalent parallel or series electrical circuits. This suggests, in general, that the magnitude of thermal conductivity and its temperature dependence in composites can be controlled by the proper choice of components and their distribution within the composite.

Acknowledgments

Specimen preparation was performed at the Army Materials and Mechanics Research Center. The measurement of the thermal diffusivity was performed as part of a larger program supported by the Office of Naval Research.

References

1. M. E. Belitskii and D. S. Yas, "Erosion Wear of Mica-Ceramic Materials," Sov. Powder Met. Metal Ceramic (Engl. Translation), 4, (76), 303-05 (1969).
2. J. W. McCauley and S. J. Acquaviva, "Property Characterization of Ba-Mica/Al_2O_3 Composites," Amer. Ceram. Soc. Bull., 52, 364 (1973).
3. C. C. Seaton and J. W. McCauley, "Thermal Shock Characteristics of Ba-Mica/Al_2O_3 Composites," Amer. Ceram. Soc. Bull, 52, 708 (1973).
4. K. Chyung, "Fracture Energy and Thermal Shock Resistance of Mica Glass-Ceramics", pp. 495-508 in Fracture Mechanics of Ceramics, Vol. 2. Ed. by R. C. Bradt, D. P. H. Hasselman and F. F. Lange, Plenum Press (1974).
5. D. G. Grossman, "Machinable Glass-Ceramics Based on Tetrasilisic Mica," J. Am. Ceram. Soc., 55, 446 (1974).
6. J. W. McCauley, "Structural and Chemical Characterization of Processed Crystalline Ceramic Materials," Chptr 7 in Characterization of Materials in Research, Ceramics and Polymers, Syracuse University Press, Syracuse, N. Y. (1975).
7. R. P. Tye and J. W. McCauley, "The Thermal Conductivity and Linear Expansion of Ba-Mica/Alumina Composite Materials," Rev. Int. Htes Temp. et Refract., 12, 100-05 (1975).
8. J. W. McCauley, "Fabrication and Properties of Ba-Mica/Al_2O_3 Composites," Amer. Ceram. Soc., Bull. 51, 434 (1972).
9. H. J. Siebeneck, K. Chyung, D. P. H. Hasselman and G. E. Youngblood, "Effect of Crystallization on the Thermal Diffusivity of a Mica Glass-Ceramics," J. Amer. Ceram. Soc., 60, 375-76 (1977).

References (Cont'd)

10. J. W. McCauley (in preparation).

11. Y. S. Touloukian, R. W. Powell, C. Y. Ho and M. C. Nicolaou, Thermophysical Properties of Matter, Vol. 10: Thermal Conductivity-Non-Metallic Solids. IFI/Plenum, New York, (1973).

12. A. Simpson and A. D. Stuckes, "The Thermal Conductivity of Highly Oriented Pyrolytic Boron Nitride," J. Phys. C: Solid St. Phys., 4, 1710-18 (1971).

13. E. K. Sichel and R. E. Miller, "Thermal Conductivity of Highly Oriented Pyrolytic Boron Nitride," pp. 11-17 in Thermal Conductivity 14, Ed. by P. G. Klemeus and T. K. Chen, Plenum Press, N. Y. (1974).

14. Takoho Tanaka and Hiro Shige Suzuki, "The Thermal Diffusivity of Pyrolytic Graphite at High Temperatures," Carbon, 10, 253-57 (1972).

15. S. Nasu, T. Takahashi and T. Kikuchi, "Anisotropy Ratio of Thermal Diffusivity in Pyrolytic Graphite over the Temperature Range from 300 to 1600°C," J. Nucl. Mat. 43, 72-74 (1972).

TABLE I. Composition and Density of Ba-Mica/Al_2O_3 Composites.

Ba-Mica Content (Vol.%)	Density (gms/cc)
5	3.935
15	3.845
20	3.750
30	3.695
40	3.625
50	3.540

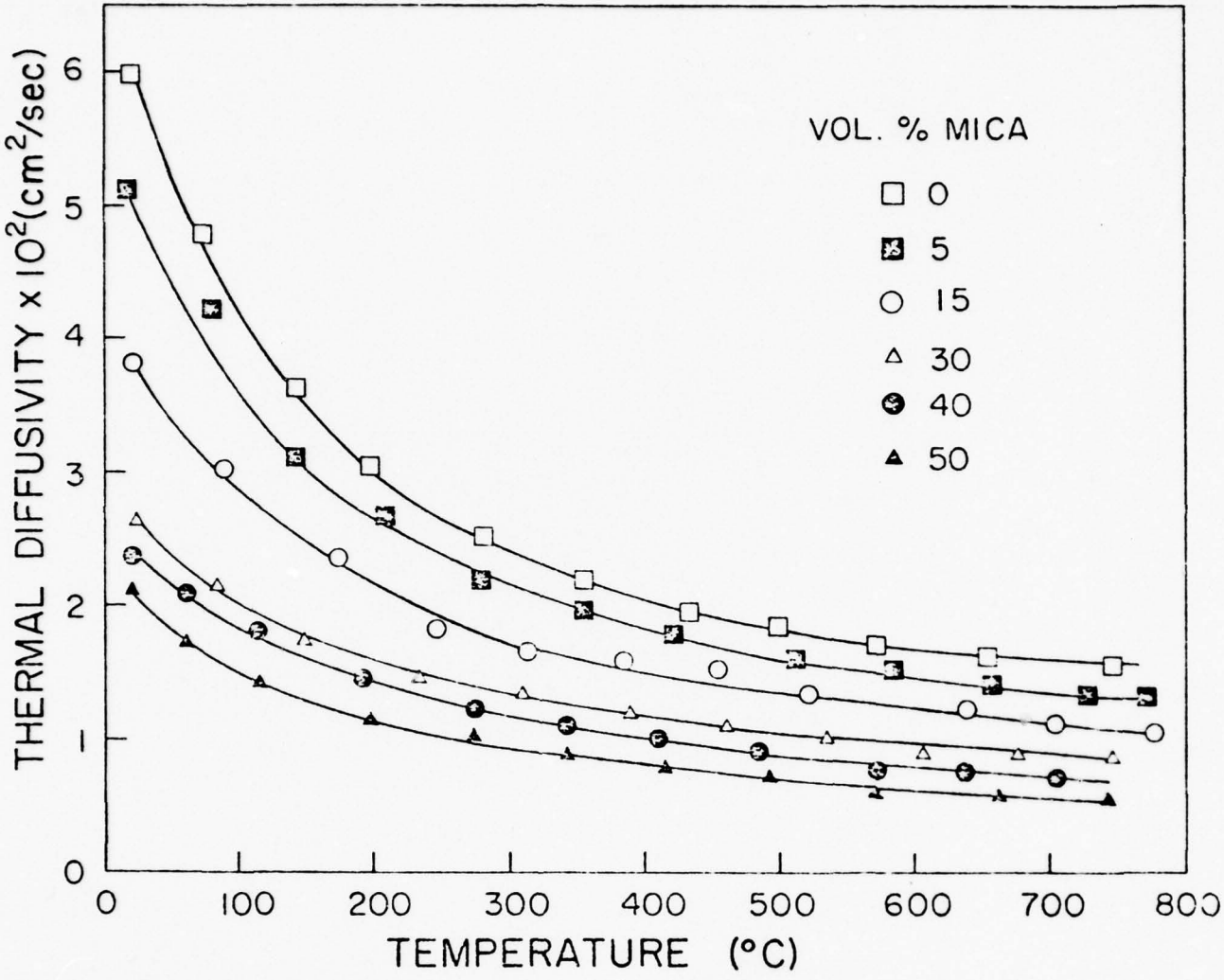

Fig. 1. Effect of Temperature on the Thermal Diffusivity of Ba-Mica-Alumina Composites.

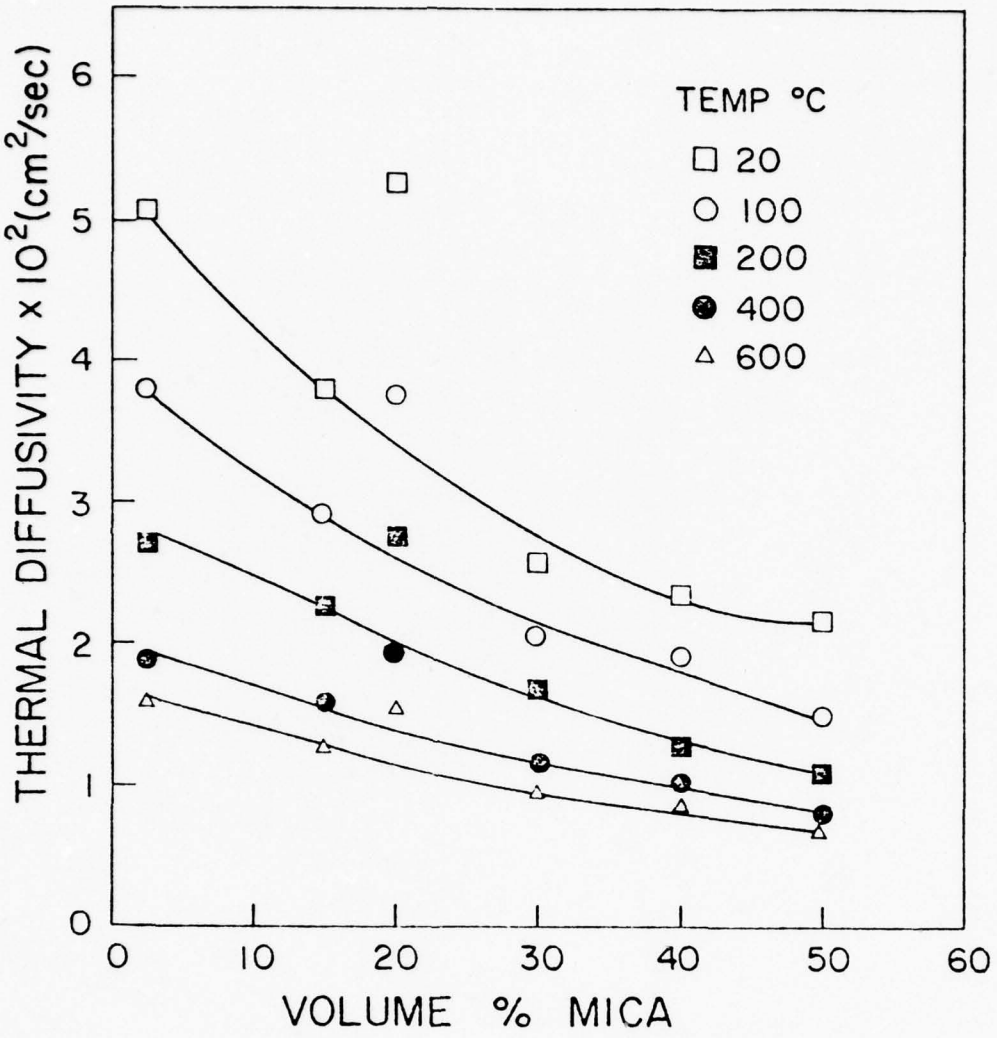

Fig. 2. Effect of Composition on the Thermal Diffusivity of Ba-Mica-Alumina Composites.

CHAPTER X.

EFFECT OF ALUMINA DISPERSIONS ON THE THERMAL CONDUCTIVITY/ DIFFUSIVITY AND THERMAL STRESS RESISTANCE OF A BOROSILICATE GLASS

EFFECT OF ALUMINA DISPERSIONS ON THE THERMAL CONDUCTIVITY/DIFFUSIVITY AND THERMAL STRESS RESISTANCE OF A BOROSILICATE GLASS

by

D. P. H. Hasselman*, J. C. Swearengen†, E. K. Beauchamp†
and
W. A. Zdaniewski*

*Department of Materials Engineering
Virginia Polytechnic Institute and State University
Blacksburg, Virginia 24061

†Sandia Laboratories
Albuquerque, New Mexico 87115

Hot-pressed glass-crystal mixtures are used as model materials for studies of the properties of brittle matrix composites. Properties such as elastic behavior[1,2,3], strength[2,4] and fracture toughness[3,4] have been studied extensively for glass matrices with an alumina dispersed phase. However, such composites in their own right are also candidate materials for engineering applications involving thermal stress. This note presents data for the thermal conductivity and thermal diffusivity of glass-alumina mixtures, which permits making an assessment of the effect of the crystalline phase on thermal stress resistance.

The specific glass-alumina specimens in this study were prepared in a program addressing the fracture toughness[3] of a borosilicate glass with alumina dispersions. The glass consisted of 70 mole % SiO_2 plus B_2O_3 and Na_2O in a molar ratio of 0.67. The alumina dispersions were spherical with a diameter of 25 ± 7 μm. Details for the specimen preparation and microstructure were presented earlier[3]. This particular glass-alumina system was selected because of the close match between the coefficients of thermal expansion of the two phases, in order to minimize or eliminate the formation of micro-cracks due to internal stresses; such cracks could have significant effect on the thermal conductivity[5].

The thermal diffusivity of the composites was measured over the temperature range from room temperature to about 600°C by the laser-flash diffusivity technique[6] using equipment described in detail elsewhere[7], with the transient temperatures of the specimens during the test being monitored by IR-detectors. The thermal conductivity was calculated from the thermal diffusivity using values for the density

of the alumina and the glass of 3.987 and 2.454 $g.cc^{-1}$ resp. and literature data for the specific heat of alumina[8] and a borosilicate glass of composition similar to the glass of the present study[9].

Figure 1 shows the experimental data for the thermal diffusivity as a function of temperature for a number of compositions for which the volume fractions were determined from the composite densities after hot-pressing[3]. For some of these compositions, fig. 2 shows the calculated values of thermal conductivity. The relative effect of temperature and composition on the thermal diffusivity and conductivity of these composites can be explained on the basis of the general heat conduction processes in dielectric materials. Due to the relative differences in elastic properties and degree of crystallinity, the thermal conductivity and diffusivity of the glass is expected to exhibit much lower values and a lower temperature dependence than the corresponding values for the alumina. For these reasons, addition of alumina particles to the glassy phase is expected to increase the magnitude of the thermal diffusivity with a corresponding increase in its temperature dependence, in agreement with observations. The positive temperature dependence of the thermal diffusivity of the glass at the higher temperatures most likely is attributable to a contribution of internal radiation to the heat transfer process.

The values of the thermal conductivity show a much lower relative temperature dependence than the thermal diffusivity, because the positive temperature dependence of the specific heat compensates for the negative temperature dependence of the thermal diffusivity. It may be noted that at the highest volume fraction the variation in thermal conductivity with volume content alumina lies above the values calculated by the Rayleigh-

Maxwell theory[10,11], which is appropriate only for dilute concentrations of spherical inclusions.

An assessment of the anticipated effect of the alumina phase on thermal stress resistance can be made on the basis of its influence on thermal stress resistance parameters. As a measure of the resistance of a brittle material to the initiation of thermal fracture two well-known[12] parameters are: $R = S_t(1-\nu)/\alpha E$ and $R' = S_t(1-\nu)K/\alpha E$, in which S_t is the tensile strength, ν is Poisson's ratio, α is the coefficient of thermal expansion, E is Young's modulus and K is the thermal conductivity. The resistance of crack propagation and corresponding loss in load-bearing ability after thermal fracture initiation described is given by the parameters[13], $R_{st} = (G/\alpha^2 E)^{\frac{1}{2}}$ and $R'_{st} = (GK^2/\alpha^2 E)^{\frac{1}{2}}$ for stable crack propagation and $R'''' = GE/S_t^2$ for unstable catastrophic crack propagation. In these latter parameters G is the fracture energy, related to the critical stress intensity factor, $K_{Ic} = (2GE)^{\frac{1}{2}}$. Figure 3 shows the relative variation of these parameters with volume fraction alumina as calculated from the thermal conductivity and mechanical[3] property and strength[14] data for these materials. The location of the curves for the parameters R_{st}, R'_{st} and R'''' must be considered only approximate in view of the lack of sufficient data points to plot the curves accurately. Nevertheless, sufficient data were available to indicate that these parameters vary significantly with alumina content.

As judged by the variation of the parameters R and R', the addition of the alumina phase has only a minor influence on the thermal conditions required to initiate fracture. In fact, the variation in R indicates that the alumina phase actually decreases thermal stress resistance.

The parameter R' increases primarily because the increase in K exceeds the increase in E. As indicated by experimental data, the values of R and R' could be increased by increasing the composite strength by decreasing the alumina particle size.

The major increases in the parameters R_{st} and R'_{st} and especially R"", indicate that the alumina crystalline phase has a large effect on the nature of crack propagation following thermal fracture. Specifically, under conditions of both stable and unstable fracture the extent of crack propagation should be reduced appreciably accompanied by a major increase in the retention of load-bearing ability or any other property affected by cracks. The general shape of the curves in fig. 3 for R_{st}, R'_{st} and R"" indicates that optimum resistance to thermal crack propagation can be obtained at approximately 20 vol.% alumina.

These results suggest that by incorporating a high conductivity crystalline phase in the glassy material, the resistance to the initiation and the catastrophic nature of thermal fracture of a glass can be improved significantly. Well controlled thermal stress experiments to confirm this conclusion should be of interest.

ACKNOWLEDGMENTS

The specimens used in this study were prepared at Sandia Laboratories, where also their mechanical properties were measured with support by the Department of Energy. The measurement of the thermal diffusivity, data interpretation and manuscript preparation in part was supported by Virginia Polytechnic Institute and State University and in part by the Office of Naval Research under contract #N00014-78-C-0431.

References

1. D. P. H. Hasselman and R. M. Fulrath, "Effect of Alumina Dispersions on Young's Modulus of a Glass," J. Amer. Ceram. Soc., 48 (4) 218-19 (1965).

2. F. F. Lange, "Fracture Energy and Strength Behavior of a Sodium Borosilicate Glass-Al_2O_3 Composite System." J. Amer. Ceram. Soc., 54 (12) 614-20 (1971).

3. J. C. Swearengen, E. K. Beauchamp, R. J. Eagan, "Fracture Toughness of Reinforced Glasses," pp. 973-87 in Fracture Mechanics of Ceramics, Vol. 4. Ed. by R. C. Bradt, D. P. H. Hasselman and F. F. Lange, Plenum Press, N.Y. pp. 987 (1978).

4. D. P. H. Hasselman and R. M. Fulrath, "Proposed Fracture Theory of a Dispersion-Strengthened Glass Matrix," J. Amer. Ceram. Soc., 49 (2) 68-72 (1966).

5. D. P. H. Hasselman, "Effect of Cracks on Thermal Conductivity," J. Composite Materials, (in press).

6. W. J. Parker, R. J. Jenkins, C. P. Butler and G. L. Abbott, "Flash Method of Determining Thermal Diffusivity, Heat Capacity and Thermal Conductivity," J. Appl. Phys., 32 (9) 1679-84 (1961).

7. H. J. Siebeneck, D. P. H. Hasselman, J. J. Cleveland and R. C. Bradt, "Effect of Microcracking on the Thermal Diffusivity of Fe_2TiO_5," J. Am. Ceram. Soc., 59 [5-6] 241-44 (1976).

8. Y. S. Touloukian, R. W. Powell, C. Y. Ho and P. G. Klemans, Thermophysical Properties of Matter, Vol. 2: Specific Heat: Nonmetallic Solids, The TPRC Data Series, IFI/Plenum, New York, NY (1970).

9. A. Goldsmith, T. E. Waterman and H. J. Hirschhorn, Handbook of Thermophysical Properties of Solid Materials, Vol. 3: Ceramics. The MacMillan Comp. New York (1961).

10. L. Rayleigh, "On the Influence of Obstacles Arranged in Rectangular Order Upon the Properties of a Medium," Phil. Mag. 34, 481-507 (1892).

11. J. C. Maxwell, A Treatise on Electricity and Magnetism, I, 3rd Ed. p. 440, Oxford University Press, Oxford, U.K. (1904).

12. W. D. Kingery, "Factors Affecting Thermal Stress Resistance of Ceramic Materials," J. Amer. Ceram. Soc., 38 [1] 3-15 (1955).

13. D. P. H. Hasselman, "Unified Theory of Thermal Shock Fracture Initiation and Crack Propagation in Brittle Ceramics," J. Amer. Ceram. Soc., 52 (11) 600-04 (1969).

14. J. C. Swearengen, E. K. Beauchamp and R. J. Eagan, (Unpublished results).

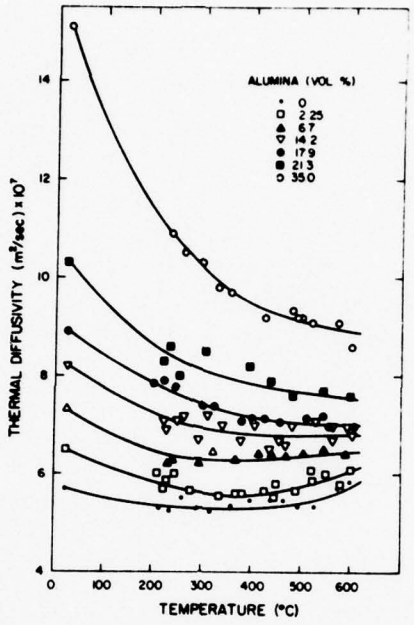

Fig. 1. Effect of temperature and composition on thermal diffusivity of glass-alumina composite.

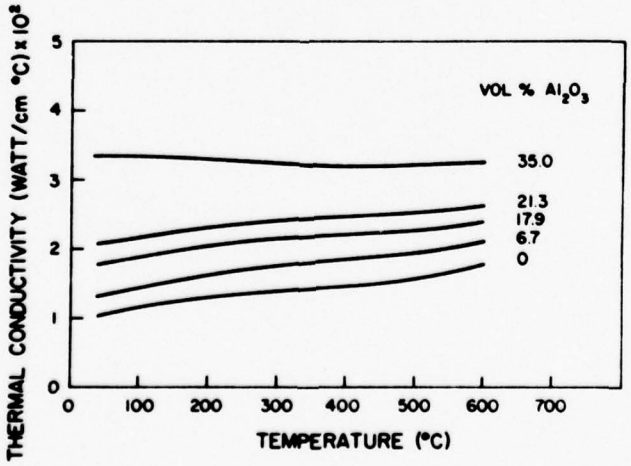

Fig. 2. Calculated thermal conductivity of glass-alumina composites.

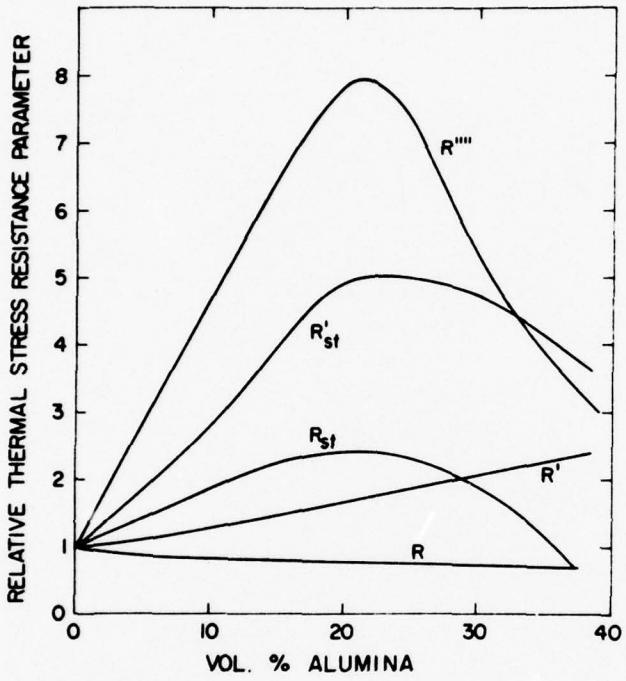

Fig. 3. Relative thermal stress resistance parameters of glass-alumina composites.

CHAPTER XI.

FIGURES-OF-MERIT FOR THE THERMAL STRESS RESISTANCE OF HIGH-TEMPERATURE BRITTLE MATERIALS: A REVIEW.

FIGURES-OF-MERIT FOR THE THERMAL STRESS RESISTANCE OF HIGH-TEMPERATURE BRITTLE MATERIALS: A REVIEW

by

D. P. H. Hasselman
Whittemore Professor of Materials Engineering
Department of Materials Engineering
Virginia Polytechnic Institute and State University
Blacksburg, Virginia 24061 USA

ABSTRACT

A review is presented of the selection rules for brittle structural ceramics subjected to severe thermal stress. A total of twenty-two figures-of-merit are presented for a total of twenty-nine different heat transfer environments and/or criteria of thermal stress resistance, involving steady-state or transient heat transfer, internal heat generation, thermal buckling as well as thermal fatigue and unstable crack propagation.

1. Introduction

Materials of construction for high-temperature structures and/or components, in spite of such properties as high melting points, low vapor pressure, high creep resistance and other favorable characteristics, tend to be highly brittle. As a direct result of this brittleness, high-temperature materials are highly susceptible to catastrophic failure under thermal conditions which involve appreciable levels of thermal stress. In order to avoid thermal stress failure it is essential that the structure or component be designed to minimize the conditions which lead to the generation of thermal stresses, and that the material of construction be selected with a combination of properties such that the magnitude of thermal stress is minimized. In order to achieve this latter objective it is critical that the role of the pertinent material properties which govern thermal stress fracture be well understood. For this purpose, a large number of analytical expressions have been presented in the literature devoted to materials science and engineering for the thermal stress resistance of brittle materials for a wide range of thermal environments and criteria of thermal stress resistance in terms of the appropriate material properties and geometric variables. From these expressions figures-of-merit or so-called thermal stress resistance parameters can be derived which form the basis for the selection of the optimum material for a particular thermal environment and criterion of thermal stress resistance. These thermal environments include steady-state heat flow, transient heat flow involving convective or radiative heat transfer, thermal fatigue, thermal stability as well as thermal stress resistance controlled by stable or unstable catastrophic crack propagation.

The present writer some nine years ago presented a compendium of the approximately ten or twelve thermal stress resistance parameters available at that time. Since then, the total number of non-redundant equations for thermal stress resistance and number of thermal stress resistance parameters has grown appreciably. In fact, the total number of parameters has grown to some twenty-two. This indicates that the selection or development of material with optimum thermal stress resistance for a given thermal environment is a highly complex task. In view of this complexity and the gain in understanding achieved during the last decade, it appears justified to present a review of the thermal stress figures-of-merit in order to present the reader with the latest information. The presentation of such a review represents the primary objective of this paper, which is organized as follows:

For a given thermal environment and criterion of thermal stress resistance, a literature equation is presented for a single geometry. On dimensional grounds, for the same thermal environment and criterion of thermal stress resistance, with exception of the geometric constant, the equation presented also is appropriate for other geometries. For this reason a general thermal-stress-resistance figure-of-merit can be derived appropriate to the specific thermal environment and performance criterion independent of geometric considerations. The appropriate figure-of-merit is given immediately following the equation given. Depending on the condition of external constraints or geometry, Poisson's ratio can enter in various terms such as $(1-\nu)$, $(1-2\nu)$, $(1+\nu)$ etc., or may even be absent. For purposes of brevity, these terms involving Poisson's ratio are considered part of the geometric constant, which will keep the total number of expressions to be presented to a manageable number. Nevertheless,

appropriate literature references involving terms for Poisson's ratio will be given whenever available.

Again for purposes of brevity, the expression to be presented will be given with an adequate but brief description of the thermal environment or other pertinent conditions. For details of the mathematics, assumptions, boundary conditions, etc., the reader is referred to the original papers. If an expression or figure-of-merit has not appeared in the literature previously, it will be so stated.* Whenever possible, the symbols used in the equations are those recommended by the American Ceramic Society and are listed separately.[2]

2. Equations and Figures-of-Merit

A. Steady-State Heat Flow

a. Circular hollow cylinder; radial heat flow, ΔT_{max} across wall[3,4]:

$$\Delta T_{max} = S_t(1-\nu)C/\alpha E \tag{1a}$$

Figure-of-merit:

$$R = S_t(1-\nu)/\alpha E \tag{1b}$$

b. In terms of maximum heat flow, Q_{max}, eq. 1 becomes:

$$Q_{max} = S_t(1-\nu)KC'/\alpha E \tag{2a}$$

Figure-of-merit:

$$R' = S_t(1-\nu)K/\alpha E \tag{2b}$$

* The use of the term "can be derived" implies that the equation presented can be derived readily from the reference cited.

c. Circular hollow cylinder, radial heat flow: Stress relaxation by linear creep. Maximum rate of temperature change[5]:

$$\dot{\Delta T}_{max} = S_t(1-\nu)C/\alpha\eta \tag{3a}$$

Figure-of-merit:

$$R_{cr} = S_t(1-\nu)/\alpha\eta \tag{3b}$$

d. In terms of maximum rate of change of heat flow, eq. 3a becomes[5]:

$$\dot{Q}_{max} = S_t(1-\nu)C'K/\alpha\eta \tag{4a}$$

Figure-of-merit:

$$R'_{cr} = S_t(1-\nu)K/\alpha\eta \tag{4b}$$

e. Linear heat flow around spherical cavity. Maximum temperature gradient[6] can be derived to be:

$$\nabla_{max} = 2S_t(1-\nu)/\alpha Eb \tag{5a}$$

Figure-of-merit:

$$R = S_t(1-\nu)/\alpha E \tag{5b}$$

f. Eq. 5a in terms of maximum heat flow becomes:

$$Q_{max} = 2S_t(1-\nu)K/\alpha Eb \tag{6a}$$

Figure-of-merit:

$$R' = S_t(1-\nu)K/\alpha E \tag{6b}$$

From other solutions[7] figures-of-merit can be obtained for inclusions other than pores.

B. Internal Heat Generation

g. For solid circular rod with uniform internal heat generation (H), the maximum rate of heat generation is[8]:

$$H_{max} = 8S_t(1-\nu)K/\alpha Eb^2 \tag{7a}$$

Figure-of-merit:

$$R' = S_t(1-\nu)K/\alpha E \tag{7b}$$

C. Transient Heat Transfer

h. Flat plate; Linear rate of increase of surface temperature. Maximum rate of increase[9]:

$$\dot{T}_{max} = 3S_t(1-\nu)a/\alpha Eb^2 \tag{8a}$$

Figure-of-Merit:

$$R'' = S_t(1-\nu)a/\alpha E \tag{8b}$$

i. Convective (Newtonian) heat transfer. Spherical body subjected to heating and cooling over temperature range ΔT[10].

$$\Delta T_{max} = \frac{2.5\ S_t\ (1-\nu)}{\alpha E}\ \{1 + 2/\beta\} \quad \beta = bh/K \tag{9}$$

For severe heat transfer, $\beta \to \infty$

$$\Delta T_{max} = 2.5\ S_t(1-\nu)/\alpha E \tag{10a}$$

Figure-of-Merit:

$$R = S_t(1-\nu)/\alpha E \tag{10b}$$

For mild heat transfer, $\beta << 1$

$$\Delta T_{max} = 5S_t(1-\nu)K/\alpha Ebh \tag{11a}$$

Figure-of-merit:

$$R' = S_t(1-\nu)K/\alpha E \tag{11b}$$

j. Radiation heat transfer. Spherical body at low initial temperature and wavelength independent emissivity. Instantaneously uniformly subjected to black-body radiation. Maximum radiation temperature[11]:

$$T_{max} = \{5S_t(1-\nu)K/\rho b\alpha E\varepsilon\}^{1/4} \tag{12a}$$

Figure-of-merit:

$$R_{rad} = \{S_t(1-\nu)K/\alpha E\varepsilon\}^{1/4} \tag{12b}$$

k. Radiation heat transfer. If body transparent to radiation at wavelength, $\lambda < \lambda_o$ eq. 12a becomes[12]:

$$T_{max} = \{5S_t(1-\nu)K/\rho b(1-F_{\lambda o})\alpha E\varepsilon\}^{1/4} \tag{13a}$$

Figure-of-merit:

$$R_{trans} = \{S_t(1-\nu)K/(1-F_{\lambda o})\alpha E\varepsilon\}^{1/4} \tag{13b}$$

l. Transient heat transfer with inertial effects. Rod of length L, freely suspended. Rod is very rapidly exposed to uniform temperature increase ΔT in time period, t_o. Compressive stresses will occur because of finite time required for expansion to take place.[13]

The maximum temperature increase of the rod, without compressive failure can be derived to be:

$$\Delta T_{max} = S_c/\alpha E \quad \text{for} \quad t_o \leq t_m \tag{14a}$$

Figure-of-merit:

$$R_{in} = S_c/\alpha E \tag{14b}$$

and

$$\Delta T_{max} = S_c c\ t_o/\alpha EL \quad \text{for} \quad t_o \geq t_m \tag{15a}$$

Figure-of-merit:

$$R'_{in} = S_c c/\alpha E \tag{15b}$$

m. Transient heat transfer. Time-to-failure. Sphere. Surface temperature raised instantaneously by temperature difference, ΔT. Time to maximum stress[14]:

$$t^* = 0.0574\ b^2/a \tag{16a}$$

Figure-of-merit:

$$R_t = a^{-1} \tag{16b}$$

D. Thermal Buckling

n. Straight column prevented from expanding against rigid constraint. Heated by temperature difference ΔT. Critical temperature difference required for column instability[15]:

$$\Delta T_c = \pi^2 I/L^2 A\alpha \tag{17a}$$

Figure-of-merit:

$$R_{1b} = \alpha^{-1} \tag{17b}$$

o. Post-thermal buckling of straight column. Originally straight column prevented from expanding against rigid constraints, heated over temperature difference, $\Delta T > \Delta T_c$ to be subjected to bending in post-thermal buckling.

Maximum temperature difference required for failure of square column as the result of tensile bending stresses[16]:

$$\Delta T_{max} = \pi^2 d^2/12L^2\alpha + S_t^2 L^2/\pi^2 \alpha E^2 d^2 \tag{18a}$$

Figure-of-Merit:

$$R_{2b} = S_t^2/\alpha E^2 \tag{18b}$$

p. Column with slight initial curvature (radius R) prevented from expanding against rigid constraints. Heated by temperature difference ΔT. Critical temperature difference required for column fracture due to bending moment[17]:

$$\Delta T_{max} = (S_t/\alpha^2 E)^{1/2}(16\ Rd^3/15L^4)^{1/2} \tag{19a}$$

Figure-of-merit:

$$R_{3b} = (S_t/\alpha^2 E)^{1/2} \tag{19b}$$

q. Column initially straight subjected to transverse temperature gradient ∇ and prevented from expanding against rigid constraints. Heated by temperature difference ΔT. Critical temperature difference for fracture of column due to bending moment (for given gradient ∇)[7]:

$$\nabla T_{max} = (S_t/\alpha^3 E)^{1/2}(16d^3/15\nabla L^4)^{1/2} \tag{20a}$$

Figure-of-merit:

$$R_{4b} = (S_t/\alpha^3 E)^{1/2} \tag{20b}$$

r. Initially straight column subjected to transverse temperature gradient ∇ and prevented from expanding against rigid con-

straints. Heated by temperature difference ΔT. Critical temperature gradient at fixed ΔT, required for column fracture[17]:

$$\nabla_{max} = (S_t/\alpha^3 E)\ \{16d^3/15(\Delta T)^2 L^4\} \tag{21a}$$

Figure-of-merit:

$$R_{5b} = (S_t/\alpha^3 E) \tag{21b}$$

Eq. 21a in terms of maximum heat flow becomes[16]:

$$Q_{max} = (S_t K/\alpha^3 E)\ \{16d^3/15(\Delta T)^2 L^4\} \tag{22a}$$

Figure-of-merit:

$$R_{6b} = (S_t K/\alpha^3 E) \tag{22b}$$

E. Crack-Propagation

s. Fatigue. Subcritical crack growth. Constant thermal stress. Material subjected at t = o to a steady-state thermal stress. $\sigma = C\alpha E\Delta T/(1-\nu)$, with $\sigma << S_t$, the fracture stress. The material undergoes subcritical crack growth with a crack velocity, $V = AK_I^n \exp(-Q/RT)$. For $K_I = Y\sigma_a \sqrt{a}$ and K_{Ii} (t=o) $<< K_{Ic}$, for the condition that over the total time period, the total extent of crack growth does not affect the compliance, the time to failure (t_f) is[18]:

$$t_f \simeq \frac{2(1-\nu)^2 \exp(Q/RT)}{C(\alpha E\Delta T)^2 Y^2 A(n-2) K_{Ii}^{(n-2)}} \tag{23a}$$

Figure-of-merit:

$$R_f = \frac{(1-\nu)^2 \exp(Q/RT)}{\alpha^2 E^2 (n-2) A} \tag{23b}$$

If in analogy to eq. 2a, ΔT in eq. 23a is related to a heat flux Q, with $\Delta T = C'Q/K$, the time to failure becomes[18]:

$$t_f \simeq \frac{2(1-\nu)^2 K^2 \exp(Q/RT)}{\mathcal{C}(\alpha E \Delta T C' Q)^2 Y^2 A (n-2) K_{Ii}^{(n-2)}} \tag{24a}$$

Figure-of-merit:

$$R'_f = \frac{(1-\nu)^2 K^2 \exp(Q/RT)}{\alpha^2 E^2 (n-2) A} \tag{24b}$$

t. Crack stability. Onset of catastrophic crack propagation. Flat plate with crack. Heat flow perpendicular to crack. Maximum temperature gradient to avoid crack propagation[19]:

$$\nabla_{max} = 8(G/2\pi\alpha^2 E\ell^3)^{1/2} \tag{25a}$$

Figure-of-merit:

$$R_{st} = (G/\alpha^2 E)^{1/2} \tag{25b}$$

Eq. 25a in terms of maximum heat flow becomes:

$$Q_{max} = 8(GK^2/2\pi\alpha^2 E\ell^3)^{1/2} \tag{26a}$$

Figure-of-merit:

$$R'_{st} = (GK^2/\alpha^2 E)^{1/2} \tag{26b}$$

u. Flat plate with N cracks per unit area. Plate cooled by temperature difference ΔT and prevented from shrinking by uniaxial rigid constraints. Critical temperature difference

of cooling[20]:

$$\Delta T_{max} = (2G/\pi \ell \alpha^2 E)^{1/2}(1+2\pi N \ell^2) \tag{27a}$$

Figure-of-merit:

$$R_{st} = (G/\alpha^2 E)^{1/2} \tag{27b}$$

For three-dimensionally constrained body with penny-shaped cracks[21] ΔT_{max} yields same figure-of-merit as eq. 27b.

F. Catastrophic crack propagation and resulting change in strength behavior:

v. Flat plate undergoing catastrophic (unstable) fracture by simultaneous propagation of N cracks per unit area. The final crack length at crack arrest[20]:

$$\ell_f = S_t^2/4NGE \tag{28a}$$

Minimum extent of crack propagation requires high values of the figure-of-merit:

$$R'''' = GE/S_t^2 \tag{28b}$$

The same figure-of-merit is obtained for penny-shaped crack undergoing crack propagation in three-dimensional body[21]. In order to avoid redundancy, the figure-of-merit, $R''' = E/S_t^2$, proposed previously is not included in the present review.

w. Strength retained (S_f) by plate which has undergone crack propagation with final crack length, ℓ_f can be derived to be:

$$S_f = \frac{GE}{S_t}\left(\frac{8N}{\pi}\right)^{1/2} \tag{29a}$$

Figure-of-merit:

$$R_f = GE/S_t \tag{29b}$$

For other geometries eq. 29a can take on somewhat different form[22].

3. Discussion and Conclusions

The expressions and figures-of-merit presented above indicate that the selection of a material with optimum thermal stress resistance can be a complex task. A total of twenty-nine independent equations are given for the thermal stress resistance of brittle materials for a number of different thermal environments, failure mechanisms and measures of thermal stress resistance. These twenty-nine equations lead to a total of twenty-two different thermal stress figures-of-merit summarized in Table I. It should be noted that some of these figures-of-merit, such as R, R' and R_{st}, apply to more than one and in the case of R' to as many as four different thermal environments and criteria of thermal stress resistance. It should be noted that the present review does not include the figure-of-merit[23], $R''' = E/S_t^2$ which implicitly is contained within the figure-of-merit, R''''. For this reason, the figures-of-merit presented are non-redundant. On the other hand, a figure-of-merit, R_t is introduced, equal to the reciprocal of the thermal diffusivity. Other factors being constant, this figure-of-merit maximizes the time-of-maximum-stress (i.e., time-of-failure) of a brittle material subjected to transient heating or cooling. Material selection on the basis of this parameter is appropriate to structures or components which have a specific function for a relatively short duration. Note also that the velocity of sound in a material has been introduced as a material property which can affect thermal stress resistance.

For the proper choice of figure-of-merit, it is essential that the heat transfer environment, the criterion of thermal stress resistance and failure mechanism be firmly established, before a choice can be made of the material with optimum thermal stress resistance. This choice of figure-of-merit is rendered even more complex by the temperature dependence of the physical properties, as well as the temperature dependence of heat transfer mechanisms. Due to these temperature dependencies, the relative thermal stress resistance of any two materials may well be interchanged for different levels of temperature at which the materials are susceptiple to thermal stress failure.

In summary, a review is presented of all thermal-stress figures-of-merit available at the time of preparation of this paper. It is hoped that this review will make a contribution to the general understanding of the nature of thermal stress failure of brittle materials and the selection of the material with the best thermal stress resistance.

Acknowledgments

Preparation of this review was carried out as part of a research program on the thermo-mechanical and thermal behavior of structural ceramics supported by the Office of Naval Research.

4. List of Symbols

A. Material Properties

α - coefficient of linear thermal expansion

A - constant in $V = AK_I^n \exp(-Q/RT)$

a - thermal diffusivity

c - speed of sound

ε - emissivity

E - Young's modulus

η - viscosity

G - fracture surface energy

K - thermal conductivity

K_{Ic} - critical stress intensity factor

λ_o - wave-length above which dielectric material is opaque and below which it is transparent

n - constant in $V = AK_I^n \exp(-Q/RT)$

ν - Poisson's ratio

Q - activation energy for sub-critical crack growth

S_c - compressive strength

S_t - tensile strength

B. Environmental, geometric variables and physical constants

A - cross-sectional area of column

b - thickness of plate, column, radius of cylinder, sphere or spherical cavity

β - Biot number, $\beta = bh/K$

C,C' - geometric constants

d - thickness of column

∇ - temperature gradient

∇_{max} - maximum temperature gradient

$F_{\lambda o}$ - fraction of total energy from black-body radiation below frequency, λ_o

H_{max} - maximum rate of internal heat generation

h - convective heat transfer coefficient

I - cross-sectional moment of inertia of column

ℓ - crack half-length

L - length of column, rod

N - number of cracks per unit area of volume

Q_{max} - maximum heat flux or flow

$\dot{Q}_{max}$ - maximum rate of change of heat flux or flow

ρ - Stefan-Boltzmann constant

σ - stress

T_{max} - maximum temperature of black-body radiation

ΔT_c - critical temperature difference

ΔT_{max} - maximum temperature difference

$\dot{\Delta T}_{max}$ - maximum rate of change of ΔT_{max}

t_o - time period of rapidly heating rod by ΔT

t - time

t* - time-to-maximum stress

t_f - time-to-failure

$t_m = L/c$

References

1. D. P. H. Hasselman, American Ceram. Soc. Bull., 49 (1970) 1033.
2. See Symposium on Thermal Fracture, J. Amer. Ceram. Soc., 38 (1955) 1-54.
3. C. H. Kent, J. Appl. Mech., 54 (1932) 185.
4. R. L. Coble and W. D. Kingery, J. Amer. Ceram. Soc., 38 (1955) 33.

5. D. P. H. Hasselman, J. Amer. Ceram. Soc., 50 (1967) 459.

6. A. L. Florence and J. N. Goodier, J. Appl. Mech., 26 (1959) 293.

7. T. R. Tauchert, J. Comp. Mat., 2 (1968) 478.

8. Z. Zudans, T. C. Yen and W. H. Steigelmann, Thermal Stress Techniques in the Nuclear Industry, American Elsevier Publishing, New York 1965, p. 493.

9. W. R. Buessum, Sprechsaal, 93 (1960) 137.

10. W. B. Crandall and J. Ging, J. Amer. Ceram. Soc., 38 (1955) 55.

11. D. P. H. Hasselman, J. Amer. Ceram. Soc., 46 (1963) 229.

12. D. P. H. Hasselman, J. Amer. Ceram. Soc., 49 (1966) 103.

13. H. Bargmann p. 174 in Topics in Applied Continuum Mechanics, ed. by J. L. Zeman and F. Ziegler, Springer Verlag, Vienna (1974).

14. G. Gruenberg, Z. Phys. 35 (1925) 548.

15. Y. B. Fridman, Strength and Deformation in Nonuniform Temperature Fields, Consultants Bureau (1964) p. 3.

16. D. P. H. Hasselman, J. Amer. Ceram. Soc., 61 (1978).

17. D. P. H. Hasselman, J. Amer. Ceram. Soc., (in press).

18. D. P. H. Hasselman and W. Zdaniewski, J. Amer. Ceram. Soc., (in press)

19. J. N. Goodier and A. L. Florence, Proc. XIth Int. Cong. of Appl. Mech. Munchen (1964) p. 562.

20. D. P. H. Hasselman, pp. 89-103 in Ceramics in Severe Environments, ed. by W. W. Kriegel and Hayne Palmour III, Plenum Press, New York (1971).

21. D. P. H. Hasselman, J. Amer. Ceram. Soc., 52, 600 (1969).

22. J. A. Coppola, D. A. Krohn and D. P. H. Hasselman, J. Amer. Ceram, Soc., 55 (1972) 481.

23. D. P. H. Hasselman, J. Amer. Ceram. Soc., 46 (1963) 535.

TABLE I

SUMMARY OF THERMAL STRESS FIGURES-OF-MERIT FOR BRITTLE MATERIALS

A. Steady State Heat Flow:

$$S_t(1-\nu)/\alpha E;\quad S_t(1-\nu)K/\alpha E;\quad S_t(1-\nu)/\alpha\eta;\quad S_t(1-\nu)K/\alpha\eta$$

B. Transient Heat Transfer:

$$S_t(1-\nu)a/\alpha E;\quad S_t(1-\nu)/\alpha E;\quad S_t(1-\nu)K/\alpha E;\quad (S_t(1-\nu)K/\alpha E\varepsilon)^{1/4};$$

$$(S_t(1-\nu)K/(1-F_{\lambda o})\alpha E\varepsilon)^{1/4};\quad S_c/\alpha E;\quad S_c c/\alpha E;\quad a^{-1}$$

C. Thermal Buckling:

$$\alpha^{-1};\ S_t^2/\alpha E^2;\ (S_t^2/\alpha^2 E)^{1/2};\ (S_t/\alpha^3 E);\ (S_t K/\alpha^3 E);\ (S_t/\alpha^3 E)^{1/2}$$

D. Crack Propagation and Change in Strength:

$$(1-\nu)^2[\exp(Q/RT)]/\alpha^2 E^2(n-2)A;\ (1-\nu)^2K^2[\exp(Q/RT)]/\alpha^2E^2(n-2)A;$$

$$(G/\alpha^2E)^{1/2};\quad (GK^2/\alpha^2E)^{1/2};\quad GE/S_t^2;\quad GE/S_t$$

BASIC DISTRIBUTION LIST December 1978

Technical and Summary Reports

Organization	No. of Copies
Defense Documentation Center Cameron Station Alexandria, Virginia 22314	(12)
Office of Naval Research Department of the Navy	
Attn: Code 471	(1)
Code 102	(1)
Code 470	(1)
Commanding Officer Office of Naval Research Branch Office 495 Summer Street Boston, Massachusetts 02210	(1)
Commanding Officer Office of Naval Research Branch Office 536 South Clark Street Chicago, Illinois 60605	(1)
Office of Naval Research San Francisco Area Office 760 Market Street, Room 447 San Francisco, California 94102 Attn: Dr. P. A. Miller	(1)
Naval Research Laboratory Washington, D.C. 20390	
Attn: Code 6000	(1)
Code 6100	(1)
Code 6300	(1)
Code 6400	(1)
Code 2627	(1)
Naval Air Development Center Code 302 Warminster, Pennsylvania 18974 Attn: Mr. F. S. Williams	(1)
Naval Air Propulsion Test Center Trenton, New Jersey 08628 Attn: Library	(1)
Naval Construction Batallion Civil Engineering Laboratory Port Hueneme, California 93043 Attn: Materials Division	(1)
Naval Electronics Laboratory Center San Diego, California 92152 Attn: Electron Materials Sciences Division	(1)
Naval Missile Center Materials Concultant Code 3312-1 Point Mugu, California 93041	(1)
Commanding Officer Naval Surface Weapons Center White Oak Laboratory Silver Spring, Maryland 20910 Attn: Library	(1)
David W. Taylor Naval Ship R&D Center Materials Department Annapolis, Maryland 21402	(1)
Naval Undersea Center San Diego, California 92132 Attn: Library	(1)
Naval Underwater System Center Newport, Rhode Island 02840 Attn: Library	(1)
Naval Weapons Center China Lake, California 93555 Attn: Library	(1)
Naval Postgraduate School Monterey, California 93940 Attn: Mechanical Engineering Dept.	(1)
Naval Air Systems Command Washington, D.C. 20360	
Attn: Code 52031	(1)
Code 52032	(1)
Code 320	(1)

BASIC DISTRIBUTION LIST (Cont'd)

Organization	No. of Copies
Naval Sea System Command Washington, D.C. 20362 Attn: Code 035	(1)
Naval Facilities Engineering Command Alexandria, Virginia 22331 Attn: Code 03	(1)
Scientific Advisor Commandant of the Marine Corps Washington, D.C. 20380 Attn: Code AX	(1)
Naval Ship Engineering Center Department of the Navy CTR BG #2 3700 East-West Highway Prince Georges Plaza Hyattsville, Maryland 20782 Attn: Engineering Materials and Services Office, Code 6101	(1)
Army Research Office Box CM, Duke Station Durham, North Caroling 27706 Attn: Metallurgy & Ceramics Div.	(1)
Army Materials and Mechanics Research Center Watertown, Massachusetts 02172 Attn: Res. Programs Office (AMXMR-P)	(1)
Air Force Office of Scientific Research Bldg. 410 Bolling Air Force Base Washington, D.C. 20332 Attn: Chemical Science Directorate	(1)
Electronics and Solid State Science Directorate	(1)
Air Force Materials Lab (LA) Wright-Patterson AFB Dayton, Ohio 45433	(1)

Organization	No. of Copies
NASA Headquarters Washington, D.C. 20546 Attn: Code RRM	(1)
NASA Lewis Research Center 21000 Brookpark Road Cleveland, Ohio 44135 Attn: Library	(1)
National Bureau of Standards Washington, D.C. 20234	
Attn: Metallurgy Division	(1)
Inorganic Materials Division	(1)
Defense Metals and Ceramics Information Center Battelle Memorial Institute 505 King Avenue Columbus, Ohio 43201	(1)
Director Ordnance Research Laboratory P.O. Box 30 State College, Pennsylvania 16801	(1)
Director Applied Physics Laboratory University of Washington 1013 Northeast Forthieth Street Seattle, Washington 98105	(1)
Metals and Ceramics Division Oak Ridge National Laboratory P.O. Box X Oak Ridge, Tennessee 37380	(1)
Los Alamos Scientific Laboratory P.O. Box 1663 Los Alamos, New Mexico 87544 Attn: Report Librarian	(1)
Argonne National Laboratory Metallurgy Division P.O. Box 229 Lemont, Illinois 60439	(1)

BASIC DISTRIBUTION LIST (Cont'd)

Organization	No. of Copies
Brookhaven National Laboratory Technical Information Division Upton, Long Island New York 11973 Attn: Research Library	(1)
Library Building 50 Room 134 Lawrence Radiation Laboratory Berkeley, California	(1)

SUPPLEMENTARY DISTRIBUTION LIST

Technical and Summary Reports

Advanced Research Project Agency
Materials Science Director
1400 Willison Boulevard
Arlington, VA 22209

Mr. George Boyer
Sensor Systems Program
Office of Naval Research
Code 222
Arlington, VA 22217

Professor R. Bradt
Ceramics Section
Materials Sciences Department
The Pennsylvania State University
University Park, PA 16802

Professor L E. Cross
The Pennsylvania State University
Materials Research Laboratory
University Park, PA 16802

Dr. A. G. Evans
Department Materials Science
and Engineering
Hearst Mining Building
University of California
Berkeley CA 94720

Dr. Gene Haertling
Motorola Corporation
3434 Vassar, NE
Albuquerque, NM 87107

Mr. W. B. Harrison
Honeywell Ceramics Center
1885 Douglas Drive
Golden Valley, MN 55422

Dr. L. L. Hench
Department of Metallurgy
University of Florida
Gainesville, FL 32603

Dr. A. A. Heuer
Professor of Ceramics
Case Western Reserve University
University Circle
Cleveland, OH 44106

Dr. Paul Jorgensen
Stanford Research Institute
333 Ravenswood Avenue
Menlo Park, CA 94025

Dr. R. N. Katz
Army Materials and Mechanics
Research Center
Watertown, MA 02172

Dr. H. Kirchner
Ceramic Finishing Company
P. O. Box 498
State College, PA 16801

Dr. B. G. Koepke
Honeywell, Inc.
Corporate Research Center
10701 Lyndale Avenue South
Bloomington, MN 55420

Mr. Frank Koubek
Naval Surface Weapons Center
White Oak Laboratory
Silver Spring, MD 20910

Dr. J. Lankford
Southwest Research Institute
8500 Culebra Road
San Antonio, TX 78284

Dr. R. E. Loehman
University of Florida
Ceramics Division
Grainesville, FL 32601

Professor P. B. Macedo
The Catholic University of America
Washington, DC 20017

Dr. N. Perrone
Code 474
Office of Naval Research
800 N. Quincy Street
Arlington, VA 22217

Dr. R. Rice
Naval Research Laboratory
Code 6360
Washington, DC 20375

SUPPLEMENTARY DISTRIBUTION LIST (Cont'd)

Dr. A. M. Alper
GTE Sylvania, Inc.
Towanda, PA 18848

Dr. W. H. Rhodes
GTE Laboratories Inc.
40 Sylvan Rd.
Waltham, MA 02154

Dr. D. C. Larson
IIT Research Inst.
10 W. 35th Str.
Chicago, IL 60616

Dr. B. Butler, Chief
Materials Branch
Solar Energy Research Institute
1536 Cole Blvd
Golden, CO 80401

Dr. M. J. Noone
Certain Teed Corp.
P.O. Box 860
Valley Forge, PA 19482

Dr. M. Berg
AC Spark Plug Division
General Motors Corp.
1601 N. Averill Ave.
Flint, MI 48556

Dr. I. K. Naik
Airesearch Casting Corp.
Garrett Corp.
2525 W. 190th Str.
Torrance, CA 90509

Dr. R. J. Bratton
R&D Center
Westinghouse Electric Corp.
Pittsburgh, PA 15235

Dr. W. Reilly, Director
PPG Industries
P.O. Box 31
Barberton, OH 44203

Dr. W. D. Syniuta
Amtech Inc.
141 California Str.
Newton, MA 02158

Dr. Wm. Kessler
AFML
Wright-Patterson Air Force Base
OH 45433

Dr. S. F. Galasso
United Aircraft Research Laboratories
East Hartford, CN 06108

Dr. J. A. Coppola
The Corborundum Comp.
P.O. Box 1054
Niagara Falls, NY 14302

Dr. W. D. Tuohig
Bendix Research Laboratories
Southfield, MI 48076

Dr. Robert Ruh
AFML/LLM
Wright-Patterson AFB
OH 45433

Dr. R. A. Penty
Hagne International
3 Adams Str.
South Portland, Maine 04106

Dr. S. Musikant
General Electric Company
3198 Chestnut Str.
Philadelphia, PA 19101

Dr. D. W. Richerson
Airesearch Man. Comp. Code 503-44
Garrett Corp.
111 S. 34th Str., Box 5217
Pheonix, Arizona 85034

Dr. T. J. Whalen
Process Research Department
Ford Motor Company
20000 Rotunda Drive
Dearborn, Michigan 48121

SUPPLEMENTARY DISTRIBUTION LIST (Cont'd)

Dr. Frank Recny
General Electric Company
Court Street
Plant Building C
Box 1122
Syracuse, NY 13201

Dr. J. H. Rosolowski
General Electric Company
Research and Development Center
P. O. Box 8
Schenectady, NY 02301

Dr. J. H. Simmons
Catholic University of America
Washington, DC 20064

Dr. P. L. Smith
Naval Research Laboratory
Code 6361
Washington, DC 20375

Dr. R. W. Timme
Naval Research Laboratory
Code 8275
Underwater Sound Reference Division
P.O. Box 8337
Orlando, FL 32806

Dr. Charles C. Walker
Naval Sea Systems Command
National Center #3
2531 Jefferson Davis Highway
Arlington, VA 20390

Dr. Paul D. Wilcox
Sandia Laboratories
Division 2521
Albuquerque, NM 87115

Dr. N. S. Corney
Ministry of Defense
(Procurement Executive)
The Adelphi
John Adam Street
London WC2N 6BB
UNITED KINGDOM

Dr. Murray Gillen
Australian Embassy
Washington, DC 33801

Prof. R. H. Doremus
Rensselaer Polytechnic Institute
Troy, NY 12181

Dr. D. J. Godfrey
Admiralty Materials Laboratory
Ministry of Defense
(Procurement Executive)
Holton Heath
Poole, Dorset
BH16 6JU
UNITED KINGDOM

Globe-Union, Inc.
5757 North Green Bay Avenue
Milwaukee, WI 53201
Attn: G. Goodman

Prof. P. J. Gielisse
Dept. of Chemical Engineering
University of Rhode Island
Kingston, RI 02881

Mr. W. B. Crandall
Alfred University
Alfred, NY 14802

Dr. J. T. A. Roberts
Electric Power Research Institute
3412 Hillview Avenue
P.O. Box 10412
Palo Alto, CA 94303

Dr. W. R. Manning
Champion Spark Plug Company
20000 Conner Avenue
Detroit, MI 48234

Dr. B. A. Wilcox
Ceramics Program, Room 336
Metallurgy and Materials Research
National Science Foundation
Washington, DC 20550

Dr. H. E. Bennett
Naval Surface Weapons Center
Research Department Code 601
China Lake, CA 93555

Dr. R. J. Charles
General Electric Company
Research and Development Center
Schenectady, NY 12301

Dr. A. R. C. Westwood
Martin-Marietta Laboratories
1450 South Rolling Road
Baltimore, MD 21227

SUPPLEMENTARY DISTRIBUTION LIST (Cont'd)

Dr. D. E. Niesz
Battelle Memorial Institute
505 King Avenue
Columbus, OH 43201

Dr. C. O. Hulse
United Aircraft Research Labs
United Aircraft Corporation
East Hartford, CT 06108

Dr. S. M. Wiederhorn
Physical Properties Section
Bldg. 223, Rm. A355
National Bureau of Standards
Washington, DC 20234

Dr. P. F. Becher
Code 6362
U.S. Naval Research Laboratory
Washington, DC 20375

Mr. J. F. McDowell
Sullivan Park
Corning Glass Works
Corning, NY 14830

Dr. E. K. Beauchamp, Div. 5846
Sandia Laboratories
Albuquerque, NM 87185

Dr. J. C. Swearengen
Materials Science Division
Sandia Laboratories
Livermore, CA 94550

Dr. J. A. Rubin
Kyocera International, Inc.
8611 Balboa Avenue
San Diego, CA 92123

Dr. M. I. Mendelson
Government Products Division
Pratt and Whitney Aircract Gr.
P.O. Box 2691
West Palm Beach, FL 33402

Dr. W. V. Kotlensky
Materials Technology Department
TRW, Inc.
One Space Park
Redondo Beach, CA 90278

Dr. L. M. Long
Engineering Division
Tennessee Eastman Company
Kingsport, TN 37662

Dr. R. E. Engdahl
Deposits and Composites, Inc.
318 Victory Dr.
Herndon, VA 22070

Professor W. D. Kingery
Ceramics Div. Rm 13-4090
MIT
77 Mass. Ave.
Cambridge, MA 02139

Dr. F. W. Clinard, Jr.
Los Alamos Scientific Lab.
MS 546
P.O. Box 1663
Los Alamos, NN 87544

Dr. D. DeCoursin
Fluidyne Eng.
5900 Olson Memorial Hwy.
Minneapolis, MN 55422

Dr. F. F. Lange
Rockwell International
P.O. Box 1085
1049 Camino Dos Rios
Thousand Oaks, CA 91360

Dr. T. Vasilos
AVCO Corporation
Research and Advanced Development
Division
201 Lowell Str.
Wilmington, MA 01887

Dr. M. O. Marlowe
General Electric Comp.
1900 South 10th St.
San Jose, California 95125

Dr. N. N. Ault
NORTON Comp.
One New Bond Str.
Worcester, MA 01606

SUPPLEMENTARY DISTRIBUTION LIST (Cont'd)

Dr. J. E. Doherty
Mat. Eng and Res. Lab.
Pratt and Whitney Aircraft
Middletown, CN 06457

Dr. J. E. Hove
Institute for Defense Analysis
400 Army-Navy Dr.
Arlington, VA 22202

Dr. R. A. Krakowsky
Mail St. 641
Los Alamos Scientific Lab.
Los Alamos, NM 87544

Dr. Hayne Palmour III
Engineering Research Division
N.C. State University
P.O. Box 5995
Raleigh, NC 27650

Dr. W. J. Smothers
Homer Research Laboratory
Bethlehem Steel Corp.
Bethlehem, PA 18016

Dr. L. Steinhauer
Mathematical Sciences NW
Box 1887
Bellevie, Wash. 98009

Dr. D. Ulrich
AFOSR, Code NC
Chemical Sciences Div.
1400 Wilson Blvd
Arlington, VA 22209

Dr. C. Zweben
General Electric Space Div.
P. O. Box 8555
Philadelphia, PA 19101

Dr. C. Hoenig
Lawrence Livermore Lab.
Livermore, CA.

Dr. V. J. Tennery
Oak Ridge Nat. Lab.
Oak Ridge, TN 38730

Dr. E. D. Lynch
Lynchburg Research Center
Babcock and Wilcox Co.
Box 1260
Lynchburg, Va. 24505

Dr. S. L. Blum
Northern Energy Corp.
70 Memorial Dr.
Cambridge, MA 02142

Dr. W. R. Prindle
National Materials Adv. Brd.
2101 Const. Avenue
Washington, DC 20418

Mr. R. Palicka
CERADYNE Inc.
P.O. Box 11030
3030 South Red Hill Ave.
Santa Ana, CA 92705

Dr. S. Dutta
NASA-Lewis Research Center
Mail Stop 49-3
21000 Brookpark Rd.
Cleveland, OH 44135

Mr. B. Probst
NASA-Lewis Research Center
21000 Brookpark Rd.
Cleveland, OH 44135

Dr. K. Chyung
Sullivan Park
Corning Glass Works
Corning, NY 14830

Dr. S. W. Freiman
Deformation and Fracture Group
Physical Properties Section, Bldg 223
National Bureau of Standards,
Washington, DC 20234

Mr. W. Trombley
Garrett Corporation
1625 Eye Str. NY
Suite 515
Washington, DC 20006

Dr. S. C. Dixon
SDD-Thermal Structures Branch
Mail Stop 395
NASA Langley Research Center
Hampton, VA 23665

Mr. R. T. Swann
MD-Materials Research Branch
Mail Stop 396
NASA Langley Research Ctr.
Hampton, VA. 23665

SUPPLEMENTARY DISTRIBUTION LIST (Cont'd)

Dr. Clifford Astill
Solid Mechanics Program
National Science Foundation
Washington, DC 20550

Dr. D. I. Roberts, Manager
Structural Materials Dept.
General Atomic Comp.
P. O. Box 81608
San Diego, CA 92138

Dr. M. Bohon
Black and Veatch
P. O. Box 8405
Kansas City, MO 64114

Dr. R. J. Cottschall
U.S. Dept. of Energy
Div. of Matls. Science
Mail Stop J309
Washington, DC 20545

Metals and Ceramics Information Center
Batelle Columbus
Columbus, OH

Dr. K. H. Holko, Manager
Materials Applications
General Atomic Company
P. O. Box 81608
San Diego, CA 92138

Dr. S. Pohlman
Solar Energy R. I.
1365 Cole Blvd.
Golden, CO. 80401

Dr. D. C. Larson
IIT Research Institute
Mechanics of Materials Division
Chicago, IL 60616